High-Performance Aptasensors: Poly(ethylene glycol)-tethered Surface Construction to Quench Bio-fouling and Enhance Sensitivity

Thangavel Lakshmipriya

February 2014

High-Performance Aptasensors: Poly(ethylene glycol)-tethered Surface Construction to Quench Bio-fouling and Enhance Sensitivity

Thangavel Lakshmipriya
Doctoral Program in Materials Science

Submitted to the Graduate School of
Pure and Applied Sciences
in Partial Fulfillment of the Requirements
for the Degree of Doctor of Philosophy in Engineering

at the
University of Tsukuba

Table of Contents

List of Figures

Page

List of Tables

Page

Chapter 1

General Introduction

1.1. High-performance sensing

Reporting clinically relevant biomolecular interactions is mandatory in the field of medical diagnosis. Recognition of biomolecular interaction is considered as an important event to convey the importance for a wide range of disciplines to understand the events of disease and gene regulations. A biosensor is an analytical device, made by a combination of a biological component with a physicochemical detector that assists in the detection of biomolecular interactions. A biosensor detects extremely small amounts of biochemical agents, such as proteins, nucleic acid, bio-mimetic polymers, in a given sample. First reported biosensor was in 1962 having signal recognition elements and transducers, as the basic for sensor development.[1] Nanomaterials can facilitate signal transduction with electroactive tags for sensing and imaging purposes. Benefits obtained from nanotechnology mainly depend on specific tailored materials designed with essential structures at the nanoscale level to achieve a specific goal, thus greatly extending the range of applications, including diagnosis.

1.1.1. Gold sensing surface

Among several nanomaterials that have been fabricated, gold (Au) is an ideal material that is widely used in the development of sensors, owing to its unique characteristics, such as easy water dispersal, compatibility with surface functionalization, biological non-reactivity, anti-oxidation, high-conductivity and ability to be tailored with uniform and different nano-sizes.[2,3,4] Original Au material does not have any charges, however, getting surface charges when undergo the preparation of nanostructures. Gold nanostructures consist negative surface charges in most of the cases and positive charged nanostructures can also be prepared. Au sensing surface can be chemically functionalized by Au-S linkage and exchange reaction with thiolated compounds, examples mercaptohexadecanoic acid and mercaptopropionic acid. Au adsorb in the visible light spectrum around 520 nm (green light) due to the excitation of plasmons in the particle and this wavelength can be adapted to several optical sensors.[5,6] In the past, several attractive Au-based sensing surfaces have emerged, and the applications of these surfaces have expanded to sensor development

in conjunction with various fields.[7-14] Usually thin layer of Au tends to be less stable and it can be overcome by making a hybridized surface of Au with other materials such as, chromium and silica.

1.1.2. Silica sensing surface

Other than Au, sensors on silicon (Si) and silica or dioxide of silicon (SiO_2) substrates are widely used in the analysis of biomoecular interactions.[15-17] Si is an abundant, low-cost material as compared to noble metals. Amourpous and variety of crystal forms of SiO_2 materials are quite common; in addition due to smoothness of crystal form of SiO_2, it is more suitable for sensing applications. SiO_2 will occur as a non-crystalline oxidation product on the surface of Si or Si compounds. These materials can be prepared by Czochralski technique has been conventionally used crystal growth method for the growth of single crystal ingots. Quartz, tridymite and cristobalite are three forms of crystalline forms of SiO_2. A high quality SiO_2 layer grown on the Si and SiO_2 always carry the positive charges. These substrates can be made with wide variations in the degree of packing leads to differences in the densities, thicknesses, and morphologies of the deposited films.[18] Furthermore, Si and SiO_2 are inert against most chemicals and physical conditions. SiO_2 materials are very commonly chemically functionalized by silane (amine) coupling reagents. The above described two materials (Au and SiO_2) are highly preferable in sensing surface developments, their high performances are displayed when hybridized with other materials such as polymers.

1.1.3. Polymer-hybridized sensing surface

The major prerequisite of biosensors includes measuring the specific target in a sample containing mixture of compounds, without compromising the convenience and sensitivity. Even though, the sensitivity varies with the different systems depends on various parameters, sensitivity is the determining factor for the quality of the sensor.[19] One of the most important factors in improving the effectiveness of the sensor is the correct orientation of immobilized biomolecules on the sensing surface.[20] It is also important to minimize non-specific biofouling as much as possible to improve the

signal to noise ratio (S/N). Natural polymers such as albumin, casein, and dextran are considered as candidates for suppressing the non-specific interaction on the sensor surface.[21] However, the efficiency of these natural polymers is not completely satisfactory. High-performance surface modification techniques using synthetic polymers are highly anticipated to overcome these issues. Nagaoka and his co-workers in 1982 first reported that about a 'poly(ethylene glycol) (PEG) polymer brush', represents PEG chain-end immobilized on a sensing surface which forms a tethered chain. Several reports on PEG-chain-tethered surfaces have been published after their report.[20] It was reported previously that a densely packed PEG tethered-chain surface shows high resistance to biofouling. In particular, a combination of long and short PEG chains greatly reduces non-specific adsorption of proteins onto the substrate surface. It is interesting to note that sensitivity is also increased when antibody was co-immobilized on mixed-PEG chain hybridized surface.[22] For effective immobilization of PEG-derivatives on substrate surfaces, suitable anchoring strategies must be designed using specific interactions. It was also reported that multi-anchoring is one of the most effective ways of stably immobilizing PEG derivatives onto the substrate surface.[23] Several types of PEG-based block copolymers, but not graft-type copolymers, have been used to construct highly stable, tether-like chains on the substrate surface. PEG block copolymers such as PEG-*b*-polycations, PEG-*b*-polyanions, and PEG-*b*-hydrophobic polymers have proven to be versatile materials.

The objective of this work is stated below to establish high-performance PEG hybridized aptasensors on SiO_2 and Au sensing surfaces. The following targets, polymers and sensors were chosen to carry out this study.

(i) To reduce the bio-fouling and to increase the non-fouling characters with higher specificity using poly(ethylene glycol)-block polymers (PEG-*b*-polymers), such as PEG-*b*-poly(acrylic acid) (PEG-*b*-PAAc), pentaethylenehexamine-terminated PEG (N6-PEG) and PEG-b-poly[2-(N,N-dimethylamino)ethyl methacrylate] (PEG-*b*-PAMA) as a blocking agents.

(ii) Human coagulating factor IX protein (FIX) was chosen as a model analyte to interact anti-FIX aptamer, because FIX has extremely low availability *in vivo* and important to detect defects in human blood coagulation system. Further, anti-influenza aptamers were generated to demonstrate and diagnosis of intact influenza viruses.

(iii) Sensor surfaces (SiO_2 or Au) of Evanescent-field-coupled Waveguide-mode (EFC-WM), Surface Plasmon Resonance (SPR) and Surface Plasmon Fluorescence Spectroscopy (SPFS) were used to demonstrate the aptamer-protein interactions.

The potential characteristics of the above molecules on PEG-*b*-polymer hybridized sensing surfaces are described below.

1.2. PEG-*b*-polymers

PEG is one of the popular polymers, which is chemically inert, provides terminal hydroxyl groups that can be used as anchors for functional groups, is nontoxic and disperable in water due to hydrogen bonding between water molecules and ether oxygen of PEG chain. PEG-*b*-polymers are attracted the researchers in the past especially in the fields of biotechnology, pharmaceutical and medicine for the purposes of bio-recognition, cosmetics, drug delivery systems and microsystems.[24,25] PEG-based polymers are also driven an efficient role in the development of biointerfaces and for the applications of non-ionic surfactants, lubricants, and adhesives.[20,26] PEG has been used as a blocking agent for the preventing nonspecific adsorption of binding materials when co-immobilized with ligands for targets such as antibodies and oligonucleotides.[20] Surface modification with PEG (so-called PEGylation) is shown to have non-fouling due to biocompatibility of the polymers such as hydrophilic, and flexiblility.[27-29] Grafting of nanostructures with PEG resulting the enhanced stability of suspensions due to steric repulsion.[30] Moreover, PEGylated nanoparticles are connected with external stimuli-responsive such as pH, temperature and ionic strength.[31-34] These properties makes the PEG to be applicable to nano- or microscale particles.[35] PEG-*b*-polymers found to reduce the nonspecificity to higher extend due to its characteristics such as low interfacial free energy in water and high chain

mobility, which stimulates excluded-volume effects.[36] The length and density of the constructed polymers are grately play a role in the improvement of sensitivity and specificity of a given sensor. However, increased chain-length tend be less densed due to steric exclusion of PEG-chains on the immobilized surface .[37,38] Instead, mixture of long and short PEG-chain overcome the density issues, by the occupying properties of short chain between the interface of two long chains.[39] Even though, different methods used to construct PEG tethered chains on sensing surfaces, two main techniques are common, known as the 'grafting-from' and 'grafting-to' methods; the former is used to construct PEG chains by the polymerization of vinyl monomers from a surface, and the latter involves the immobilization of polymer to a surface.[20] Figure 1.1. summarizes different ways of immobilization of polymers on sensing substrate.

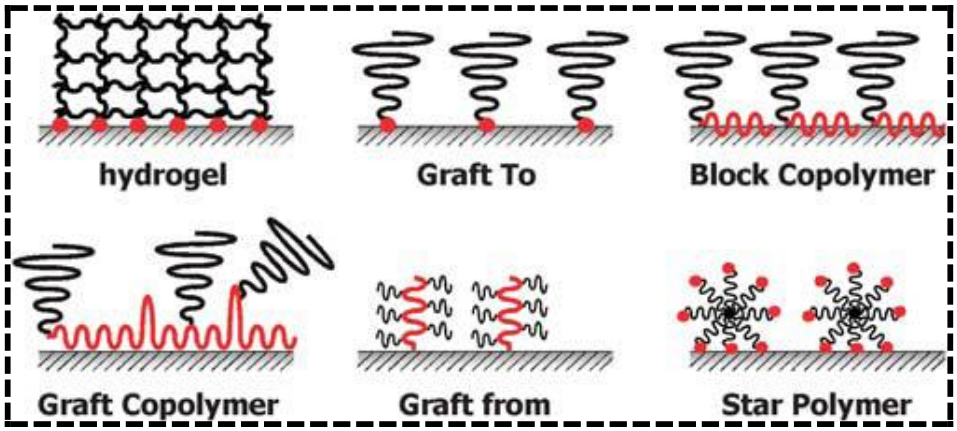

Figure 1.1. PEG-tethered surface modifications. Immobilization of different polymers is shown. Depends on the sensing surface to be preferred, the suitable polymer will be chosen (This figure is reproduced from Nagasaki, 2011).[20]

These polymers are drastically reduce the back-ground noice and improve the sensitivity. Another advantages of polymers are having lower molecular weights (less than 10 kDa) than other blocking agents such as Bovine serum albumin (BSA) (66 kDa), casein (>20 kDa) and gelatin (>100 kDa). Higher molecular weight blocking cause interference with molecular recognition site of ligand

and analyte.[20] To demonstrate the applications of PEG-*b*-polymers for the sensing applications, three types of polymers are desired to use in the present study for surface construction, namely, PEG-*b*-PAAc, N6-PEG and PEG-*b*-PAMA (Figure 1.2).

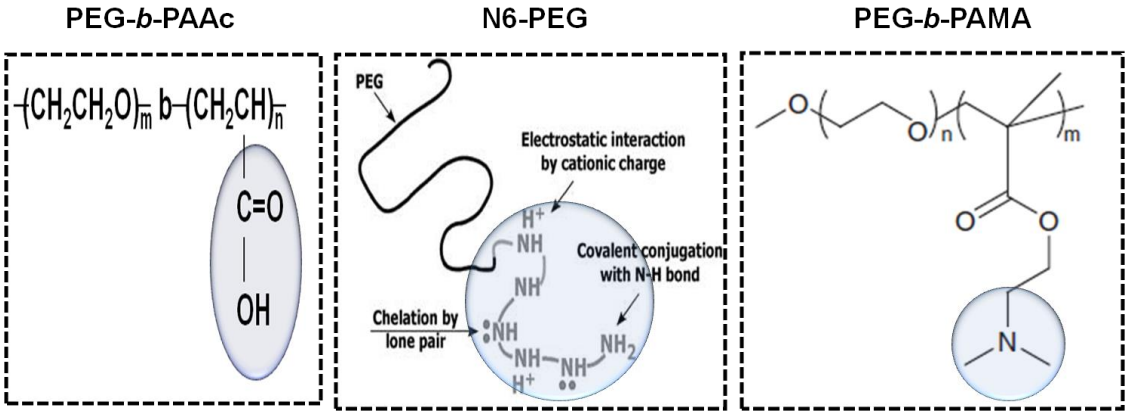

Figure 1.2. PEG-*b*-polymers. Three kinds (PEG-*b*-PAAc, N6-PEG and PEG-*b*-PAMA) of polymers were used. The chemical structures of polymers are shown. Negative charged PEG-*b*-PAAc can bind on the positively charged amine surfaces. Polyvalent interactions between the end amino groups of N6-PEG interact on the Au surface. Polyamine segment of PEG-*b*-PAMA interacts with a Au surface via multipoint coordination by the tertiary amino groups. Regions of interaction are encircled (This figure is reproduced from Nagasaki, 2011).[20]

1.2.1. PEG-*b*-poly(acrylic acid) (PEG-*b*-PAAc)

Negative charged PEG-*b*-PAAc can bind on the positively charged surfaces, such as amine. Another example, PEG-*b*-PAAc effectively covers Y_2O_3 nanoparticles via an electrostatic interaction resulting from the positive charge of the yttrium oxide surface.[40] It was reported that poly(acrylic acid)(PAAc) adsorbed nanoparticles can disperse in aqueous solutions due to electrostatic repulsion of the carboxyl groups of polymer.[41] Hemmer et al. have reported that PEG-*b*-PAAc provides the chemical durability leads a good *in vitro* biocompatibility.[42] They analysed bare and PEG-*b*-PAAc modified Erbium and ytterbium doped gadolinium oxide (Gd_2O_3:Er^{3+},Yb^{3+}) nanostructures and investigated of their *in vitro* cytotoxicity with B-cell hybridomas and macrophages and noticed no cytotoxic effect towards B-cell hybridomas, however, bare nanostructures shown a toxic effect on macrophages. The same team also tested the effect of PEG-*b*-PAAc modification on the *in vitro*

cellular up-take of Gd_2O_3:Er^{3+},Yb^{3+} nanostructures by macrophages.[43] PEG-*b*-PAAc can be availed commercially. PEG-*b*-PAAc modifications on nanostructures provide a protecting layer and PEG-*b*-PAAc is suitable for providing chemical durability, dispersion stability, and noncytotoxic behaviour for biomedical applications[30]. In this work, the author used PEG-*b*-PAAC for the blocking agent on the amine modified surfaces.[44]

1.2.2. Pentaethylenehexamine-terminated PEG (N6-PEG)

PEG-*b*-polyamine is more suitble for the modification of Au surfaces for specific biorecognition. Polyvalent interactions between the end amino groups of N6-PEG interact on the Au surface. The coordination of the lone pair of the amino groups to the Au surface is involved in this reaction.[22] This poly-amine interaction with Au-surface is long-term stable than a common Au-S linkage under varied physiological conditions.[20,45] The coordination lone pair of the amino group is low with Au (3–6 $kcalmol^{-1}$) than Au-S linkage (~50 $kcalmol^{-1}$) implies the strong interaction of N6-PEG.[46] Concerning chain density on sensing surface by N6-PEG, was found to be 3 times higher than mono-amine-ended PEG. Moreover, electrostatic force of N6-PEG is totally differing from mono-ended chain. N6-PEG has both protonated and non-protonated amines in each PEG molecule and it show the pKa values of 2-10. Apart from Au surface, N6-PEG is also recommended for other surfaces, particularly active-ester surface. N6-PEG coated magnetic beads are having more stable dispersion than BSA coated beads.[20] N6-PEG can be availed commercially and greatly reduce the nonspecific binding of biomolecules, it's considered as good blocking and specific recoganising agent for Au surface. The author used N6-PEG as the blocking agent on Au surface for this study.

1.2.3. PEG-*b*-poly[2-(N,N-dimethylamino)ethyl methacrylate] (PEG-*b*-PAMA)

The polyamine segment of PEG-*b*-PAMA interacts with a Au surface via multipoint coordination by the tertiary amino groups. Co-ordination of nitrogen atom with amine groups on PEG plays

an important part in immobilization process on Au surface, three nitrogen atoms on the PEG chain are sufficient for polyvalent coordination with Au.[23] Miyamoto et al.[47] have prepared a novel PEG-*b*-PAMA, having water-soluble, biocompatibility with controlled molecular weight. Co-immobilization of PEG-*b*-PAMA and ssDNA promotes the sensitive detection, this might be due to, PEG-*b*-PAMA co-immobilized Au surface with SH-ssDNA inhibits the interaction of nucleobase of oligo and Au,[21] leads to upright confirmation of immobilized ssDNA. This confirmation further supports by the proper duplex formation.[48,49] Moreover, PEG-*b*-PAMA co-immobilized gold nanoparticle (GNP) with siRNA shown to have higher interference efficiency.[50] It was found that adsorption of PEG-*b*-PAMA on the Au surface was not affected by strong ionic condition and it indicates interaction of polyamine on the Au, rather than minor electrostatic attraction between polyamine and Au.[51] The pKa value of the amino groups of PEG-*b*-PAMA is 7.0, indicates amino groups in the PAMA will depronate completely at pH 10.0. This statement suggest that GNP can be stablilized by the neutral PEG-*b*-PAMA, through co-ordination of amino nitrogen atoms.[23] However, it was surprising that the purified PEG-GNP were stable at neutral pH, even though they are deprotonated, indicates after immobilize PEG on Au, they are stable and also cause changes in the pKa value of amino groups.[23]

1.2.3.1. Synthesis of PEG-*b*-PAMA

To synthesize PEG-*b*-PAMA, the procedure outlined by Miyamoto et al. can be followed.[47] In brief, the purified Hydroxyl-terminated PEG (MeO-PEG-OH, MW: 5000) (50 g) by reprecipitation was dissolved in commercial tetrahydrofuran (THF, Kanto Chemical Co., Ltd.). The polymer was precipitated by pouring this solution into 2-propanol. Centrifugation at 2300 x *g* at 4 °C was followed to separate precipitated polymer and washed several times with 2-propanol and dried by evaporation. The residue was dissolved in 20 mL of benzene, lyophilized overnight and the purified MeO-PEG-OH (5 g) was dissolved in THF under a nitrogen atmosphere. MeO-PEG-OH (300 mg) was dissolved in 30 mL of THF under a nitrogen atmosphere. MeO-PEG-O−K+ was prepared by adding potassium naphthalene, which was used as an initiator for the anionic addition polymerization. PEG-*b*-PAMA was

obtained via block copolymerization through the addition of 2-(*N*,*N*-dimethylamino)ethyl methacrylate (AMA). The precipitate was dissolved in distilled water and adjusted to pH 4.5 by adding 1 M HCl. After lyophilization, the protonated PEG-*b*-PAMA was purified by Soxhlet extraction with THF. The quality of the product was characterized, and its purity was determined by gel permeation chromatography and proton nuclear magnetic resonance spectroscopy.[47,49] The author used PEG-*b*-PAMA on Au surface for this study.

The comparison of basic characteristics of the above three PEG-*b*-polymers are shown in Table 1.1. It is expected that PEG-derived polymers hybridized biological probe and target interactions on sensing surface will yield potential output. On the above PEG-*b*-polymer(s) hybridized sensing surface(s), the interactions of RNA-aptamers and target stated below (FIX or influenza virus), were analyzed.

Characteristics	PEG-*b*-PAAc	N6-PEG	PEG-*b*-PAMA
Molecular weight	7.8 kDa	6 kDa	11 kDa
Interaction	Electrostatic to amine	Coordination of the lone pair to Au	Coordination of amino nitrogen atoms to Au
Suitability	Positive charged surface	Au and active-ester surface	Au surface
Active chain	Carboxylic group	6 amino	Amino group

Table 1.1. Comparison among different PEG-*b*-polymers. Different methods of preparations are involved. The sizes and the chain lengths can be varied with the preparation.

1.3. Generation of RNA-based probe for sensing applications

Developing nucleic acid probes (RNA or DNA) have been followed for several decades, because most of the biological functions are performed by the involvement of nucleic acids. A functional probe such as nucleic acid must possess the genotype and phenotype that enables the survival of the molecule within its population. Early investigations by Sol Spiegelman and colleagues performed

Darwanian evolution in the test tube using RNA bacteriophage Qβ that produces copies of the viral Genome,[52] by repeating several generations of the Qβ replicase-mediated RNA. This was the first experiment that attested the self-replicating property of the RNA that have the phenotype and genotype to 'reproduce' and to evolve *in vitro* in the presence of selection pressure. This groundbreaking work pioneered the effort to look further into the other phenotypic capability of the RNA sequence, such as the ability of the RNA sequence in recognizing target with high binding affinity and specificity. Using this work as the basic foundation, several artificially evolved molecules have been generation by mutations (Figure 1.3a). Further, library of mutants or completely randomized biomolecules was used to select the best molecules a so-called 'aptamer' (Figure 1.3b).

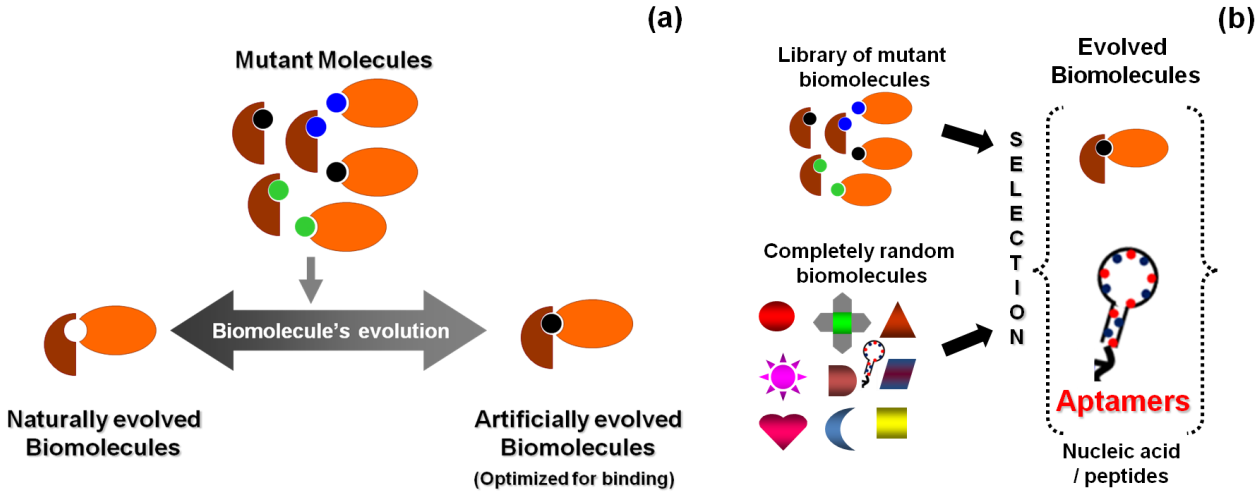

Figure 1.3. Strategies of molecular generation. (a) generation of artificial molecules from naturally evolved molecules by mutation. (b) Selection of high affinity molecules from library of mutants or completely random molecules.

1.4. Aptamers

Aptamers are artificially evolved molecules against specific targets, from small molecules to whole cells, which can be generated by the separation and amplification processes by making the complex of randomized RNA or DNA libraries with target. This strategy involving an *in vitro* selection process, called 'systematic evolution of ligands by exponential enrichment' (SELEX). This selection process mimics the natural selection of aptamers as reported in the case of riboswitches.[53] A typical

aptamer generation process starts with library contains huge number of molecules and repeatation under stringent conditions. Only high-affinity molecules are retained through successive selection cycles (Figure 1.4). SELEX was developed by 3 independent researchers in 1990 as an approach to identifying selective molecules among a randomized combinatorial library of molecules, against different targets.[54-56] Using the basic SELEX strategies, there are several other SELEX strategies have been generated (Figure 1.5).

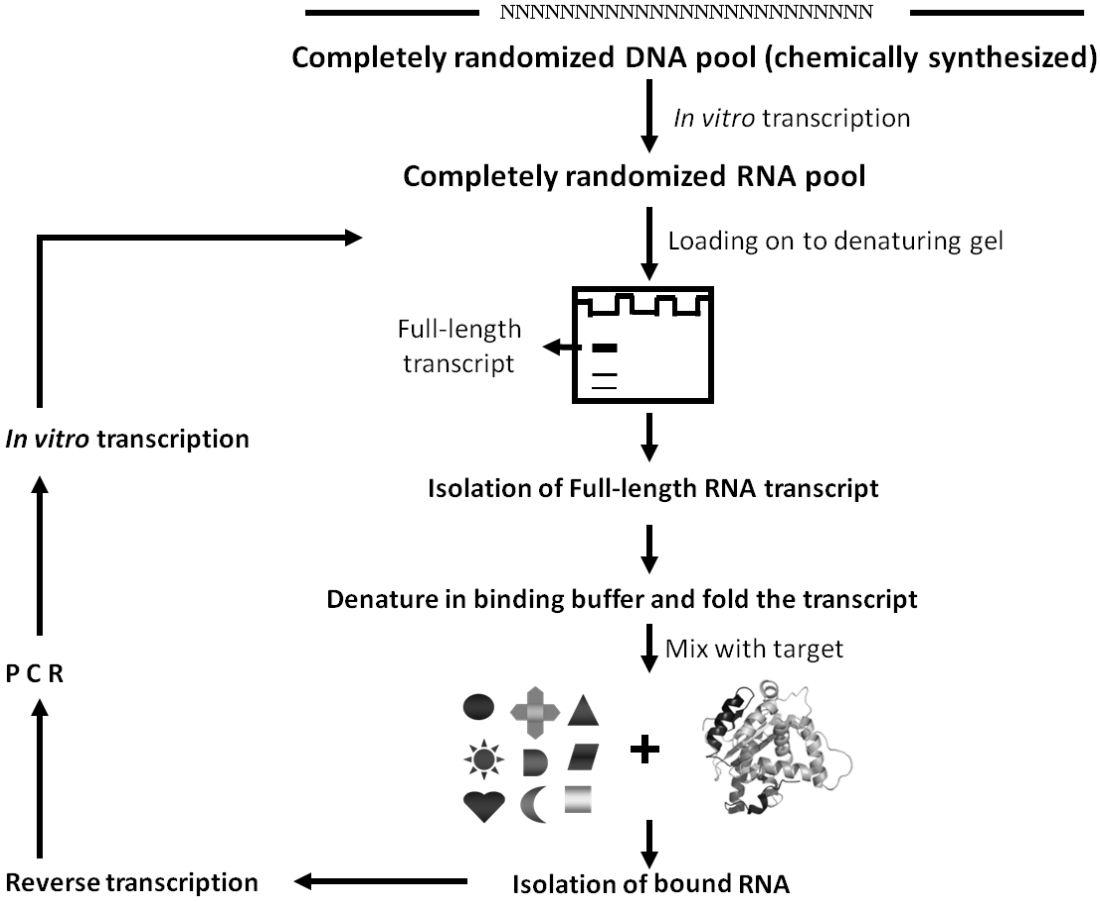

Figure 1.4. Basic strategy and methods involved in the SELEX for RNA aptamer. SELEX involves complex formation, separation and regeneration. The size of the initial library can be altered.

Selected aptamer undergo specific binding when the appropriate target such as, protein is available. These binding are accomplished due to either protein-induced aptamer folding or aptamer-induced protein folding or co-induced folding.[57] (Figure 1.6). Aptamers are having the potential characteristics equal to the antibodies, in addition aptamers have appealing characters over antibodies (Table 1.2).

Figure 1.5. Different strategies of SELEX. The number of selection cycles and molecular generation are varied with each strategy.

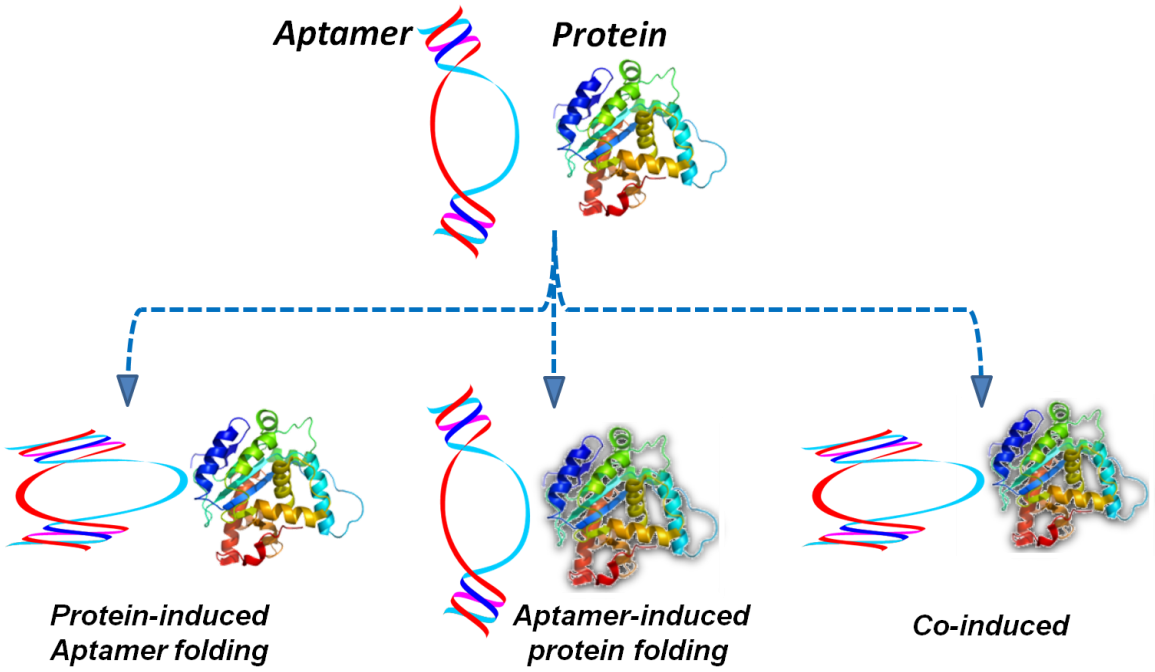

Figure 1.6. Strategies of aptamer-protein interactions. Three possible structural changes occurred during interactions are shown.

Characteristics	Aptamers	Antibodies
Binding affinity	Low picomolar to femtomolar	Low nanomolar to picomolar
Size	Molecular weight ~6 kDa	Molecular weight ~150 kDa
Method of selection	Usually *in vitro*	Usually *in vivo*
Time and cost	Fast & cheap	Time consuming & expensive
Activity	No batch variation	Batch to batch variations
Binding site	Can be determined	Difficult
Chemical modification	Easier	Difficult
Stability	Stable under varied temperatures	Sensitive
Shelf-life	Unlimited	Limited
Immunogenicity	Non-immunogenic	Immunogenic

Table 1.2. Comparison of characteristics of aptamers and antibodies. Aptamer can behave similar to antibody and also have several advantages.

Aptamers are analogues of antibodies, have been reported with high affinities to their targets, having dissociation constants of low-picomolar to femtomolar level, comparable even better than antibodies.[58] Aptamers are more thermodynamically stable, having lower molecular weight. Moreover, the production of aptamer is not influenced by the physiological conditions as in antibody generation. Antibody generation relies on the *in vivo* parameters in animal body, whereby the recognition of the target by the antibody is strictly based on the suitable *in vivo* parameters. Size of the aptamer (usually ~6,000 daltons) compared to antibodies (~150,000 daltons) have made aptamers object of intense interest in many target detection systems. Antibodies can only be raised against immunogenic targets in animals, while aptamers can be generated against virtually any target molecules. Once aptamer sequence is identified, large amounts of aptamers can be chemically synthesized, which confers no batch to batch variations. Aptamers can also be easily modified by adding extra sequences.

Enhancement of the aptamer stability will make these aptamers more amenable to subsequent applications. Modification of the pyrimidines to 2'-amino, (2'-NH_2), 2'-fluoro (2'-F) and purines to 2'-O-methyl increase the stability of the RNA aptamer due to the less reactivity of these functional groups.

Some modification can be done in the initial library itself by 2'-ribose modification which confers thermodynamic stability to the nucleic acids compared to the naturally occurring counter-parts. *In vitro* generation aptamer has expanded to the several fields, such as molecular biology, molecular evolution, and molecular recognition to analyse the functional and structural aspects. Aptamers have been selected against a wide range of important targets irrespective of sizes, playing a vital role in the clinical front for therapy to prevent and treat disorders. As very efficient molecular probes, aptamers are widely used in a number of applications including biomedical, analytical, diagnostics and therapeutics by amalgamating with several methods to transduce the molecular recognition event of aptamer-target binding. Several aptamer-based drugs are now under different phases of clinical trials. The first therapeutic aptamer generated against the vascular endothelial growth factor (VEGF) for the treatment of neovascular age-related macular degeneration, was commercialized in 2004.[59] The selected aptamers in the past have possessed significant (>10,000-fold) abilities to discriminate between closely related molecules.[60,61] Aptamers can also distinguish between closely related viral sub-types and clotting factors.[62,63] These discrimination abilities of aptamers can be used as the biorecognition elements, led to the development of high-performance sensors. All other applications that use aptamers are highly connected with sensors for clinical diagnosis and imaging purposes in the front of nanotheranostics.

1.5. Aptasensors

After the invention of aptamers in the 90s, several aptamer-based sensors (so called "aptasensors") were designed and these devices were used for several applications in interdisciplinary sciences. Applications of aptamers in the medical and immunodiagnostic fields have suggested that an aptasensor could be an alternate to other antibody-based sensors. Aptamers can be used to analyze target interactions, to generate inhibitors to be used for pharmacological purposes, to detect a target in a complex mixture, and for screening the drug library in medicinal chemistry. The aptamer can be a ligand when a mixture contains an analyte, whereas the aptamer is an analyte if it is in the

sample that is being analyzed. Usually, ligands are the interacting molecules immobilized on the sensor surface, can be done physically on the sensor surface or through pre-treated chemical linkage (Figure 1.7). The physical immobilization of molecules is mainly the result of electrostatic interaction, hydrogen bonding or van der Waals force. For the immobilization of aptamers through chemical linkages, any general strategy can be used because aptamers can be easily modified with linkers.

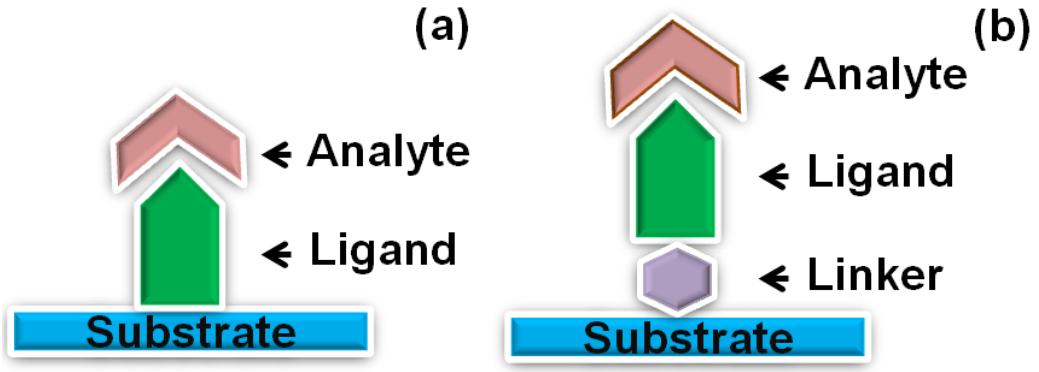

Figure 1.7. Ligand-analyte interactions on sensing surface. The ligand can be immobilized by physical means (a) or through chemical linkers (b). The scheme (b) is followed in most of the cases.

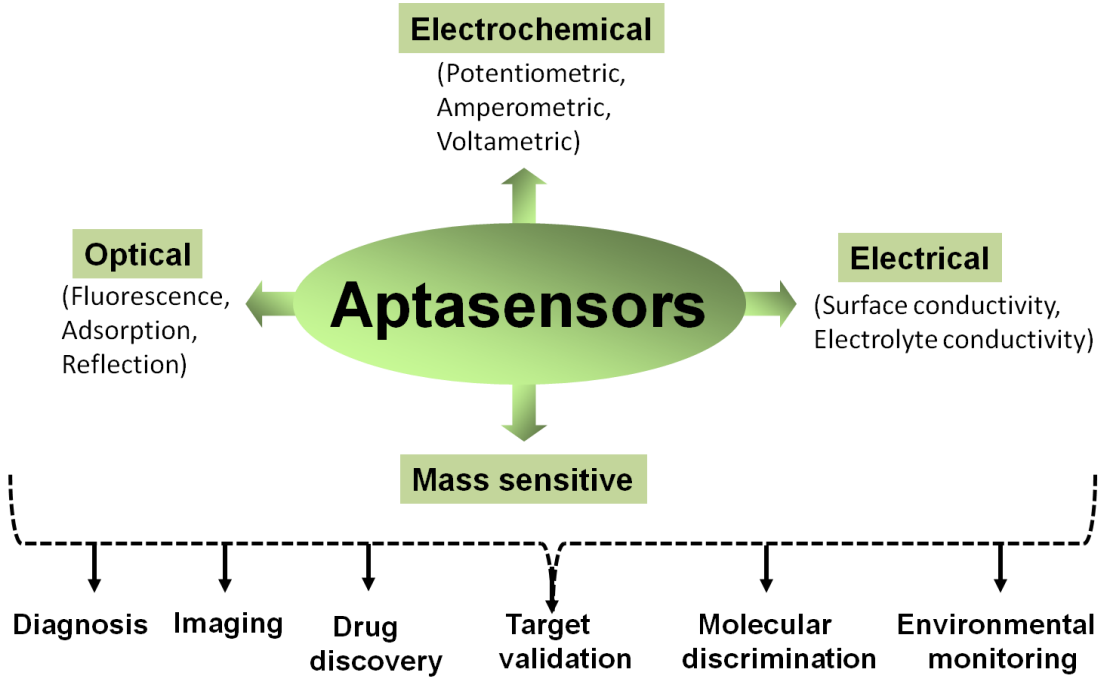

Figure 1.8. Classifications and applications of aptasensors. Each sensor has different advantages. The choice of sensor is based on the purpose.

Aptamers can fold into versatile structures because they have basic stem-loop arrangements that form proper three-dimensional structures, in order to facilitate the formation of a complex with the target molecule and influence the target's function. For molecules with higher affinity, the aptasensor can be used without involving any labeling stategy, whereas for low-affinity molecules or a low abundance of target molecules, labeling with chemical tags or metal nanoparticles have been performed for signal enhancement. Aptasensors include electrochemical, electrical, chemiluminescence, fluorescence, quantum dot-based, colorimetric, reflection-based mass spectroscopic detections,[13] play roles for several applications and are classified according to the detection mechanisms (Figure 1.8).

1.6. Targets for aptasensor development

Aptamer can be generated against any size of molecules irrespective of sizes and these targets can be ions, vitamins, peptides, proteins, whole cell. In the present study, to evaluate the aptamer and protein interactions in the presence of potential PEG-*b*-polymers, two kinds of clinically relevant samples, namely FIX of human blood coagulating system, intact influenza virus and a surface membrane protein (Hemagglutinin-HA) of influenza virus were chosen.

1.6.1. Importance of human clotting factor IX (FIX)

Blood coagulation process is a sequential interactive event that leads to the formation of a hemostatic plug following the injury and about 30 interacting proteins are involved in clotting process. Intrinsic and extrinsic are two pathways involved in the blood coagulation cascade. FIX is inactive unless activated by factor XIa in the intrinsic pathway or by factor VIIa and tissue factor complex in the extrinsic pathway. FIX has ability to interact with factors XIa, VIIIa, Va and factor VIIa/tissue factor complex and therefore, FIX is important in the overall coagulation process (Figure 1.9).[64,65] Anti-FIX is shown to reduce bleeding risks in animal models, as the better reagent than currently using anti-coagulant agent heparin.[66]

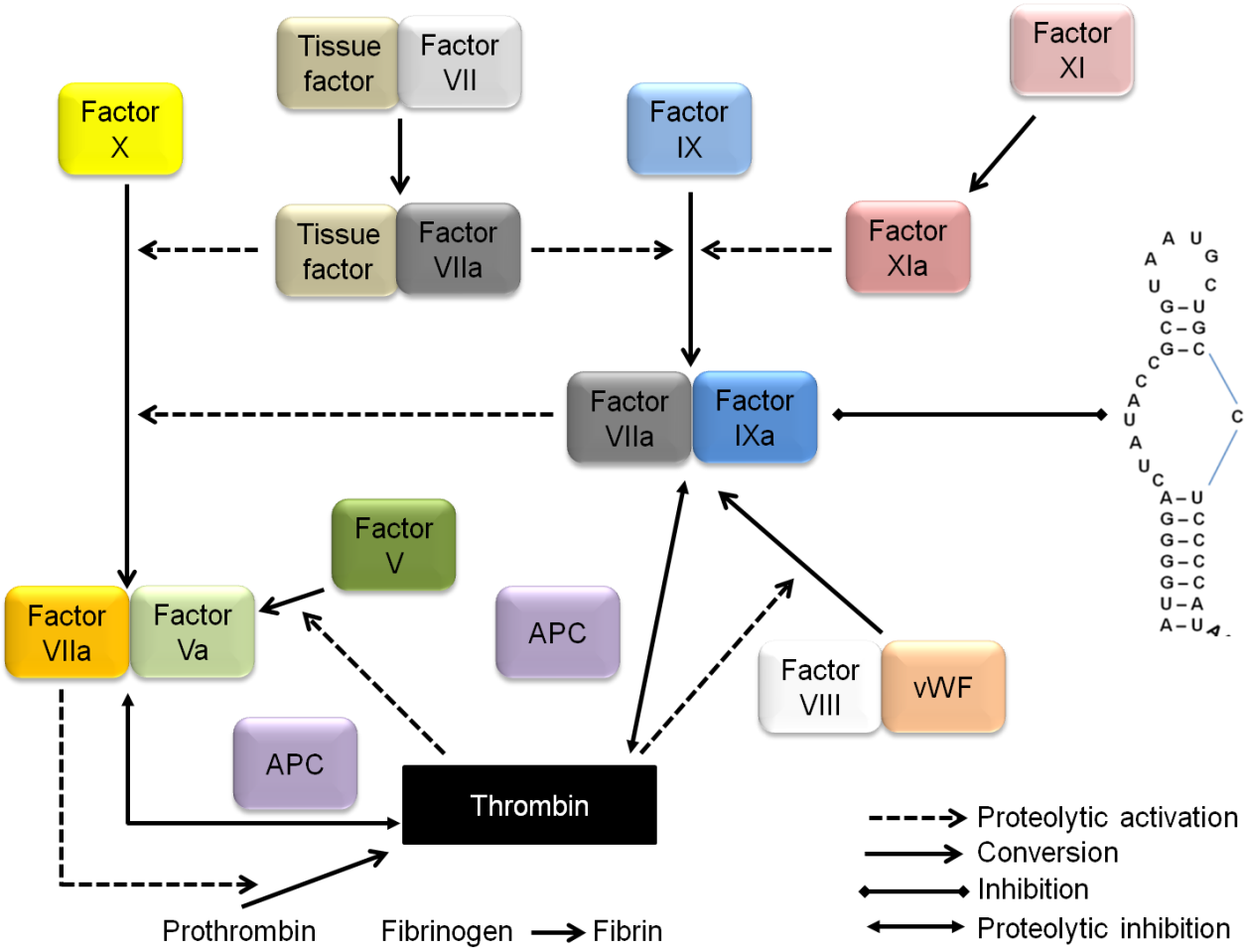

Figure 1.9. Human blood coagulating cascade. Different clotting factors are involved and linked through cleavages and convertions.[64]

Rusconi et al.[67] found a highly potent anti-coagulant aptamer against human FIXa which can prolong the coagulation of plasma from human and animal species under *in vitro* condition. Rusconi et al.[67] tested the effect of 2′-fluoropyrimidines modified stable anti-FIXa aptamer under *in vitro* and attached the PEG to the end of aptamer for *in vivo* analyses. In addition, since aptamer is targeted on FIXa, it can reduce the bleeding risks and required minimal dose. Based on their thorough analyses, they suggested that the anti-FIXa aptamer can block the cleavage of FX by the complex of FIXa-FVIIIa. Gopinath et al.[65] found that the selected anti-FIXa aptamer has ability to bind FIX as well. FIX is about 55 kDa and the amino acid sequence (Figure 1.10a; GenBank Accession number CAA01607) and crystal structure (Figure 1.10b; Protein Data Bank code: 1RFN) are available in the data bank.

Anti-FIXa aptamer was thoroughly analysed by both *in vitro* and *in vivo*, based on these studies, probably anti-FIX aptamer may bind to the vicinity of EGF1 and EGF2 domains.[65,67]

(a)

```
          10        20        30        40        50        60        70        80
    ....|....|....|....|....|....|....|....|....|....|....|....|....|....|....|....|
1   mimaespgliticllgyllsaectvfldhenankilnrpkrynsgkleefvqgnlerecmeekcsfeearevfentertt

          90        100       110       120       130       140       150       160
    ....|....|....|....|....|....|....|....|....|....|....|....|....|....|....|....|
81  efwkqyvdgdqcesnpclnggsckddinsyecwcpfgfegknceldvtcnikngtceqfcknsadnkvvcsctegyrlae

          170       180       190       200       210       220       230       240
    ....|....|....|....|....|....|....|....|....|....|....|....|....|....|....|....|
161 nqkscepavpfpcgrvsvsqtskltraeavfpdvdyvnsteaetildnitqstqsfndftrvvggedakpgqfpwqvvln

          250       260       270       280       290       300       310       320
    ....|....|....|....|....|....|....|....|....|....|....|....|....|....|....|....|
241 gkvdafcggsivnekwivtaahcvetgvkitvvagehnieeteht eqkrnviriiphhnynaainkynhdiallel depl

          330       340       350       360       370       380       390       400
    ....|....|....|....|....|....|....|....|....|....|....|....|....|....|....|....|
321 vlnsyvtpiciadkeytniflkfgsgyvsgwgrvfhkgrsalvlqylrvplvdratclrstkftiynnmfcaglhegard

          410       420       430       440       450
    ....|....|....|....|....|....|....|....|....|....|.
401 scqgdsggphvteve gtsfltgiiswgeecamkgkygiytkvsryvnwikektklt
```

(b)

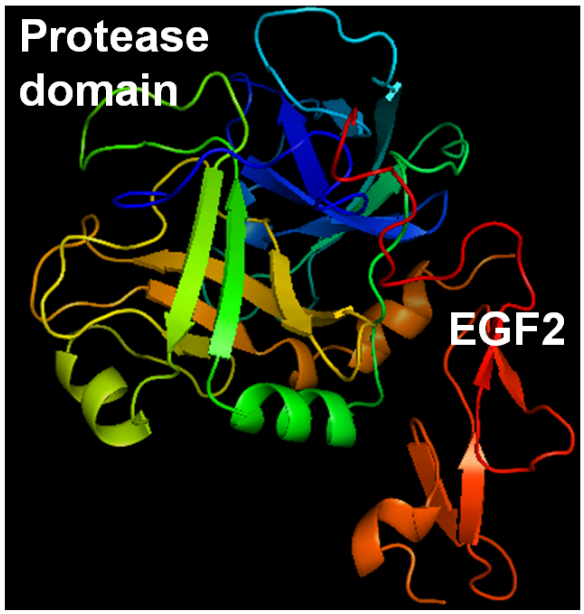

Figure 1.10. Factor IX from human blood coagulating cascade. Amino acid sequence (a) and crystal structure (b) are displayed.

1.6.2. Influenza Virus

Influenza viruses cause severe illness and infect mainly the upper respiratory tract regions such as nose, throat, bronchi and lungs. Influenza viruses has the diameter of about 80-120 nm and they are spherical or filamentous and enveloped.[68] There are three major classess of influenza viruses namely, influenza A, B, and C. Influenza A is quite common, circulated among bird and mammalian, whereas influenza B is mainly found in human. Influenza C is less common may cause both illness and local epidemics. These influenza viruses, especially influenza A caused severe death to the human population and posed several issues to human health and economy. In the past several decades, pandemic influenza emerged several times, the pandemic of 1918 with H1N1 swine flu had a huge impact caused the death rate to several millions worldwide. For influenza infection, two major surface proteins glycoproteins HA and neuraminidase (NA) are play an important role. Based on these proteins influenza A virus is classified according to their H number (for HA; 17 HA reported) or N number (for NA; 10 NA reported). There are two antigenic and genetic lineages of influenza B viruses, namely Yamagata and Victoria lineages. Several new influenza strains are emerging continuously, H1N1 viral strain (pdm/2009) is the recently emerged and pandemic among humans a so called “swine flu”. Other important subtype H5N1 from Influenza A virus is known as “bird flu”, which cause illness mainly in birds. With poultry, mainly two subtypes such as H5 and H7 highly pathogenic, leads to 100% mortality. Recent epidemiological evidence with the transmission of virulent new avian influenza A H7N9 was first reported in China by the World Health Organization on April 1, 2013. The antigens, HA and NA on the virus are the dominant target for the host antibody response. However, minor mutations in the amino acid sequences on these surface antigens occur frequently and this enables the viruses to evade the host immune system. Continuation in this mutation process is called ‘antigenic drift’ which makes the yearly update and administration of influenza vaccines. HA is the major viral antigen for influenza infection required for membrane fusion with host cells to mediate at the early stages of influenza infection (Figure 1.11a,b).[69]

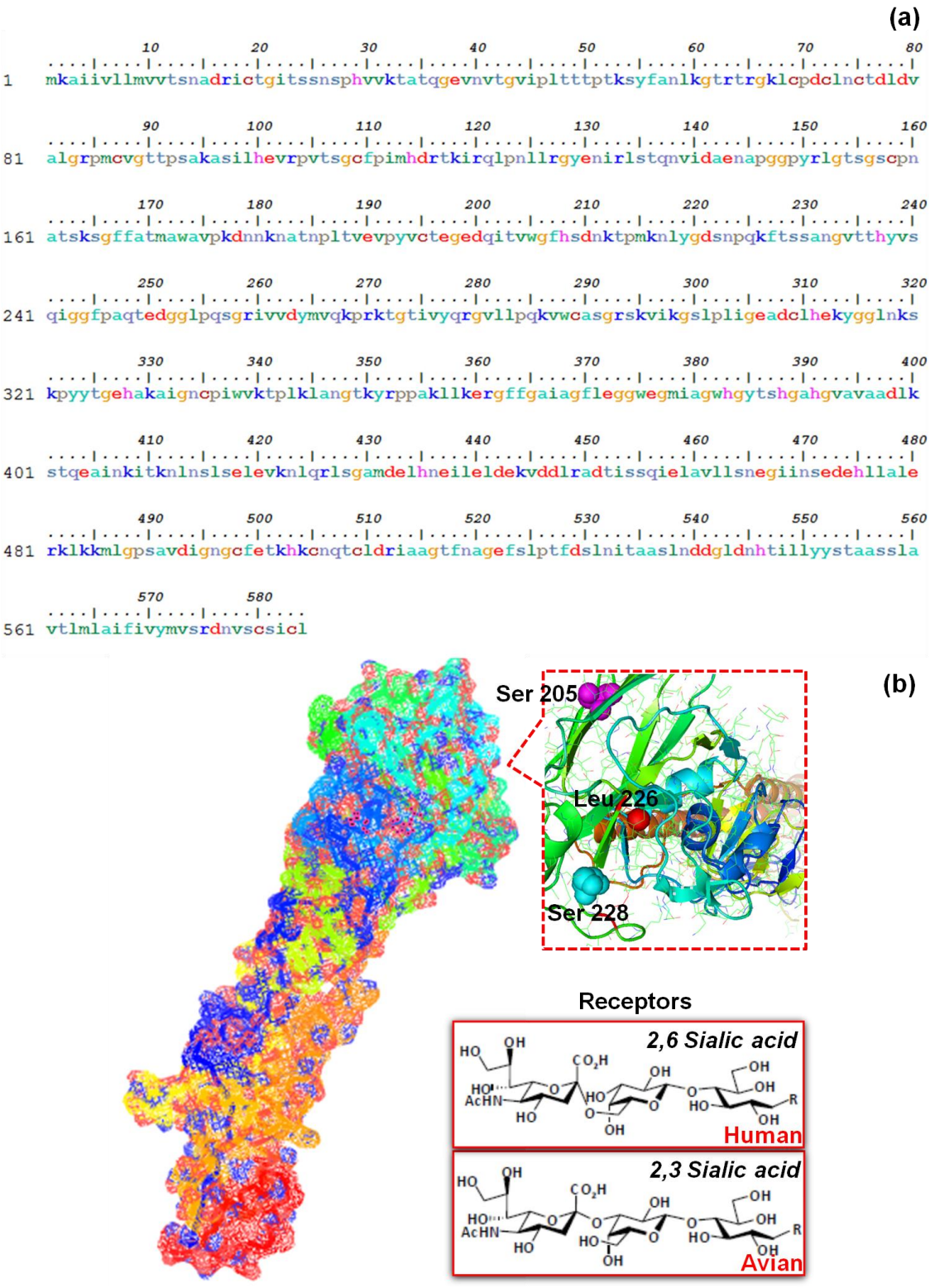

Figure 1.11. Hemagglutinin from influenza virus. Amino acid sequence (a) and crystal structure (b) are displayed. Structures of glycans from human and avian involved as the receptors for HA are shown.

During initial infection of influenza virus to the host cell, HA binds to sialic acid residues (glycans) namely Neu5Acα2,6Gal and Neu5Acα2,3Gal on human and bird cells, respectively, with the assistance of three important amino acids (Figure 1.11a). HA is a trimeric protein of about 72 kDa, the amino acid sequence (Figure 1.11a; GenBank Accession number ACF54180) and crystal structure (Figure 1.11b; Protein Data Bank code: 2VIU) are available in the data bank.

1.7. Aptasensors demonstrated in the present study

With the assistance of aforementioned three types of PEG-*b*-polymers, high-performance aptasensors were developed in this study, by analyzing aptamer-FIX or aptamer-influenza virus interactions. These sensing systems include, Evanescent-field-coupled Waveguide-mode (EFC-WM), Surface Plasmon Resonance (SPR) and Surface Plasmon Fluorescence Spectroscopy (SPFS) (Figure 1.12).

Figure 1.12. Sensing systems preferred to demonstrate the applications of PEG-*b*-polymers. All these sensors are operates based on the principle of Kretschmann configuration.

1.7.1. Evanescent-field-coupled Waveguide-mode (EFC-WM) sensor

The term "waveguide" is widely referred to as a structure capable to confine and guide electromagnetic waves.[70] The state where the light is propagating while maintaining such light intensity distribution is called the waveguide-mode. Waveguide-mode sensor is designed with Kretschmann configuration, in which modifications in the dielectric environment near the waveguide-mode sensor surfaces are detected with a high sensitivity by measuring changes in reflectivity. The

basic calculation for designing waveguide mode sensor was described[70]. The effective refractive index (N= K_x/K; K_x-progation constant) of a waveguide mode was given by the relation

$$N = [(n_C)^{-2} + (\varepsilon'_M{}^{-1}]^{-1/2}$$

Where, ε_M - dielectic constant at the metal; C-dielectic sample medium. In this configuration, the substrate is attached to a dielectric prism, and excitation light is used to irradiate the substrate through the prism at an appropriate incident angle.[71] The first waveguide was with an optical system utilizes silicon oxide-titranium oxide.[72] Planar and fiber optical waveguides are the general classes, based on the dimensions and light-guiding properties. These two waveguides are further subdivided into single-mode (only one light mode will be guided) and multimode (will allow several modes).[73] The fabrication of waveguides was done by chemical vaporation methods and categorized as, the modification of substrate materials[74] (by ion exchange in SiO_2 or $LiNbO_3$) and a waveguide layer is applied on top of a substrate material (usually with metal oxides or nitride).[75] The typical materials for waveguide-mode sensors are SiO_2, SiO_xN_y, Si_3N_4, TiO_2, Ta_2O_5 and Nb_2O_5.[73] By utilizing a compact optical system of SPR sensors as a spectral readout, the EFC-WM sensor was reported.[76] Evanescent field refers, when light is reflected, it penetrates into the medium that is reflecting the light. Under total reflection condition, light penetrates into the medium with low refractive index to about one wavelength. In the waveguide-mode sensor device any kind of solid material that reflects light and optically isolates the waveguide from the substrate can be used as the reflecting layer.

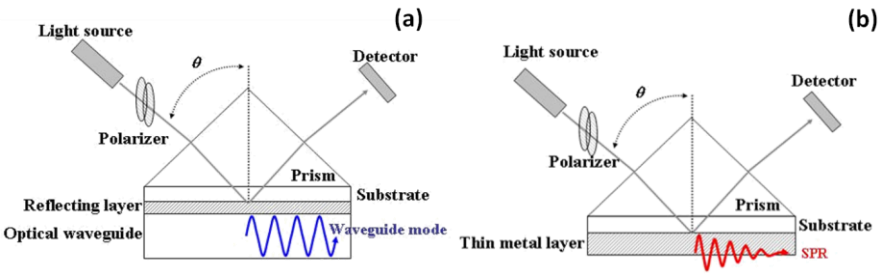

Figure 1.13. Sensing set-up of sensors. (a) waveguide mode and (b) Surface Plasmon Resonance mode. Even though, the basic operating principles are same, both mode of sensor have different advantages.

The light from the lamp was guided to a collimator lens; and the collimated light radiated into a prism, coupling of prism in a waveguide-mode sensor is a simple and the light is coupled into the waveguide through the prism mounted on the waveguide-mode sensor surface and the angle of this coupling depending on the refractive index of the waveguide,[73] where the incident angle was parallel to the bottom face of the prism. As reported before, the prism can be made of SiO_2 glass, and with the appropriate bottom angle. Waveguide mode sensors are differing from the SPR-based sensors by the propagation of light on the sensing surface (Figure 1.13).

1.7.2. Surface Plasmon Resonance (SPR) sensor

A SPR-based aptasensor is one of the predominantly established sensors to analyze different aptamer-ligand interactions as a lable-free sensing system.[77] SPR-based devises rely on optical method to measure the refractive index near a sensor surface. SPR is known as the excitation of surface plasmon by monochromatic, electromagnetic waves and the polarized light at an interface between prism and metal coated surface surrounded by biological component and liquid environment. This event relies on the change of optical parameters, derived from the alteration of the layer closest to the sensitive surface in measuring the refractive index. Absorption of molecule on the receptor layer of biosensor changes the refractive index of the layer, reporting the event of binding, detectable and quantifiable in label free approach. The surface plasmons have a penetration on the substrate to a few hundred nanometers, causes the variations in the signal obtained in concomitant with spectral changes indicate that the biomolecular interactions occurred at the interface.[78] Several SPR based biosensors were developed in a wide range of fields including biology, biomedicine and biochemistry. SPR devices are based on the attenuated total reflection and categorized as conventional SPR, long-range SPR, coupled plasmon-waveguide resonance and waveguide-coupled SPR. Even though, all these biosensors are dependent on SPR mode, their utilities are based on the exploitation in biomolecular analysis with higher specificity and sensitivity.[79]

SPR biosensor is a preferred system of measuring different biochemical recognitions, including protein-peptide,[80] protein-DNA,[81] RNA-protein,[82] cell-ligand,[83] DNA hybridization,[84] protein-protein,[85] protein-lipid,[86] and assay developments,[87] with real-time monitoring of complexes. Exhaustive surveys on SPR biosensor were carried out by Myszka and his colleague.[88,89] Different SPR-based sensors are available depending on the placement of measurement chip, surface priming, composition of buffers, immobilization procedures and so on. The development of mobile, compact, and cost-effective sensing devices with potential for field applications were made possible with miniaturized SPR sensors, using the attenuated total reflection method as an alternative to laboratory-based SPR systems.[90] A fiber optic SPR probe with wavelength interrogation was proposed and this sensor has a multimode optical fiber with locally exposed core and a thin Au film.[91] A conventional prism coupled with a rectangular thin glass substrate with SPR active metal layer was described.[92] Even though, several SPR based sensing systems have been developed in the past, SPR-based biacore system became more popular and routinely in use by several researchers,[88,89] in the present study, experiments were performed using Biacore 3000.

Biacore technology is an automated optical based system was created by a Sweden company founded in 1984 and this analytical system was launched in 1990 for biomolecular interactions and expanded by introducing three systems, namely BIAlite, Biacore 1000 and Biacore 3000. Recently, Biacore T100 system was released and it is suitable for high-throughput screening against different ligands by single assay set-up with higher sensitive advanced features (www.biacore.com and http://en.wikipedia.org). Biacore detects refractive index changes in close proximity to a metal surface.[93] Upon immobilization of ligands on the sensor's surface the interfacial refractive index is altered, which will be detected and quantified by optical system as the changes in the angle of reflectance.[94] Using biacore monitoring weak macromolecular interactions are possible that are not achieved by other sensors. Biacore is suitable for analyses of wide range of bio-molecules in real-time fashion as the label-free sensor and detected the lower concentrations.[95]

Various sensor chip-formats are constructed by either pre-immobilized ligands or modified by standard surface chemistries, to capture biomolecules. Biacore system has advantages, such as preparation of bio-specific surface, analyses of kinetic constants, measurements of analytes' concentrations and regeneration of the sensing surface for repeated use. Most commonly used sensing surface is carboxymethyl-dextran material linked on Au surface to immobilize. Using Biacore, an assay was developed by using anti-IgE DNA aptamer, with a detection limit of 2 nM.[96] On the other hand, Tombelli et al. (2005) demonstrated that Human immunodeficiency virus-1 (HIV-1) Tat protein was specifically captured by RNA aptamer, with a linear range of detection from 0 to 2.5 ppm. In addition to these common advantages, biacore system is also versatile for various purposes including high-sensitive high-throughput analyses.

1.7.3. Surface Plasmon Fluorescence Spectroscopy (SPFS)

Some of the designed aptasensor strategies are associated with fluorescence-tagged, by availing signaling by a single fluorophore, fluorophore-quencher pair, structure-switching, and fluorogenic reaction.[97] The fluorescence labeling of an aptamer at its end can be done using fluorescent tags. Fluorescence-based assays generated for thrombin binding aptamers were summarized and shown the detection limit of sub-picomolar levels.[97,98] SPFS is one of the sensors can be measured the interactions of fluorescent molecules, was implemented first in 1991, with a SPR based fluoroimmunoassay for Human Chorionic Gonadotrophin (HCG) and attained the limit of detection to <240 pM HCG in serum.[100] Later, SPFS was potentially re-established by Liebermann, and Knoll[101] with the setup based on angular modulation of SPR is combined with fluorescence spectroscopy detection for the quantitative and *in situ* discrimination of single-nucleotide mismatches in oligonucleotide double strands. SPFS is based on ehhanced electromagnetic field of a surface plasmon for the excitation of surface-confined fluorophores. Upon interaction of biomolecules the interfacial index changes and the fluorescence signals in real time fashion gives an output signal. The slight angular displacement between the minimum angle in the reflectivity scan and the

fluorescence intensity peak position is a consequence of the resonant excitation of the surface plasmon waves interfering with the directly reflected laser beam: the re-radiated and out-coupled plasmon light destructively interferes with the plane wave of the laser reflected at the prism/metal interface provided their relative phase shift corresponds to π or 180º.[102] The fluorescence signal occurs upon the resonant coupling to surface plasmons can be measured as a function of time, enables the monitoring kinetics of biomolecular reactions. The implementation of SPFS to SPR biosensors found to increase the sensitivity by several orders of magnitude and overviewed in detail.[103] Like waveguide and SPR, in most cases, the Kretschmann configuration will be the coupling scheme of choice for SPFS because the evanescent character of the surface wave being excited from the back of the prism. The alternative scheme for surface plasmon excitation by laser light based on a surface grating structure offers a number of advantages for biosensing in general and for SPFS. The strategies generated based on the SPFS are grating coupling for SPFS, long-range surface plasmons for SPFS, fluorescence imaging and color multiplexing and so on.[104] The SPFS is equivalently widespread as immunosensor for analyzing antigen and antibody interactions on the sensor surface[104]. It was elucidated novel applications of SPFS in monitoring multicomponent adsorption from the aqueous phase, using simultaneous information from SPR and fluorescence.[105]

The major challenges, especially in the bioscientific field are to elucidate the functions of biologically relevant molecules. Hence, developing effective bio-recognition sensors are mandatory for monitoring biomolecular interactions in real time fashion. Several successes have been reported in the past using different sensing systems owing to its convenience for the analyses of chemical and biological compounds. The applications of this sensor development include, medical diagnostics, environmental monitoring, food safety and security as reviewed before (Homola, 2008). Keeping all these facts discussed above, the present study was launched for the application of PEG-*b*-polymers on different sensing surfaces as described below with the chapters 2,3 and 4.

Chapter 2*: High-performance Evanescent-field-coupled Waveguide-mode biosensor for detection of Factor IX uses PEG-b-PAAc on SiO_2 surface and N6-PEG on Gold Nanoparticle.*

Chapter 3*: Co-immobilization of PEG-b-PAMA and N6-PEG promotes non-biofouling on Au surface of Surface Plasmon Resonance biosensor for detection of FIX in human plasma.*

Chapter 4*: Generation of anti-influenza aptamers for sensing applications on PEG-b-PAAc/fluorescent hybridized surface of Surface Plasmon Fluorescence Spectroscopy.*

1.8. References

1. Li, Y., Schluesener, H.J., Xu, S., *Gold Bulletin* **2010**, 43, 29-41.
2. Lim, Z., Li, J., Ng, C., Yung, L.L., Bay, B., *Acta Pharmacol. Sinica* **2011**, 32,983-990.
3. Upadhyayula, V.K.. *Anal. Chim. Acta* **2012**, 715, 1-18.
4. Guirgis, B.S., Sá E Cunha, C., Gomes, I., Cavadas, M., Silva, I., Doria, G., Blatch, G.L., Baptista, P.V., Pereria, E., Azzazy, H.M., Mota, M.M., Prudencio, M., Franco, R., *Anal. Bioanal. Chem.* **2012**, 402,1019-1027.
5. Nagel, J., Chunsod, P., Zimmerer, C., Simon, F., Janke, A., Heinrich, G., *Mater. Chem. Phys.* **2011**, 129, 599-604.
6. Tinguely, J., Sow, I., Leiner, C., Grand, J., Hohenau, A., Felidj, N., *BioNanoSci.* **2011**, 1, 128-135.
7. Baldrich, E., Restrepo, A., O'Sullivan, C.K., *Anal. Chem.* **2004**, 76, 7053–7063.
8. Guo, P., *J. Nanosci. Nanotechnol*. **2005**, 5,1964-1982.
9. Odenthal, K.J., Gooding, J., *Analyst* **2007**, 132, 603-610.
10. Wang, X., Zhao, M., Nolte, D.D., *Appl. Opt.* **2008**, 47, 2779-2789.
11. Song, S., Wang, L., Li, J., Zhao, J., Fan, C., *Trends Anal. Chem.* **2008**, 27,108-117.
12. Giljohann, D.A., Seferos, D.S., Daniel, W.L., Massich, M.D., Patel, P.C., Mirkin, C.A., *Angew. Chem. Int. Ed.* **2010**, 49, 3280-3294.
13. Iliuk, A.B.; Hu, L.; Tao, A.W., *Anal. Chem.* **2011**, 83, 4440–4452.
14. Zanoli, L.M., D'Agata, R., Spoto, G., *Anal. Bioanal. Chem.* **2012**, 402, 1759-1771.
15. Kumar, P., Choithani, J., Gupta, K.C., *Nucleic Acids Res.* **2004**, 32, e80.
16. Rong, G., Najmaie, A., Sipe, J.E., Weiss, S.M., *Biosens. Bioelectron.* **2008**, 23, 1572-1576.
17. Gonçalves, D., Prazeres, D.M.F., Chu, V., Conde, J.P., *Biosens. Bioelectron.* **2008**, 24, 545-551.

18. Sabate, J., Anderson, M.A., Kikkawa, H., Xu, Q., Cervera-March, S., Hill, C.G. Jr., *J. Catal.* **1992**, 134, 36-46.
19. Jing, M., Bowser, M.T., *Anal. Chim. Acta* **2011**, 686, 9–18.
20. Nagasaki, Y. *Poly. J.* **2011**, 43, 949-958.
21. Hermanson, G.T., Bioconjugate Techniques 2nd Edn. Academic Press, Waltham. **2008**.
22. Nagasaki, Y., Kobayashi, H., Katsuyama, Y., Jomura, T., Sakura, T., *J. Colloid Interface Sci.* **2007**, 309, 524-530.
23. Nagasaki, Y., *Chem. Lett.* **2008**, 37, 564-569.
24. Trubetskoy, V.S., *Adv. Drug Deliv. Rev.* **1999**, 37, 81-88.
25. Otsuka, H., Nagasaki, Y., Kataoka, K., *Adv. Drug Deliv. Rev.* **2003**, 55, 403-419.
26. Bailey, F.E.J.V.K., Alkylene oxides and their polymer. Marcel Dekker Inc., New York, **1990**.
27. Oishi, M., Sasaki, S., Nagasaki, Y., Kataoka, K., *Biomacromolecules* **2003**, 4, 1426-1432.
28. Oishi, M., Nagasaki, Y., Itaka, K., Nishiyama, N., Kataoka, K., *J. Am. Chem. Soc.* **2005**, 127, 1624-1625.
29. Oishi, M., Ikeo, S., Nagasaki, Y., *Poly. J.* **2007**, 39, 239-244.
30. Hemmer, E., Venkatachalam, N., Hyodo, H., Soga, K., *Adv. Mater. Sci. Eng.* **2012**, 2012, Article ID 748098, 15 pages.
31. Kakizawa, Y., Miyata, K., Furukawa, S., Kataoka, K., *Adv. Mater.* **2004**, 16, 699-702.
32. Iijima, M., Nagasaki, Y., *J. Polym. Sci.* **2006**, A44, 1457.
33. Oishi, M., Kataoka, K., Nagasaki, Y., *Bioconjugate Chem*. **2006**, 17, 677-688.
34. Kanayama, N., Fukushima, S., Nishiyama, N., Itaka, Jang, W.-D., Miyata, K., Yamasaki, Y., Chung, U., Kataoka, K., *ChemMedChem.* **2006**, 1, 439-444.
35. Yuan, X., Yoshimoto K., Nagasaki, Y., *Anal. Chem*. **2009**, 81,1549-1556.
36. Uchida, K., Hoshino, Y., Tamura, A., Yoshimoto, K., Kojima, S., Yamashita, K., Yamanaka, I., Otsuka, H., Kataoka, K., Nagasaki, Y., Biointerphases **2007**, 2, 126-130.
37. Malmsten, M., Emoto, K., Van Alstine, J.M., J*. Colloid Interface Sci.* **1998**, 202, 507-517.
38. Otsuka, H., Nagasaki, Y., Kataoka, K., *Langmuir* **2004**, 20, 11285-11287.
39. Satomi, T., Nagasaki, Y., Kobayashi, H., Otsuka, H., Kataoka, K., *Langmuir* **2007**, 23, 6698-6703.
40. Kamimura, M., Miyamoto, D., Saito, Y., Soga, K., Nagasaki, Y., *Langmuir* **2008**, 24, 8864-8870.
41. Yi, G.-S., Chow, G.-M., *Chem. Mater.* **2007**, 19, 341-343.
42. Hemmer, E., Yamanao, T., Kishimoto, H., Soga, K., In: IEEE Explore, proceedings of the international conference on nanoscience and nanotechnology (ICONN), Sydney, Australia, **2010**, p. 225–229.

43. Hemmer E, Takeshita, H., Yamanao T, Fujiki, T., Kohl, Y., Löw, K., Venkatachalam, N., Hyodo, H., Kishimoto, H., Soga, K., *J. Mater Sci: Mater. Med.* **2012**, 23, 2399–2412.
44. Lakshmipriya, T., Fujimaki, M., Gopinath, S.C.B., Awazu, K., Horiguchi, Y., Nagasaki, Y., *Analyst* **2013**, 138, 2863-2870.
45. Furusho, H., Kitano, K., Hamaguchi, S., Nagasaki, Y., *Chem. Mater.* **2009**, 21, 3526–3535.
46. Pong, B.- K., Lee, J.- Y., Trout, B. L., *Langmuir* **2005**, 21, 11599-11603.
47. Miyamoto, D., Oishi, M., Kojima, K., Yoshimoto K., Nagasaki, Y. *Langmuir* **2008**, 24, 5010-5017.
48. Yoshimoto, K., Matsumoto, S., Asakawa, R., Uchida, K., Nagasaki, Y., *Chem. Lett.* **2007**, 36, 1444–1445.
49. Horiguchi, Y., Miyachi, S., Nagasaki, Y., Langmuir **2013**, 29, 7369-7376.
50. Oishi, M., Nakaogami, J., Ishii, T., Nagasaki, Y., *Chem. Lett.* 2006, 35, 1046-1047.
51. Yoshimoto, K., Nozawa, M., Matsumoto, S., Echigo, T., Nemoto, S., Hatta T., Nagasaki, Y., *Langmuir* **2009**, 25, 12243-12249.
52. Spiegelman, S., Haruna, I., Holland, I.B., Beaudreau, G., Mills, D., *Proc. Natl. Acad. Sci.* USA. **1965**, 54, 919-927.
53. Breaker, R.R., *Mol. Cell* **2011**, 43, 867-879.
54. Ellington, A.D., Szostak, J.W., *Nature* **1990**, 346, 818–822.
55. Tuerk, C., Gold, L., *Science* **1990**, 249, 505–510.
56. Robertson, D.L., Joyce, G.F., *Nature* **1990**, 344, 467–468.
57. Williamson, J.R. *Nat. Struct. Biol.* **2000**, 7, 834-837.
58. Tombelli, S., Minunni, M., Luzi, E., Mascini, M., *Bioelectrochem.* **2005**, 67, 135-141.
59. Ng, E.W.M., Shima, D.T., Calias, P., Cunningham, E.T., Jr., Guyer, D.R., Adamis, A.P., *Nat. Rev.* **2006**, 5, 123–132.
60. Jenison, R.D., Gill, S.C., Pardi, A., Polisky, B., *Science* **1994**, 263, 1425–1429.
61. Geiger, A., Burgstaller, P., Eltz, H.V., Roeder, A., Famulok, M., *Nucleic Acids Res.* **1996**, 24, 1029–1036.
62. Gopinath, S.C.B., Shikamoto, Y., Mizuno, H., Kumar, P.K.R., *Thromb. Haemost.* **2006**, 95, 767–771.
63. Gopinath, S.C.B., Misono, T., Kawasaki, K., Mizuno, T., Imai, M., Odagiri, T., Kumar, P.K.R., *J. Gen. Virol.* **2006**, 87, 479–487.
64. Tuddenham, E., *Nature* **2002**, 419, 23-24.
65. Gopinath, S.C.B., Balasundaresan, D., Akitomi, J., Mizuno, H., J. Biochem. **2006**, 140, 667–676.
66. Rusconi, C.P., Roberts, J.D., Pitoc, G.A., Nimjee, S.M., White, R.R., Quick, G., *Nat. Biotechnol.* **2004**, 22, 1423–1428.

67. Rusconi, C.P., Scardino, E., Layzer, J., Pitoc, G.A., Ortel, T.L., Monroe, D., *Nature* **2002**, 419, 90–94.
68. Noda, T., Sagara, H., Yen, A., Takada, A., Kida, H., Cheng, H., Kawaoka, Y. *Nature* **2006**, 439, 490.
69. Skehel, J.J., Wiley, D.C., *Annu. Rev. Biochem.* **2000**, 69, 531-569.
70. Lukosz, W., Tiefenthaler, K., *Sens. Actuators, B: Chem.* **1995**, 29, 37-50.
71. Kretschmann, E., *Z. Phys.* **1971**, 241, 313-324.
72. Lukosz, W., *Biosens. Bioelectron.* **1991**, 6, 215-225.
73. Schmitt, K., Hoffmann, C., Eds. Zourob, M. & Lakhtakia, A., Optical Guided-wave Chemical and Biosensors I, Springer Series on Chemical Sensors and Biosensors 7, Springer-Verlag, Berlin Heidelberg, **2010**, 21.
74. Hu, H., Lu, F., Chen, F., Shi, B-R., Wang, K-M., Shen, D-Y., *J. Appl. Phys.* **2001**, 89, 5224-5226.
75. Gorecki, C., *Opt. Lasers Eng.* **2000**, 33, 15-20.
76. Fujimaki, M., Nomura, K., Sato, K., Kato, T., Gopinath, S.C.B., Wang, X., Awazu, K., Ohki, Y., *Opt. Exp.* **2010**, 18, 15732–15740.
77. Tombelli, S., Minunni, M., Mascini, M., *Methods Mol. Biol.* **2008**, 419, 109–119.
78. Chien, F.C. Chen, S.J., *Opt. Lett.* **2006**, 31, 187-189.
79. Chien, F.C. Chen, S.J., *Biosens. Bioelectron.* **2004**, 20, 633-642.
80. Shliom, O., Huang, M., Sachais, B., Kuo, A., Weisel, J.W., Nagaswami, C., Nassar, T., Bdeir, K., Hiss, E., Gawlak, S., Harris, S., Mazar, A., Higazi, A.A., *J. Biol. Chem.* **2000**, 275, 24304–24312.
81. Majka, J., Speck, C., *Adv. Biochem. Engin/Biotechnol.* **2007**, 104, 13-36.
82. Katsamba, P.S., Park, S., Laird-Offringa, I.A., *Methods* **2002**, 26, 95–104.
83. Quinn, J.G. O'Neill, S. Doyle, A. McAtamney, C. Diamond, D. MacCraith, B.D. O'Kennedy, R. *Anal. Biochem.* **2000**, 281, 135–143.
84. Peterson, A.W., Wolf, L.K., Georgiadis, R.M., *J. Am. Chem. Soc.* **2002**,124, 14601-14607.
85. Gopinath, S.C.B. *Anal. Bioanal. Chem.* **2007**, 387, 171–182.
86. Gopinath, S.C.B., Shikamoto, Y., Mizuno, H., Kumar, P.K.R., *Biochemical J.* **2007**, 405, 351-357.
87. Mazumdar, S.D., Barlen, B., Kämpfer, P., Keusgen, M., *Biosens. Bioelectron.* **2010**, 25, 967-971.
88. Rich, R.L. Myszka, D.G., *J. Mol. Recognit.* **2008**, 21, 355-400.
89. Rich, R.L. Myszka, D.G., *J. Mol. Recognit.* **2011**, 24, 892-914.
90. Vidal, M.M.B., Lopez, R., Aleggret, S., Alonso-Chamarro, J., Garces, I., Mateo, *J., Sens. Actuators B* **1993**, 11 455-459.
91. Ronot-Trioli, C., Trouillet, A., Veillas, C., Gagnaire, H., *Sens. Actuators A Phys.* **1996**, 54, 589-593.

92. Homola, J., *Chem. Rev.* **2008**, 108, 462-493.
93. Chatelier, R.C., Gengenback, T.R., Griesser, H.J., Brigham-Burke, M., O'Shannessy, D.J., *Anal. Biochem.* **1995**, 229, 112-118.
94. Stenberg, E., Persson, B., Roos, H., Urbaniczky, C., *J. Colloid Sci.* **1991**, 143, 513-526.
95. Berggård, T., Linse, S., James, P., *Proteomics* **2007**, 7, 2833-2842.
96. Wang, Z., Wilkop, T., Xu, D., Dong, Y., Ma, G., Cheng, Q., *Anal. Bioanal. Chem.,* **2007**, 389, 819-825.
97. Mok, W., Li, Y., *Sensors* **2008**, 8, 7050–7084.
98. Baldrich, E., Restrepo, A., O'Sullivan, C.K., *Anal. Chem.* **2004**, 76, 7053–7063.
99. Citartan, M., Gopinath, S.C.B., Tominaga, J., Tan, S.C., Tang, T.H., *Biosens. Bioelectron.* **2012**, 34, 1-11.
100. Attridge, J. W., Daniels, P. B., Deacon, J. K., Robinson, G. A., Davidson, G. P., *Biosens. Bioelectron.* **1991**, 6, 201-214.
101. Liebermann, T., Knoll, W., *Colloid Surf. A.* **2000**, 171, 115–130.
102. Yu, F., Yao, D., Knoll, W., *Anal. Chem.* **2003,** 75, 2610-2617.
103. Dostaleka, J., Knoll, W., *Biointerphases* **2008**, 3, FD12-FD-22.
104. Knoll, W., Kasry, A., Liu, J., Neumann, T., Niu, L., Park, H., Paulsen, H., Robeleck, R., Yao, D., Yu, F., In. Handbook of Surface Plasmon Resonance, Eds. Schasfoort, R.B.M., Tudos, A.J. The Royal Society of Chemistry, Cambridge, UK., **2008**, p 275-312.
105. Roy, S., Kim, J., Kellis, J. T., Jr, Poulose, A. J., Robertson, C. R., Gast, A. P., *Langmuir* **2002**, 18, 6319-6323.

Chapter 2

High-Performance Evanescent-field-coupled Waveguide-mode Biosensor for Detection of Factor IX Uses PEG-b-PAAc on SiO_2 Surface and N6-PEG on Gold Nanoparticle

2.1. Abstract

An evanescent-field–coupled waveguide-mode (EFC-WM) sensor utilizes monolithic SiO_2/Si/SiO_2 sensing plates having a multilayer structure and is used to evaluate a blocking agent comprising poly(ethylene glycol)-based block copolymers (PEG-*b*-polymer). Factor IX (FIX) protein was detected using its aptamer, viz., FIX was immobilized on a glutaraldehyde (Glu)-modified silica surface, and then treated with a biotinylated aptamer. The quantitative analysis of FIX was carried out using streptavidin-conjugated gold nanoparticles (SA-GNPs). The blocking polymer, poly(ethylene glycol)-*b*-poly(acrylic acid) (PEG-*b*-PAAc), was found to mask unreacted amine and Glu moieties on the SiO_2 surface, and it completely prevented the non-specific binding of SA-GNPs. By exploiting the strong blocking effect of PEG-*b*-PAAc, the author achieved high ligand–analyte interaction sensitivity (sensitive down to 100 pM). To improve the sensitivity further, the author also used pentaethylenehexamine-terminated PEG (N6-PEG) on gold nanoparticle (GNP). The improvement in sensitivity was found to be 1000-fold (to 100 fM), which was substantiated by the observation of higher number of GNPs on the sensing surface in the results of scanning electron microscopic examination. Based on the competition assay of free biotin premixed with SA-GNPs, it was concluded that some active biotin-binding sites on the streptavidin were blocked by N6-PEG, which improved the binding ability to the biotinylated sensing surface. An optimum number of binding sites on the SA-GNPs might improve their binding affinity. The strategy shown with dual polymers, viz., blocking of the sensor chip surface and coating of SA-GNPs, is recommended for developing sensors with higher sensitivity and reliability. Selective binding of the aptamer to a very small amount of FIX in the mixed sample containing FXIa and FVIIa, or albumin, makes this the optimal strategy for detecting a FIX deficiency in human blood samples.

2.2. Introduction

The development of nanobiosensors that may be used to analyze biomolecular recognition

elements is currently one of the most important targets in the field of medical diagnosis. A useful biosensing system requires some key characteristics such as specificity and sensitivity. It can be accomplished by the correct orientation of the immobilized biomolecules in order to expose to receive the analyte on the sensing surface.[1] Natural polymers are used in several instances to suppress the non-specific interaction of ligand and analyte.[2] However, the efficiency of the natural polymers (albumin, casein, and dextran) are not completely satisfactory. Natural polymers derived from animals may contain disease-causing components. The blocking performance of natural polymer is different between the lots. Synthetic polymers, by contrast, are easily reproducible and contain no contagions. Thus, high-performance surface modification techniques using synthetic polymers are highly anticipated. With synthetic PEG tethered-chain surface, there were demonstration for high-performance sensing and it shows high resistance to biofouling.[3-11] For effective immobilization of PEG-derivatives on substrate surfaces, suitable anchoring strategies must be designed using specific interactions such as hydrophobic or electrostatic interactions or covalent conjugation. PEG-*b*-polycations, PEG-*b*-polyanions, and PEG-b-hydrophobic polymers are the versatile materials, can be used on different sensing surface and a typical example is the application of PEG-*b*-PAAc on Y_2O_3 nanoparticles.[5] PEG-*b*-polyamine was used for the modification of Au surfaces for specific biorecognition.[6,7] The coordination of the lone pair of the amino groups to the gold surface is involved in this case.

Improvement in sensor performance is another target in the development of high-performance sensor systems. Herein, the author has chosen evanescent-field-coupled waveguide-mode (EFC-WM) monolithic sensing plates having SiO_2 surface[12] to demonstrate the capability of PEG-*b*-polymers as the blocking and specificity-enhancing agents. At present, SiO_2 is commonly used as the sensing surface in the development of high-sensitivity systems.[13-23] The great advantage of the waveguide sensor is that higher sensitivity can easily be obtained by metal-nanoparticle labeling.[22] The waveguide sensor system that we used was similar to that of a surface plasmon resonance (SPR)

system, and the difference was that the mode used for measurement is a waveguide mode rather than a surface mode. Unless otherwise stated, the design and configuration of the waveguide sensor is based on the principle of Kretschmann, a well-known scheme for the light irradiation of the thin film attached to the prism.[13,21-25] Biomolecular interactions can be monitored by measuring changes in the local index of refraction upon adsorption of target molecules onto the surface of the waveguide-mode sensor. EFC-WM sensor has advantages of SPR sensor makes the preference of EFC-WM sensor in this study (Table 2.1).

SPR	Waveguide
Surface mode measurements	Waveguide-mode measurements
Incident light is restricted by the material used in order to induce the surface plasmon	There is no such restriction
Usually Ag or Au used as sensing surface (less stable materials)	Stable materials such as amorphous SiO_2 can be used
Sensitivity is not easy to improve	Sensitivity can be improved by nanoholes or dyes or metal particles

Table 2.1. Advantages of waveguide mode over SPR- mode sensors

The sensitivity of EFC-WM was enhanced by nano-perforations in the waveguide layer and increasing the size of the nanoholes promotes the concomitant improvement in the sensitivity.[26] In addition, labeling analytes with colored materials or GNP-conjugates were also an effective method for enhancing the signals. Using these strategies, the detection of molecules of various sizes has been demonstrated using biomolecular interactions and assembly processes. EFC-WM sensor was proposed as an aptasensor with different surface modifications, surfaces with nano-perforations, and a color-labeling technique.[27] Sizes of EFC-WM can be minimized into to smaller sizes (Figure 2.1a) and the spectral changes are depends on the molecules to be used (Figure 2.1b).

The objective of this work is to establish a high-performance biosensor by using the EFC-WM sensor, and comprising PEG-based blocking agents for both sensor surface and nanoparticles.

Human coagulating factor IX (FIX) was selected as a model analyte because it has extremely low availability in vivo and important to detect for blood coagulation analysis. A stable RNA-aptamer generated against FIX was used as the ligand[28] and demonstrated favorable properties with regards to highlighting the potential characteristics of the preferred PEG-derived polymers.

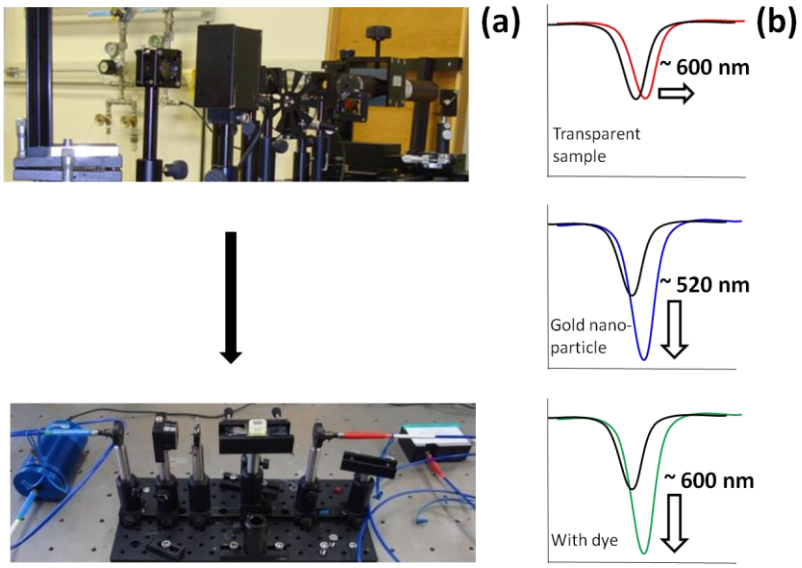

Figure 2.1. EFC-WM sensor. (a) minimized set-up (b) patterns of spectral changes with different samples.

2.3. Experimental section

2.3.1. Reagents and biomolecules

3-Aminopropyltriethoxysilane (APTES) was purchased from Sigma–Aldrich (Tokyo, Japan). Glutaraldehyde, biotin, and precast gradient polyacrylamide gel were procured from Wako Chemicals (Osaka, Japan). Gold nanoparticles (GNPs) conjugated with streptavidin (40 nm; 15-OD) were from BioAssay Works (MD, USA). The shorter oligonucleic acid (dT_{20}) conjugated with biotin at the 5′-end and the other oligonucleic acids were synthesized commercially. FIX was purchased from American Diagnostica (Stamford, CT). Pre-casted gradient polyacrylamide pre-cast gels was purchased from Wako chemicals (Osaka, Japan). Horse radish peroxidase-conjugated anti-mouse immunoglobulin G was purchased from Promega, Medison USA. Clear Blot membrane-P and nitrocellulose membranes

were purchased from ATTO (Tokyo, Japan) and Millipore (MA, USA), respectively. Triton, Tween-20, and sodium dodecyl sulfate (SDS) were from Wako Chemicals (Osaka, Japan). The enhanced chemiluminescence kit was from Amersham Pharmacia Biotech (PA, USA). PEG-b-PAAc was from General Science Corporation (Japan). N6-PEG was kindly provided by JSR (Tokyo, Japan). All samples were stored according to the suppliers' recommendations.

2.3.2. Enzymatic synthesis of aptamer

A stable 34-mer (2′-fluoro-modified) RNA-aptamer, which was previously reported by Rusconi et al.[28] was prepared and its ability to bind FIX or FIXa was verified.[28,29] The aptamer was synthesized on a synthetic DNA template by enzymatic reaction (in vitro transcription) using T7 RNA polymerase. The T7 promoter region (letters are highlighted in italics) was maintained at the 5′-end of the aptamer to generate the RNA molecules. The template, 5′-*AGTAATACGACTCACTATAGG*GATGGGGACTATACCGCGTAATGCTG-3′ was used to prepare the double-stranded DNA. A polymerase chain reaction (PCR) was carried out using the above DNA template and amplified using appropriate primers (5′-AGTAATACGACTCACTATAGG-3′ [forward] and 5′-$(T)_{24}$ATGGGGAGGCAGCATTACGCGGTATA-3′ [reverse]) using 2X PrimeSTAR Max DNA Polymerase, from Takara Bio Inc., (Japan). Twenty PCR cycles were completed at 94 °C for 70 s, 55 °C for 50 s, and 72 °C for 70 s. After proper PCR amplification, the PCR product was precipitated in ethanol and used for RNA preparation by in vitro T7 transcription. Transcription was carried out at 37 °C overnight, using a DuraScribe transcription kit (Epicentre Biotechnologies, USA). The products were treated with 2 U of DNase I (RNase free) for 20 min at 37 °C, to remove the residual template DNA, and the reaction was terminated by adding an equal volume of 2x urea buffer (7 M urea, 50 mM EDTA [ethylenediaminetetraacetic acid], 90 mM tris-borate containing 0.05% bromophenol blue). Afterwards, the reaction mixture was heated at 90 °C for 2 min and loaded onto a 12% polyacrylamide gel containing 7 M urea to fractionate. The RNA band was visualized under UV shadow and extracted

from the excised gel-piece by using the crush-and-soak method.[28] The RNAs were precipitated in ethanol and dried under vacuum, re-dissolved in RNase-free water, and the concentration was measured spectrophotometrically at 260 nm. Using the following DNA template, 5′-*AGTAATACGACTCACTATAGG*GTACCCCTGATATGGCGCATTACGAC-3′ (T7 promoter region highlighted in italics), the complementary FIX aptamer was synthesized as described above by the same T7 forward primer and the reverse primer 5′-$(T)_{24}$TACCCCTCCGTCGTAATGCGCCATAT-3′, for negative reaction.

2.3.3. Setup of the EFC-WM sensor

The evanescent-field-coupled waveguide-mode (EFC-WM) sensor consists of a multilayer sensing plate comprising a dielectric waveguide, a high-refractive index layer, and a glass substrate.[12] The sensing plate, which is illuminated using the Kretschmann configuration, operates as a sensor that is capable of detecting modifications in the dielectric environment near the waveguide surface by measuring changes in reflectivity. The optical setup is shown in Figure 2.2a. A halogen lamp was used as a light source. The light from the lamp was guided to a collimator lens and a prism was irradiated with the collimated light; the incident angle of the light was parallel to the bottom face of the prism. Then, the monolithic sensing plate placed on the bottom of a prism was illuminated and a spectrum of the reflected light was detected using a spectrophotometer (Ocean Optics, Florida, USA). The prism was made of SiO_2 glass and its bottom angle was 38°. The monolithic sensing plate consisted of a SiO_2 glass substrate, a single crystalline Si layer, and a thermally grown SiO_2 waveguide layer, where the thicknesses of the layers are 45 nm and 360 nm, respectively. The fabrication method of the sensing plate is described in elsewhere (Figure 2.2b).[12] The optical measurements in this study were taken around 520 nm to show a dip in reflectance, which corresponds to the optical absorption of GNPs. If GNPs are attached to the waveguide surface, the dip will be deepened by the optical absorption of the GNPs.[22]

2.3.4. Surface functionalization on SiO_2-sensing plate

Sensor chips were initially treated with an alkali solution for 30 min and washed thoroughly with a copious volume of buffer (10 mM HEPES [4-{2-Hydroxyethyl}-1-piperazineethanesulfonic acid]-KOH, 150 mM NaCl [pH 7.4]) to remove the free hydroxide ions, and the surface was dried.

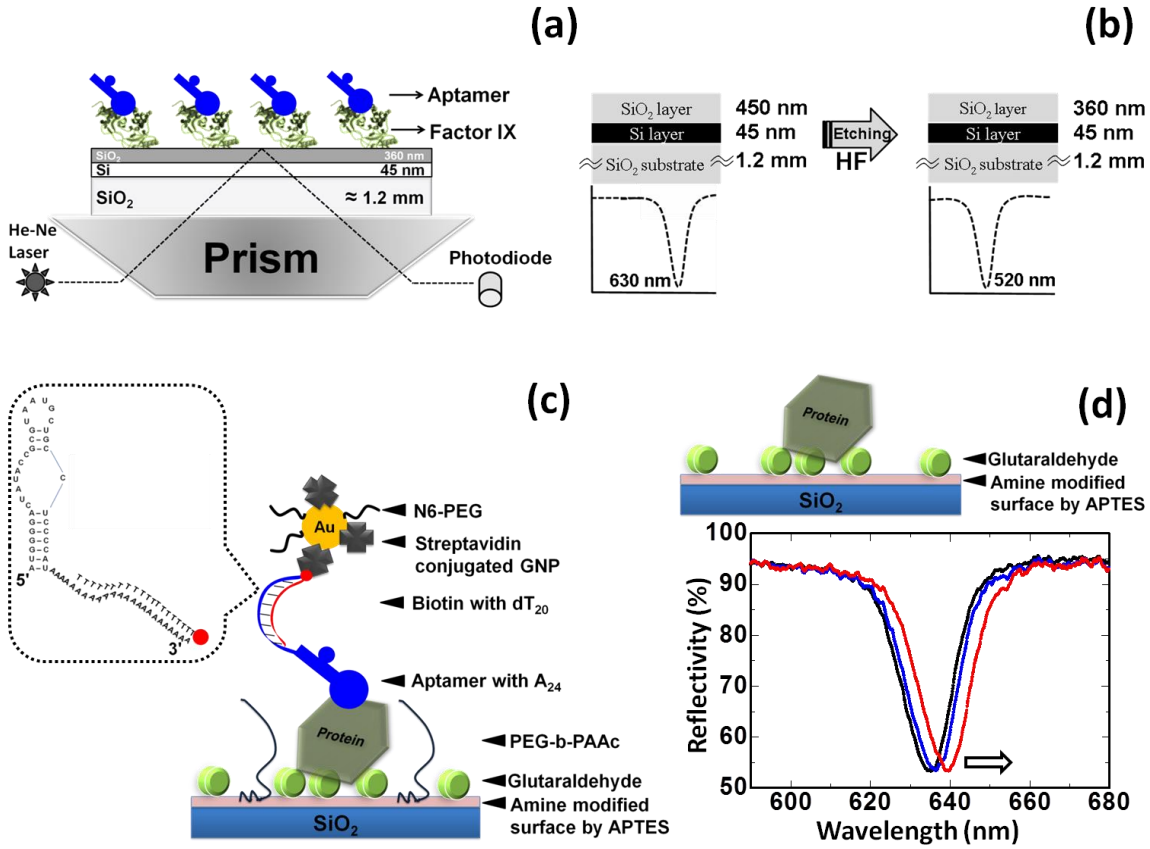

Figure 2.2. (a) Schematic diagram of the waveguide-mode sensing system. A prism, a sensing plate, and other supports are shown. Light source is from halogen lamp and light was detected using a spectrophotometer. FIX and its aptamer are attached on the surface of the top SiO_2 layer. (b) fabrication method of the sensing plate (c) Schematic of chemical surface modifications of the SiO_2 layer of the sensing plate for FIX and aptamer interactions. Glu was attached to the amine-modified surfaces, followed by FIX protein immobilization. The aptamer ending with A_{24} was attached and then biotin with dT_{20} was allowed to react. SA-GNPs (40 nm) were used as a label. Sequences of the aptamer extended at the 3′-end are shown in the dotted box. (d) Spectrum shows the stable attachment of Glu on the amine-modified surface. Black, blue and red spectra indicate buffer only, Glu attachment and FIX, respectively. Chips with the ability to measure the shifts around 630 nm were used. A red shift was observed by the attachment of Glu, because the transparent material, Glu, was attached on the surface.[12] There were no changes in the red spectrum after several washing steps, indicating that Glu was stably attached on the amine-modified surface.

Then further modification was carried out by immersion in a 0.5% (v/v) ethanol solution of APTES for 24 h. The amine group-functionalized surface of the SiO_2 waveguide layer was rinsed with ethanol and dried in a stream of nitrogen gas. The amine-functionalized SiO_2 surface was treated with a 2.5% solution of aqueous Glu for 3 h at room temperature to form an aldehyde-activated surface. After incubation, the surface was washed thoroughly with the HEPES buffer. The Glu-activated surface was made available for the covalent attachment of FIX, and then the remaining free amine sites were blocked by the introduction of PEG-*b*-PAAc. Anti-FIX aptamer extended with dA_{24} at the 3′-end was permitted to react with the FIX on the surface. The free end of the aptamer with dA_{24} was duplexed with biotin-dT_{20}. Finally, the biotin–streptavidin interactions were monitored by immobilizing the SA-GNPs in the presence or absence of N6-PEG (Figure 2.2c). The sensor surface was functionalized by Glu, which has strong affinity for amine-modified SiO_2 surfaces; the spectrum shown in figure 2.2d demonstrates that stable attachment of Glu was achieved after a long incubation and several washings. Optical density (OD) of the SA-GNP solution was measured and the dilutions were prepared using 10 mM HEPES (pH 7.4) to obtain 1 OD SA-GNP solution from the original stock supplied. Each reaction was performed for 30 min on the sensor chip, after which the sensing surface was thoroughly washed 3 times with 300 µL of HEPES buffer. In order to maintain the stability of the interaction between FIX and the aptamer, 2 mM $CaCl_2$ was added to the buffering solution, as previously recommended.[28]

2.3.5. Determination of Limit of detection

To determine the sensitivity of detection of FIX on the waveguide-mode sensor, the author performed experiments with aptamer and protein titrations using single (PEG-*b*-PAAc) and dual polymers (PEG- *b*-PAAc and N6-PEG). Surface modifications for all experiments were carried out as described above. Aptamer titrations were carried out after modification with PEG-*b*-PAAc of the Glu-modified surface of SiO_2. For this titration, the author kept the FIX (250 nM) and PEG-*b*-PAAc

concentrations (4 mg/mL) constant and titrated using different concentrations of aptamer (10 pM to 200 nM). After attaching the aptamer as described above, the DNA ends with biotin was complemented. Spectral changes were monitored by using 1 OD of SA-GNPs. Similar titration was also carried out with the addition of N6-PEG (0.5 mg/mL) to the 1 OD of SA-GNPs. To optimize the sensitivity limit of FIX, the author also performed the protein titration at 100 fM to 250 nM, keeping the aptamer (100 nM) and PEG-*b*-PAAc (4 mg/mL) concentrations constant. Limit of detection is calculated with the value 3 times higher resonance angle than the control experiment. Measurements were carried out with or without addition of N6-PEG (0.5 mg/mL) on SA-GNPs.

2.3.6. Biotin-streptavidin competitive assay

The author carried out the competition assays with the addition of different concentrations of free biotin to SA-GNPs. For this assay, the surface treatment and chemical modifications of the sensing surface were the same as described above. Biotin was used as a competitor at concentrations of 0.1 fM to 1000 fM. The biotin concentration was varied whilst maintaining a constant SA-GNP optical density (1 OD) and titrated on a biotin-immobilized sensing surface with constant aptamer concentration.

2.3.7. Scanning electron microscopy (SEM)-Nanoscale Imaging

To increase the sensitivity of the specific biomolecular interaction described above, the author mixed N6-PEG with SA-GNPs. To visually confirm the effect of the N6-PEG on the sensing performance, the author carried out microscopic analyses with field emission scanning electron microscopy (SEM; JEOL, JSM-6340F) on the SA-GNP surfaces in the presence and absence of N6-PEG. Surface modifications were as described in Fig. 2.2c. N6-PEG was premixed with SA-GNPs before being attached to the biotinylated sensing surface. The attachment of GNPs was observed using SEM. SEM measurements were carried out with 5 kV acceleration and 10 μA emission.

Images were captured at a magnification of 10000. All SEM observations were performed at a GNP-streptavidin conjugate optical density of one, as described above.

2.3.8. Selective and specific binding of aptamer with FIX on the surface

For selective binding which mimics a similar situation in the blood samples, experiments with mixed clotting proteins were carried out. Different concentrations of FIX, representing concentrations lower than the saturation points from the above assays with dual polymers, were considered. For this assay the author used a protein mixture (FIX, FXIa, and FVIIa); the author kept FXIa and FVIIa concentrations constant and titrated the binding of FIX at concentrations of 100 fM to 1 nM. All other surface chemical modifications and detection strategies were the same as those described above. The selective binding study was also performed in the presence of 84 nM of albumin with dose-dependent FIX concentrations from 100 fM to 1 nM**.** These mixtures were tested against a constant aptamer concentration (100 nM).

2.4. Results and Discussion

An improvement in biofouling resistance is necessary in biosensor development and biomolecular recognition. The steps of the sensing strategy are as follows: (i) FIX was applied to the Glu-modified SiO_2 surface to mimic blood proteins; (ii) the specific interaction of aptamer-A_{24} with the target protein (FIX in this case) takes place on the surface; (iii) the hybridization of biotinyl-dT_{20} to the aptamer-A_{24} takes place; (vi) contact is made with GNPs that are surface-modified with streptavidin; and (v) the absorption is measured using the EFC-WM sensor. During these steps, the issue of non-specific interactions of aptamer-A_{24} and GNPs is important with regard to suppressing background signals. In this study, the author has utilized 2 kinds of synthesized polymer derived from PEG, viz., PEG-*b*-PAAc and N6-PEG, in order to create high-performance sensing surfaces. The idea was to achieve the most effective blocking of both the sensor chip and the surfaces of the GNPs

using PEG-*b*-PAAc and N6-PEG. With the assistance of these blocking polymers, the author has analyzed human coagulating FIX. An aptamer against FIX was used to improve specific sensing. This 2′-fluoropyrimidine-modified stable aptamer, which binds FIXa with high affinity and specificity,[28] binds FIX with equal efficiency.[29] FIX used in this study has high purity and migrates as a single prominent protein under sodium dodecyl sulfate poly(acrylamide) gel electrophoresis (SDS-PAGE) (Figure 2.3a). The aptamer prepared by the enzymatic reaction (transcription) is a 58-mer, and contains 34-nucleotides at its 5′-end that specifically bind with human FIX (Figure 2.3b). The non-specific attachments of SA-GNP were found to occur on amine- and Glu-modified surfaces. The potential blocking effect of PEG-*b*-PAAc on these surfaces was compared with that of ethanolamine, which is a common blocking agent for sensing surfaces. Further, the improvement in the sensitivity was evaluated following the additional usage of N6-PEG on GNPs.

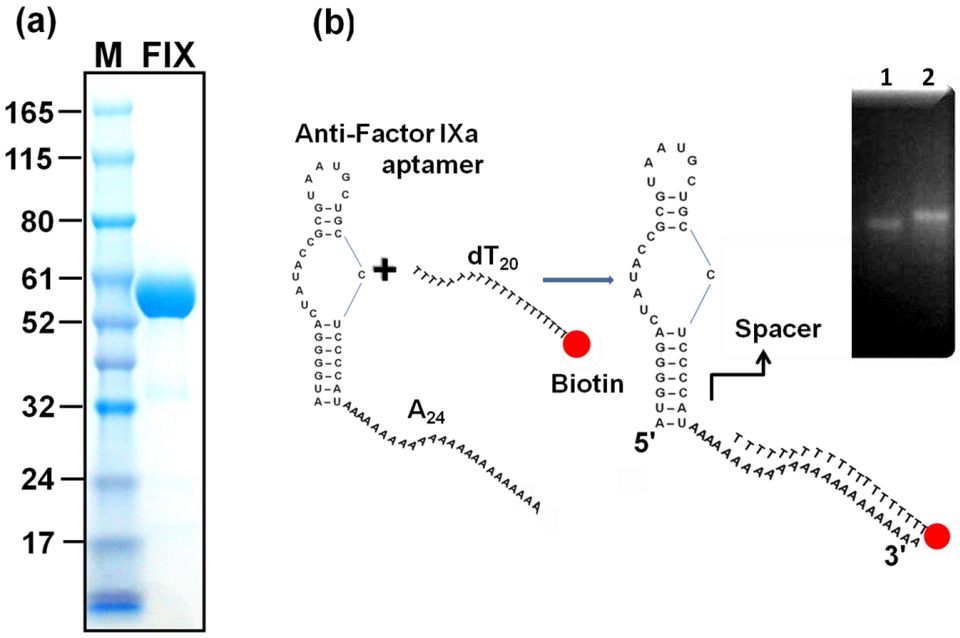

Figure 2.3. FIX and aptamer. (a) Purity of FIX on SDS-PAGE. The FIX band was migrated at ~55,000 daltons. 3 µg of FIX was loaded. (b) Schematic diagram for the duplex formation of FIX aptamer with extended 3′end (A_{24}) and biotin-dT_{20}. Spacer region was created for flexibility. Figure inset is shown for mobility of anti-FIX aptamer without (1) and with (2) poly-A tail on 4% agarose gel.

2.4.1. Influence of ethanolamine or PEG-*b*-PAAc on FIX recognition of chemically functionalized SiO_2 surface

Before optimization of the sensing of FIX by the present system, the author confirmed that the system works properly by using ethanolamine and PEG-*b*-PAAc as blocking agents. After FIX solution was contacted with the Glu-treated sensor chip, the biotinylated aptamer was reacted in the presence of a buffering agent containing $CaCl_2$, which is necessary for these ligand-analyte interactions.[28]

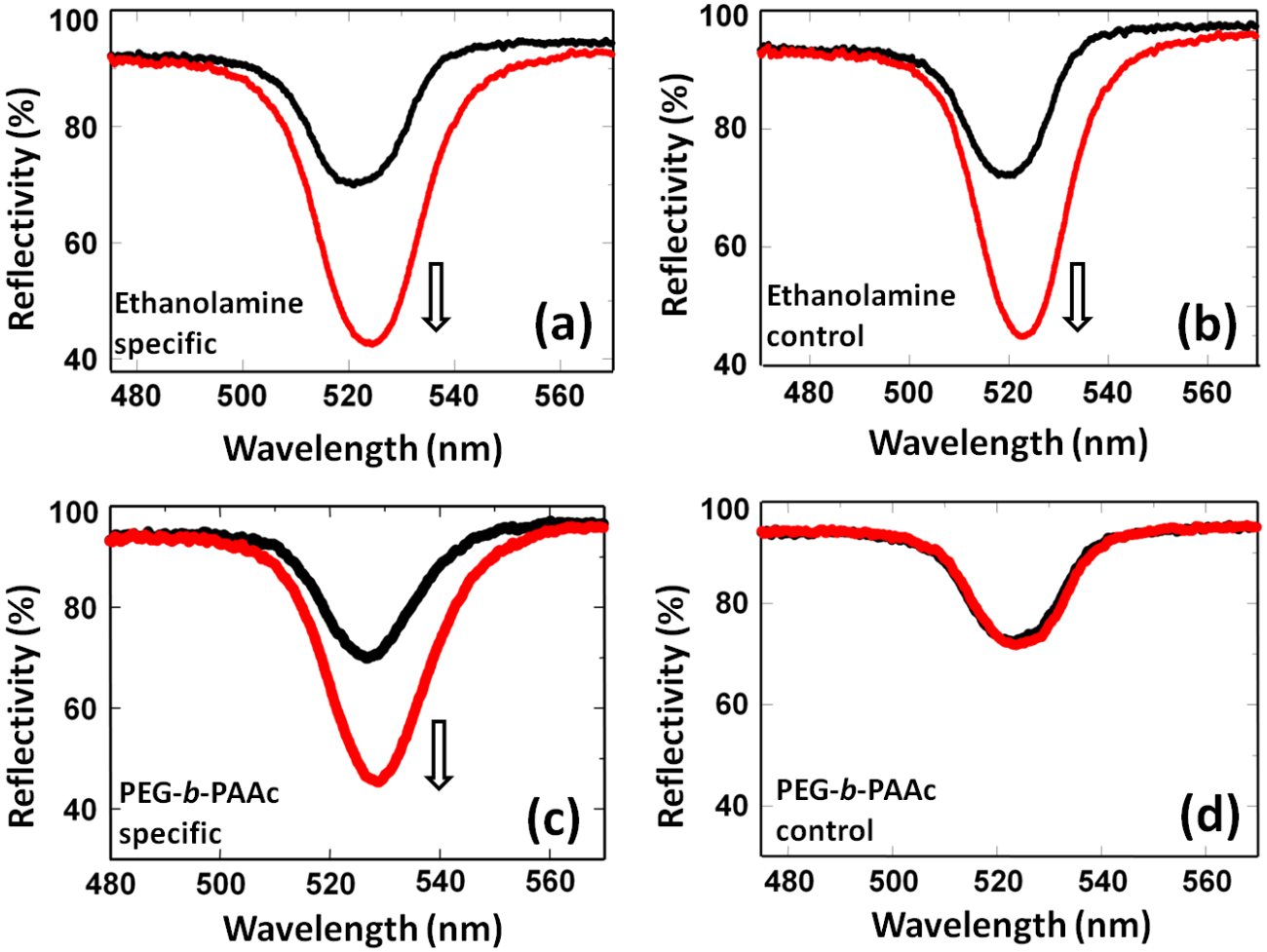

Figure 2.4. Aptamer and FIX interaction using ethanolamine or PEG-*b*-PAAc as the blocking material. (a) Specific reaction using ethanolamine (b) non-specific reaction using ethanolamine (c) specific reaction using PEG-*b*-PAAc (d) non-specific reaction using PEG-*b*-PAAc. Black and red curves are the spectra before and after the attachment of SA-GNP, respectively. Arrows indicate the direction of changes in the spectrum.

On this biotin-exposed surface, the author immobilized the SA-GNPs, which were preferably 40 nm in size and could enhance the spectral signaling to a large degree at 520 nm (suitable for Au). Biotinylated complementary aptamer sequence was used for the control experiment. Figure 2.4 clearly demonstrates the spectral changes resulting from the SA-GNP–biotin interaction on the waveguide sensor surfaces. However, in the case of the ethanolamine-treated sensing surfaces, significant spectral changes were recognized both in the specific adsorption (Figure 2.4a) and in the control experiment (Figure 2.4b).This result indicates that the ethanolamine-modified surfaces could not prevent the non-specific interaction between SA-GNPs and the waveguide sensor surfaces. In the case of sensing surfaces using PEG-*b*-PAAc as a blocking agent, the author could clearly see the difference of the spectral changes in the specific aptamer-treated surface (Figure 2.4c), and the background signal was completely suppressed (Figure 2.4d). In order to significantly improve the colloidal stability and non-fouling character of SA-GNPs, the author used N6-PEG as the blocking agent. Non-specific absorptions of SA-GNPs with and without N6-PEG were investigated on a PEG-*b*-PAAc-immobilized sensor chip surface using the EFC-WM sensor. Interestingly, no signal change was observed regardless of N6-PEG blocking, as shown in Figure 2.5. Complete protection of sensor chip surface by PEG-*b*-PAAc might prevent non-specific interaction of SA-GNPs even without N6-PEG blocking.

To check the required amount of PEG-*b*-PAAc, the author titrated the PEG-*b*-PAAc concentrations from 0.5 mg/mL. As determined in the above section, 4 mg/mL of PEG-b-PAAc was desired as the highest concentration. Initially, with lower concentration (0.5 mg/mL) of PEG-*b*-PAAc, interactions of FIX and complementary aptamer sequence were checked. A spectral change in the waveguide sensor system was found to have non-specificity and it was with the reflectivity changes of 30%. With gradually increasing concentration of PEG-*b*-PAAc, the non-specificity was reduced correspondingly. With the PEG-b-PAAc concentrations of 1 and 2 mg/mL the non-specific spectral

changes were measured as 20 and 5%, respectively. No spectral changes were found at the concentration of 4 mg/mL of PEG-*b*-PAAc, indicates under this condition PEG-*b*-PAAc was exclusively favored the specific interactions (Figure 2.5).

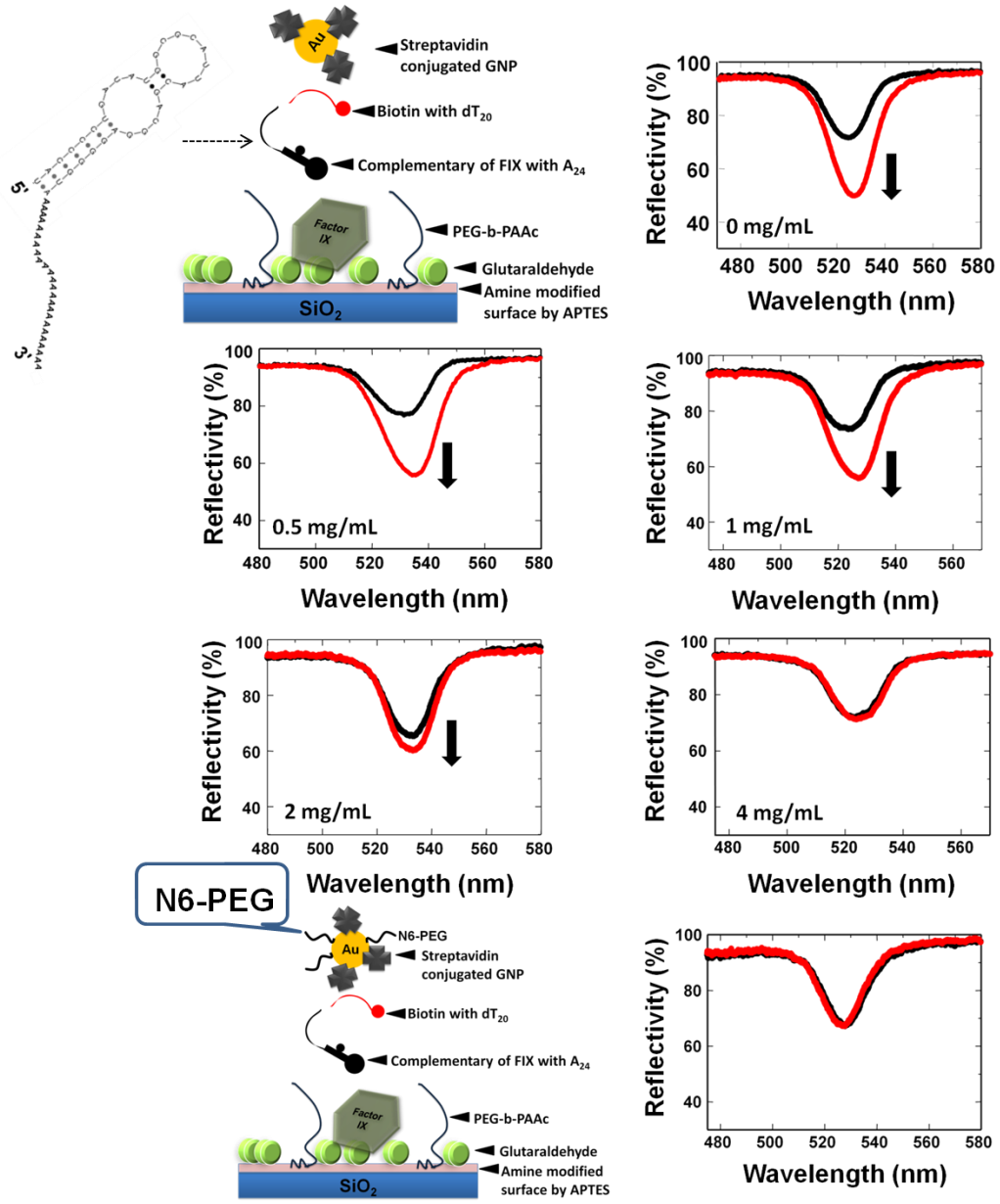

Figure 2.5. Control experiments with complementary sequences of FIX aptamer using different PEG-*b*-PAAc concentrations. Black and red spectrums indicate only buffer and attachment of streptavidin conjugated GNP, respectively. Predicted secondary structure with complementary sequences is shown. Arrows indicate the direction of changes in the spectrum. By the addition of N6-PEG (0.5 mg/mL) with SA-GNP, the spectrum remains same. 4 mg/mL of PEG-*b*-PAAc is sufficient for controlling non-specificity.

2.4.2. PEG-*b*-PAAc prevents needless binding on amine and Glu surfaces

To check the origin of non-specificity, initially it was aimed to immobilize SA-GNPs directly on the amine surfaces. SA-GNPs have shown higher spectral changes as non-specific binding on amine surface (Figure 2.6a).

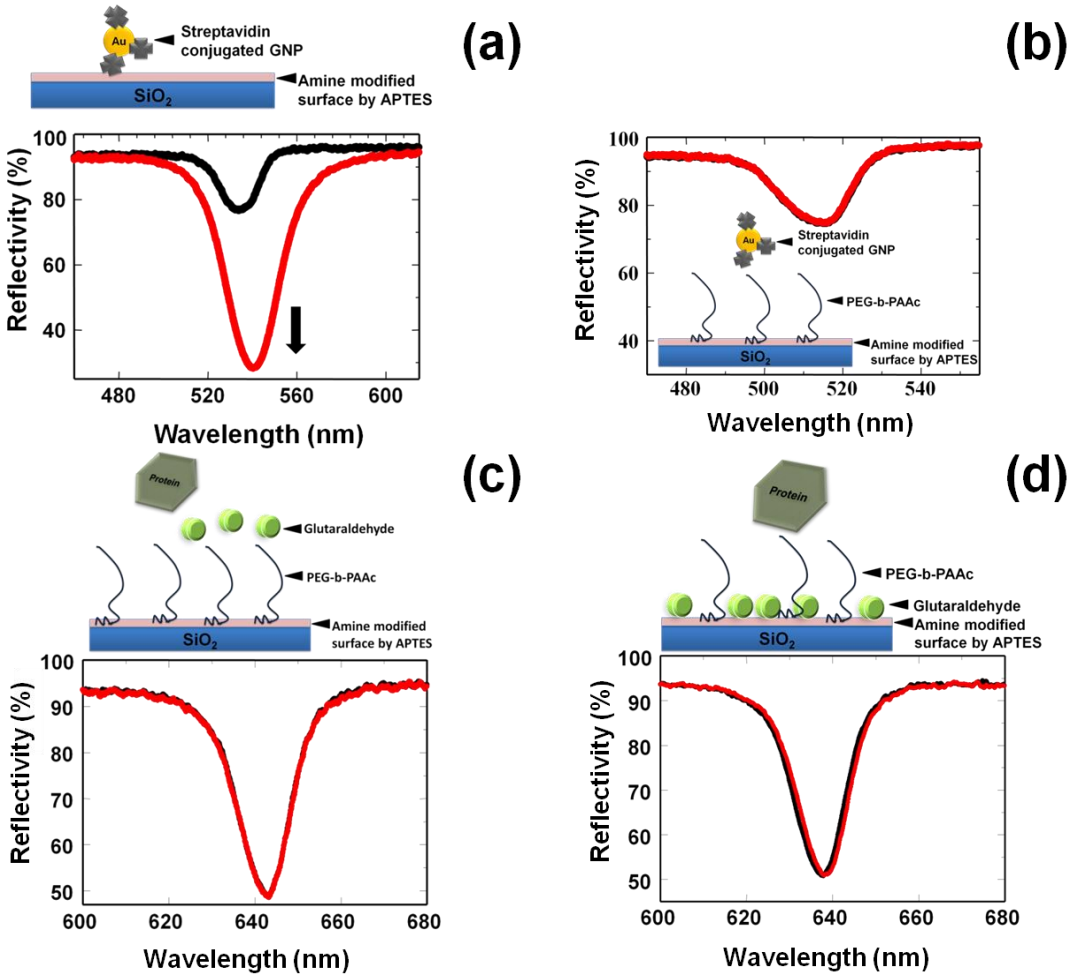

Figure 2.6. PEG-*b*-PAAc prevents the non-specific binding of SA-GNP on the amine and Glu surfaces. (a) Binding of SA-GNP on the amine surfaces. Arrow indicates the direction of changes in the spectrum. (b) PEG-*b*-PAAc prevents the binding of SA-GNP on the amine surfaces. Schematics are shown. Black and red spectrums indicate only the buffer and attachment of the SA-GNP, respectively. (c) Spectrum shows complete blocking of amine surfaces by PEG-*b*-PAAc. No spectral change was noticed. Black and red spectrums indicate only buffer and attachment of FIX, respectively. (d) Spectrum shows the complete coverage of Glu surface by PEG-*b*-PAAc. Glu was attached on the amine surface and protein was passed and FIX could not bind. Black and red spectrums indicate only buffer and attachment of FIX, respectively. Schematics are shown for each experiment. Chips suitable to measure the shifts around 630 nm were used.

This non-specific attachment is due to the electrostatic interactions occurred on amine-surface as suggested for other surfaces.[1] To sort out this issue, PEG-*b*-PAAc with concentration of 4 mg/mL was introduced on the amine surface, and then SA-GNPs were attached. Non-specific adsorption was completely quenched in the presence of PEG-*b*-PAAc (Figure 2.6b). Non-specific binding of negative-charged SA-GNPs, could be due to the consequence of attraction with the positively charged amino surfaces and it was protected by blocking with negative charged PEG-*b*-PAAc. This reaction imitates the previous report showing negatively charged anionic polymer (PEG-*b*-PAAc) binds on the positively charged rare earth ion-doped Y_2O_3 nanoparticles surfaces.[5] Based on our results, it was predicted that the bio-fouling occurred mainly because of the available free amine surfaces on the sensing surface.

To find non-specific binding of FIX on the amine, the author immobilized PEG-*b*-PAAc on amine-modified surface. Then reaction made with Glu followed by protein as the regular procedure designed for our experiments. When the author immobilized the protein on the Glu attached sensing surface, the author could not observe any changes in the spectrum by the waveguide mode sensor, even after a prolonged incubation time (Figure 2.6c). This result supports the above conclusion as PEG-*b*-PAAc can block the amine surface and it also inferred that 4 mg/mL of PEG-*b*-PAAc concentration could completely block the amine surface. The author were also keen to find the binding ability of PEG-*b*-PAAc on the Glu surface, for this notion, tried in another way in that PEG-*b*-PAAc was used after treating the sensing plate with Glu, but before treat with protein. There is no significant binding was recognized by the waveguide sensing system, as PEG-*b*-PAAc blocked the binding of protein on Glu surfaces (Figure 2.6d). In this case, PEG-*b*-PAAc masked the Glu-surfaces and also binds to the remaining amine surfaces from silane coupling reaction which is escaped from the Glu reaction. Previously, the effect of PEG-*b*-PAAc was also evidenced on other surface (rare earth ion-doped Y_2O_3 nanoparticles) and found to reduce the non-specific interactions of streptavidin and biotin.[5] It seems,

PEG-*b*-PAAc has ability to mask different surfaces, as the potential common blocking agent.

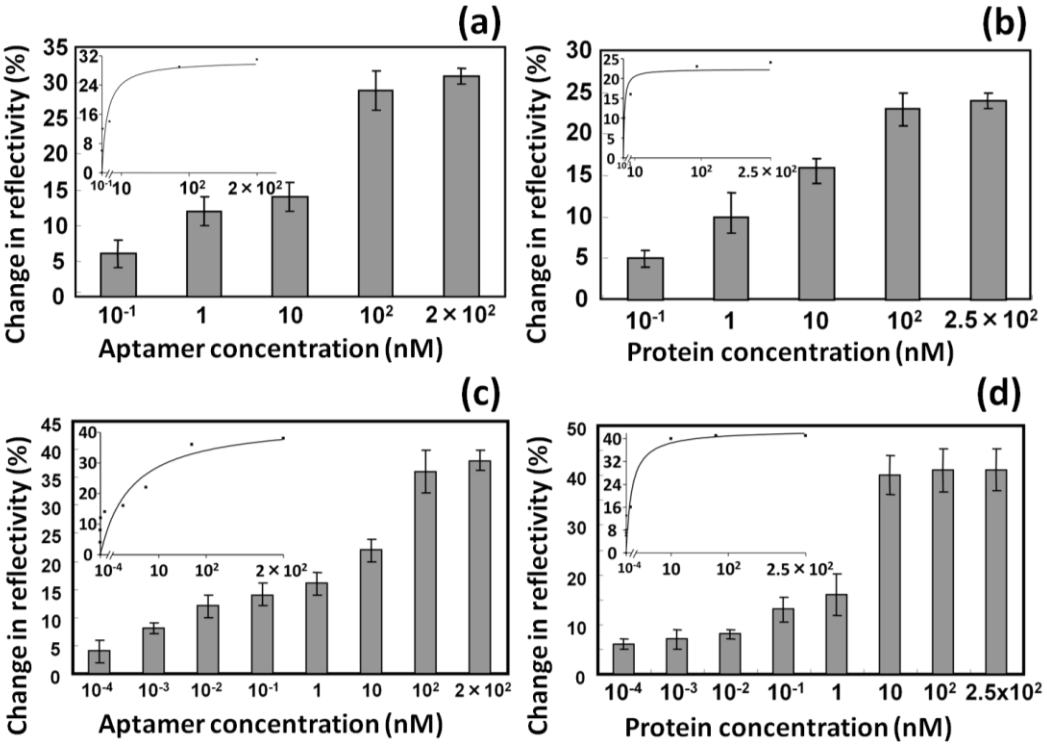

Figure 2.7. Aptamer titrations against constant FIX (250 nM). Concentrations of other biomolecules were kept constant. Graphical representation of comparative analyses for the PEGs. Reflectivity changes are shown for: (a) constant FIX (250 nM) against different concentrations of aptamers in the presence of PEG-*b*-PAAc; (b) constant aptamer (100 nM) against different concentrations of FIX in the presence of PEG-*b*-PAAc; (c) constant FIX (250 nM) against different concentrations of aptamers in the presence of PEG-*b*-PAAc on the sensing plate and N6-PEG on the SA-GNP; and (d) constant aptamer (100 nM) against different concentrations of FIX in the presence of PEG-*b*-PAAc on the sensing plate and N6-PEG on the SA-GNP. Fitting curves are shown as figure insets.

2.4.3. Determination of detection limit using single and dual PEG-polymers

The detection limit of FIX was investigated using PEG-*b*-PAAc. Initially, the aptamer concentration necessary for the saturation level was accessed by using different aptamer concentrations against constant FIX. The author found the minimal specific interaction at 100 pM of aptamer, which showed a reflectivity change of 6%. Results obtained from FIX titrations against constant aptamer and aptamer titrations against constant FIX were shown in Figure 2.7a-d. Aptamer concentration higher than 100

nM showed constant changes in the spectrum indicates the attainment of saturation (Figure 2.7a; spectra are shown in Figure 2.8).

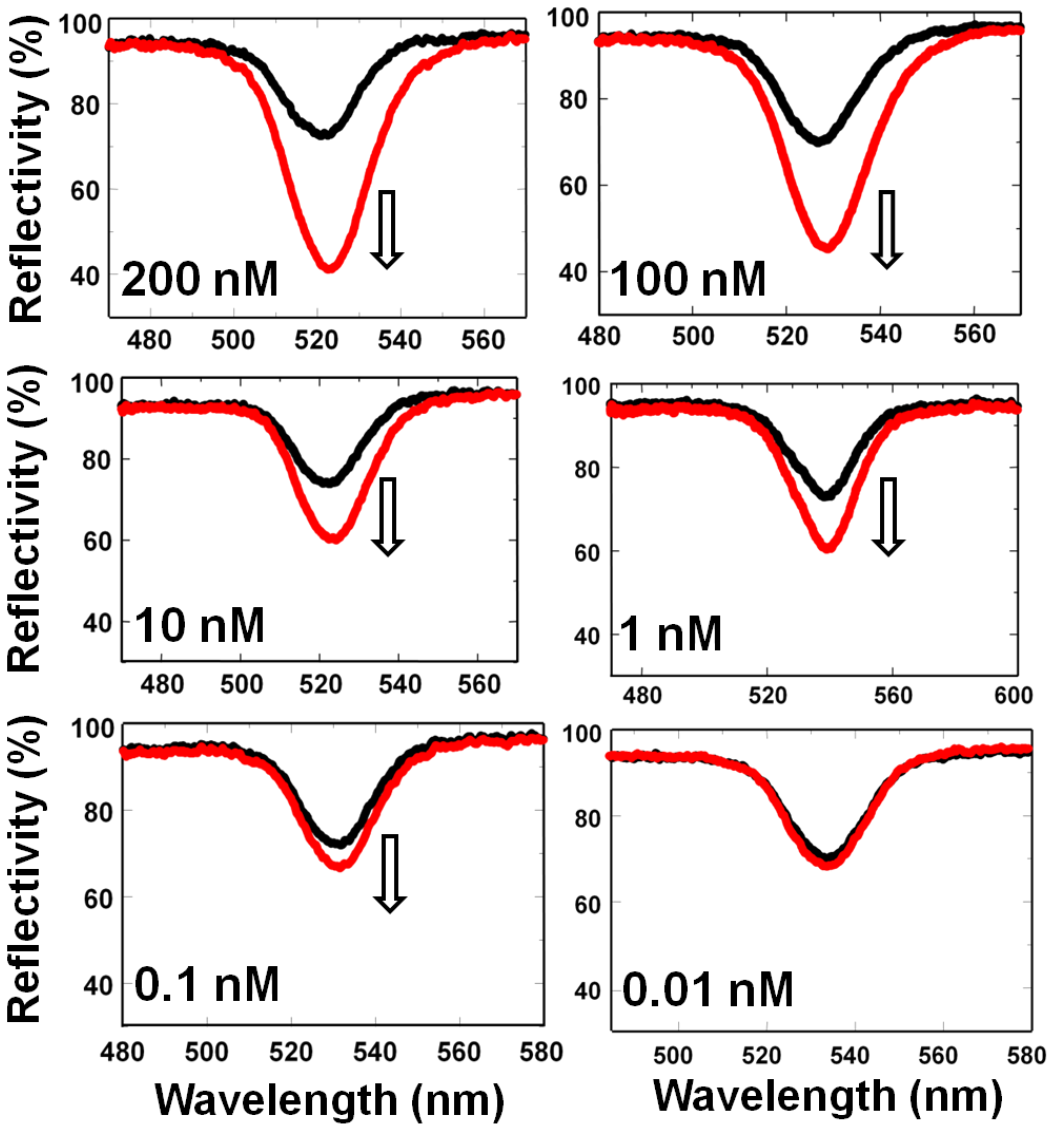

Figure 2.8. Spectra of aptamer titrations against constant FIX (250 nM). Aptamer titers were shown from higher concentration to lower concentration. Concentrations of other biomolecules were kept constant. Black and red spectra curves are the spectra before and after the attachment of SA-GNP, respectively. Arrows indicate the direction of changes in the spectrum.

Using this suitable aptamer concentration, the detetion limitl to FIX was investigated. Figure 2.7b shows the detection of FIX under a constant aptamer concentration of 100 nM; the FIX was detected at 100 pM as a 6% reflectivity change (spectra are shown in figure 2.9). It was previously reported

that the densely packed PEG chains surrounding an antibody immobilized on a sensor chip surface improve its effectiveness.[1,4,8] This might be one of the reasons that our system demonstrated a 100 pM level of sensitivity. With increasing FIX concentration, the signal changes were increased concomitantly. Similar titrations using saturated levels of aptamer (Figure 2.7c; Figure 2.10) against FIX-dose dependency were also carried out using SA-GNP with N6-PEG.

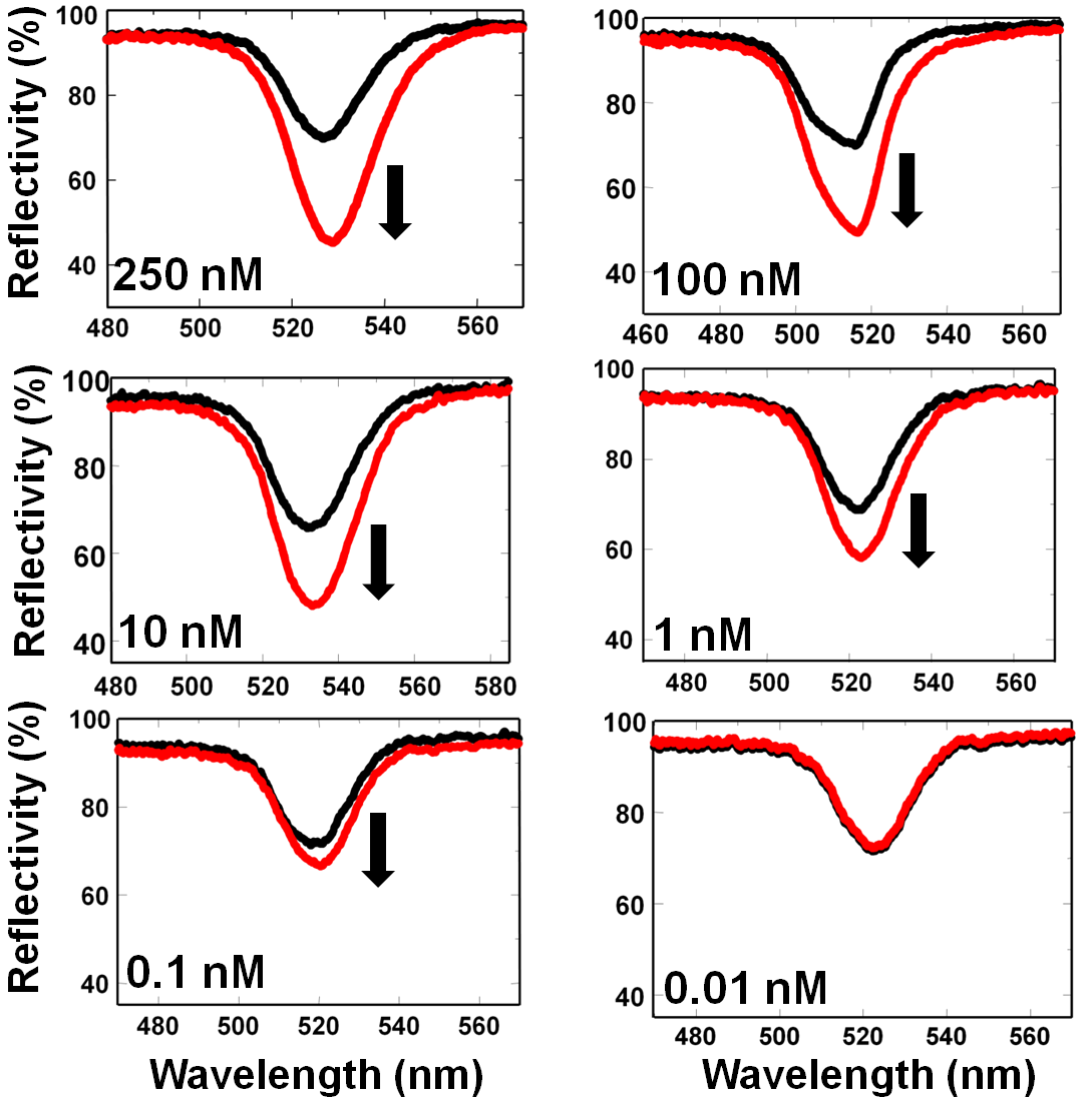

Figure 2.9. FIX titration with different concentrations against constant aptamer (100 nM). FIX titer were shown with higher concentration to lower concentration. Concentrations of other biomolecules are constant. Black and red spectrums indicate only buffer and attachment of the streptavidin conjugated GNP, respectively. Arrows indicate the direction of changes in the spectrum.

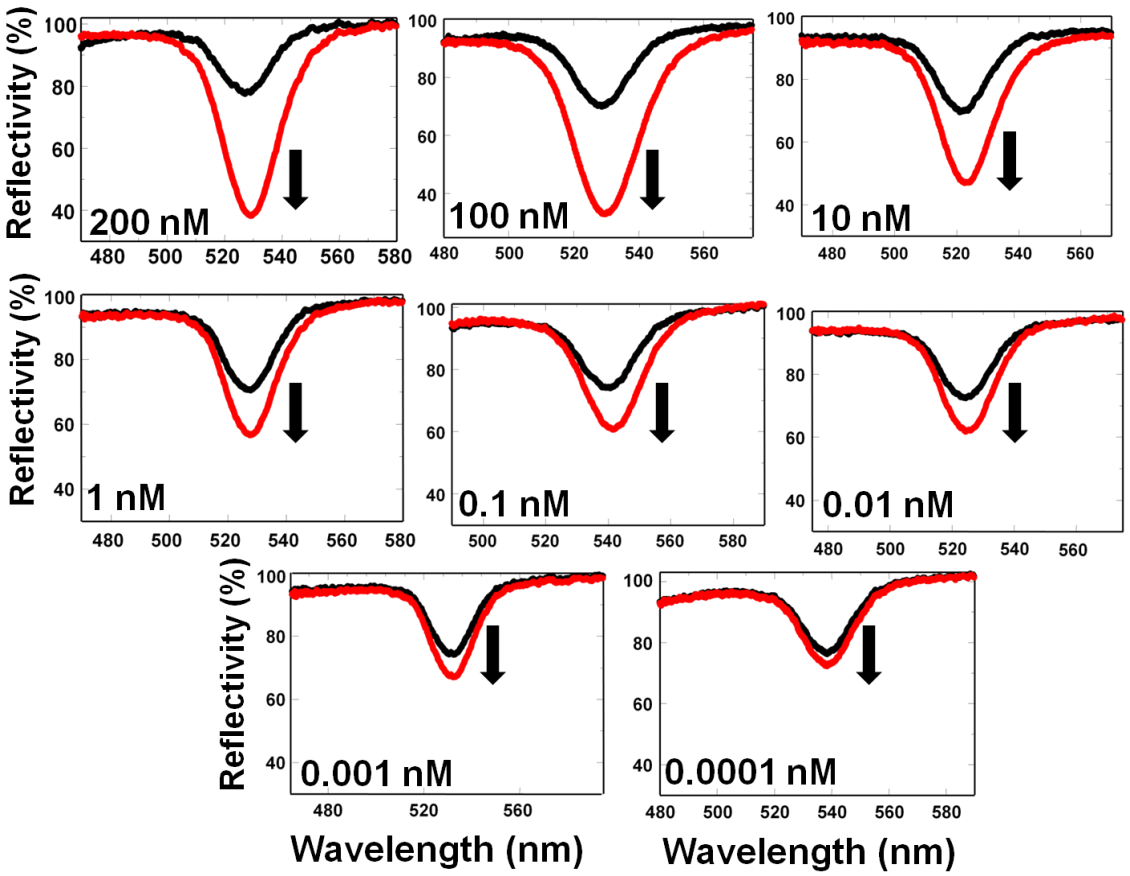

Figure 2.10. Aptamer titrations with different concentrations against constant FIX (250 nM). Aptamer titers were shown with higher concentration to lower concentration. Concentrations of other biomolecules are constant. Black and red spectrums indicate only buffer and attachment of streptavidin conjugated GNP, respectively. SA-GNP used with 0.5 mg/mL of N6-PEG. Arrows indicate the direction of changes in the spectrum.

Figure 2.7d show the detection limit of FIX using PEG-*b*-PAAc on the sensor chip surface and N6-PEG on the SA-GNP (spectra are shown in Figure 2.11). As can be seen in the figure, a large increase in the detection limit was observed when the author used both PEG-*b*-PAAc and N6-PEG. It is interesting to note that N6-PEG immobilized on SA-GNP surfaces influenced sensing ability though it did not influence suppression of non-specific binding on the sensor chip. At the sensitivity concentration determined in the earlier experiment with only PEG-*b*-PAAc (100 pM), addition of N6-PEG showed 3-fold higher spectral changes and reflectivity change at the spectral dip of 14%. Therefore, under the usage of both polymers, the detection limit was improved and the author could

monitor the FIX at 100 fM with a reflectivity change of 6% (Figures 2.7d & 2.11). This result with the addition of N6-PEG represents a 1000-fold improvement in sensitivity.

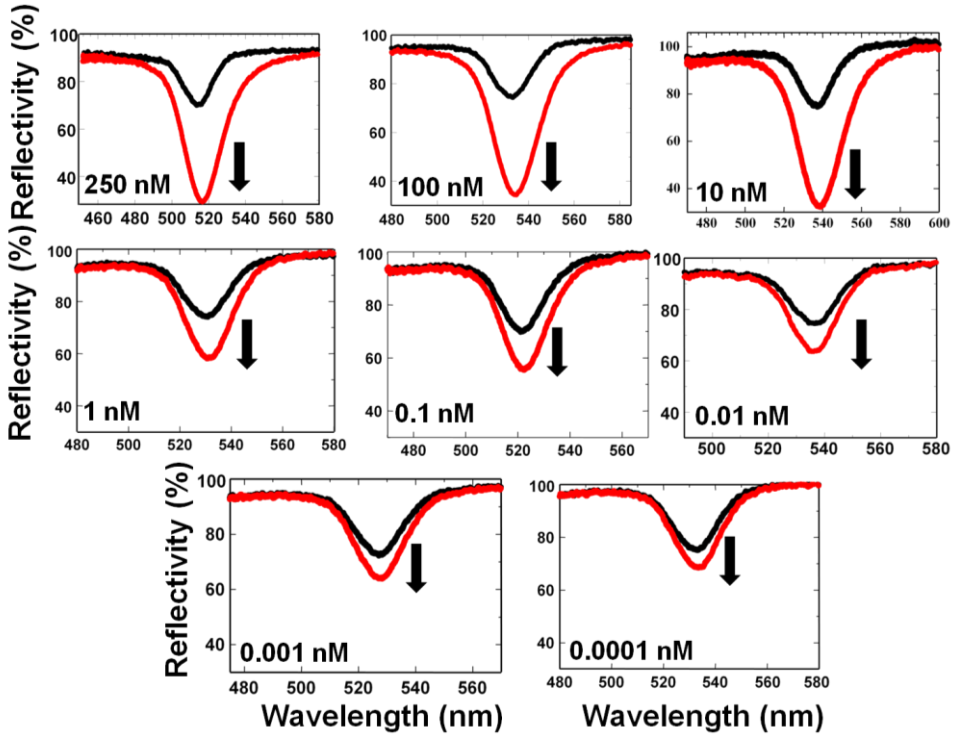

Figure 2.11. FIX titration with different concentrations against constant aptamer (100 nM). FIX titers were shown with higher concentration to lower concentration. Concentrations of other biomolecules are constant. Black and red spectrums indicate only buffer and attachment of streptavidin conjugated GNP, respectively. SA-GNP used with 0.5 mg/mL of N6-PEG. Arrows indicate the direction of changes in the spectrum.

In earlier reports, with the same aptamer and FIX interactions, the Kd values were found to be 600 and 400 pM by using a filter binding assay and a commercially established SPR-based Biocore technique, respectively. In both assays, the usage of proteins were nanomolar orders and statistical calculations were performed to calculate the Kd values.[28,29] In the routine clotting assay it was found that in the presence of FIX-aptamer at low nanomolar order, clotting was delayed.[29]

2.4.4. Biotin–streptavidin competition revealed the sensitivity enhancement

To explore the reason behind the sensitivity improvement in the presence of N6-PEG, and to

determine the genuine interactions between biotinylated aptamer and SA-GNPs, the author studied dose-dependent biotin competition on the sensor surface (Figure 2.12a &b) , viz., different concentrations of free biotin were mixed with SA-GNPs prior to application to the sensing chip.

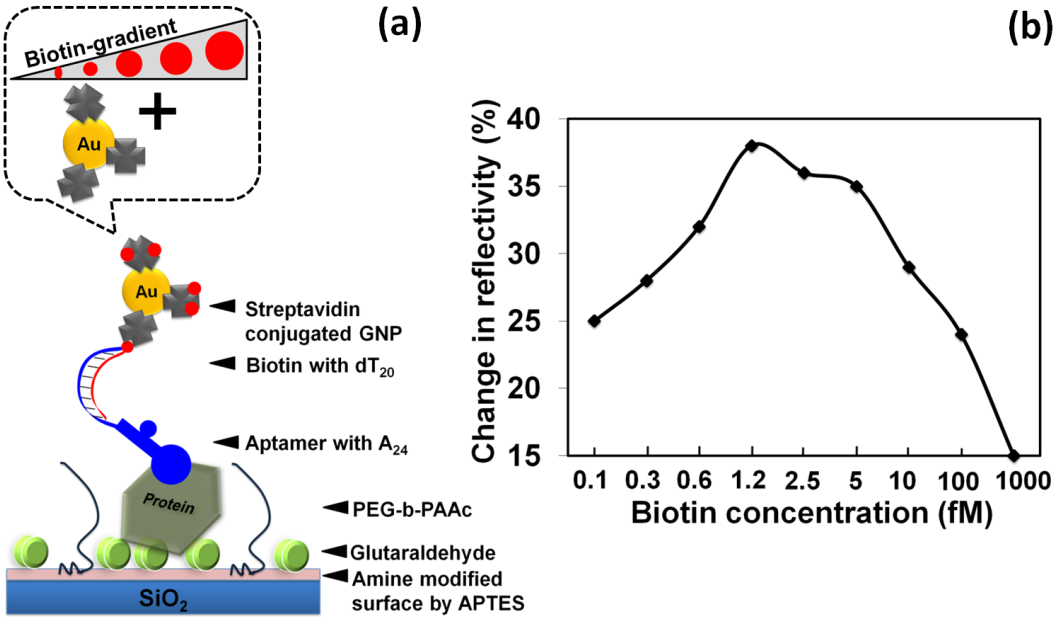

Figure 2.12. Competition assays using biotin. Different concentrations of biotin were added to SA-GNP before reacting with pre-immobilized biotinylated aptamers on the sensing surface. (a) Schematic illustrates the experimental procedure. (b) Graphic representation of changes in the reflectivity, under competition.

At low concentrations (0.1 fM of biotin), the presence of free biotin did not affect the result. However, it was interesting to note that with an increase in the biotin concentration there was a significant change in the spectral signal. These changes continued until a free biotin concentration reached 5 fM. At concentrations beyond 5 fM, there was a decline in the spectral changes of the waveguide sensor (Figure 2.13). The maximum sensitivity was seen at a free biotin concentration of around 1.5–2.5 fM, as shown in Figure 2.12b. This implies that the binding affinity of SA-GNPs with respect to the surface biotin increases with increasing free biotin concentration up to 1.2 fM, suggesting that the competitive biotin molecules at a concentration of less than 1.2 fM might occupy some of the SA-GNP active binding sites. Although streptavidin has 4 active binding sites for biotin, several sites were occupied by

the free biotin under the above competitive situation, which might increase the affinity. This kind of competition has been reported recently by Duan et al.[31] who studied the dissociation of streptavidin–biotin complexes by addition of biotin in dose-dependent manner. A similar effect might be observed in the case of N6-PEG, viz., it could mask some of the biotin-active binding sites on the streptavidin. The results of the free biotin and SA-GNPs competition assays are illustrated in figure 2.12b. The crowding property of PEG might allow more SA-GNPs to properly align with the pre-immobilized biotinylated aptamers on the sensing plate.

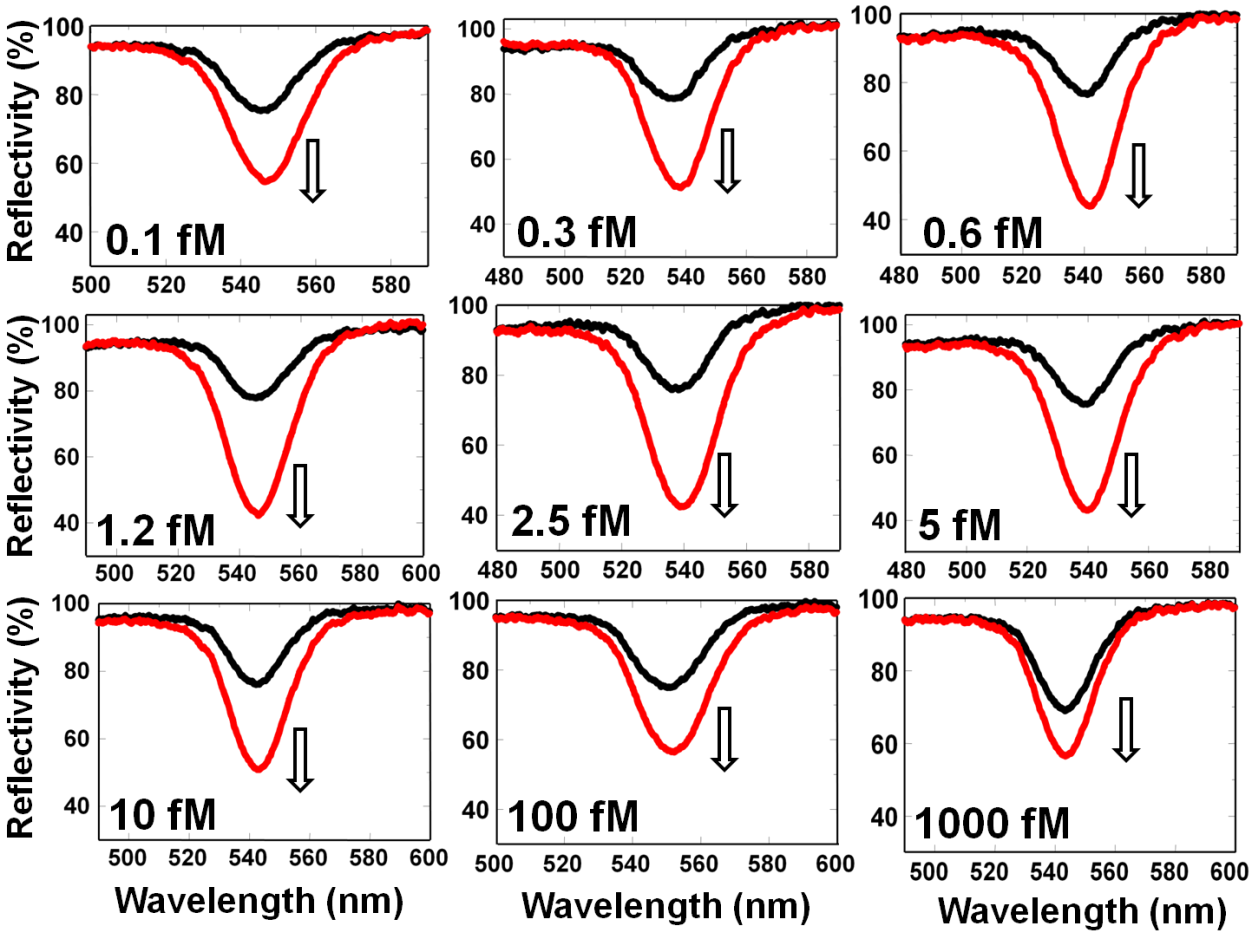

Figure 2.13. Spectrum of competition assays using biotin. Different concentrations of biotin were added to SA-GNP before reacting with pre-immobilized biotinylated aptamers on the sensing surface. Spectral changes after applying the mixture to biotinylated aptamer-immobilized sensing surface. Black and red curves are the spectra before and after the attachment of SA-GNP, respectively. The concentrations indicated in the figures are those of the biotin. Arrows indicate the direction of changes in the spectra.

2.4.5. Nanoscale imaging of captured GNPs on the sensing plate

To substantiate the above results demonstrating a 1000-fold improvement in sensitivity with N6-PEG, scanning electron microscope (SEM) analysis of the sensor chip surface was carried out. GNPs were clearly observed on the sensing plate used in the above experiments (experiments with single and double polymers) after attaching SA-GNP. Measurements were taken at different places and the number of attached GNPs was counted. The observations of the number of GNPs attached strongly corroborate the results obtained experimentally by the waveguide-mode sensor, viz., the number of GNPs from the sensing plate treated with only PEG-*b*-PAAc was about three times lower than from that treated with dual polymers (Figure 2.14a & b).

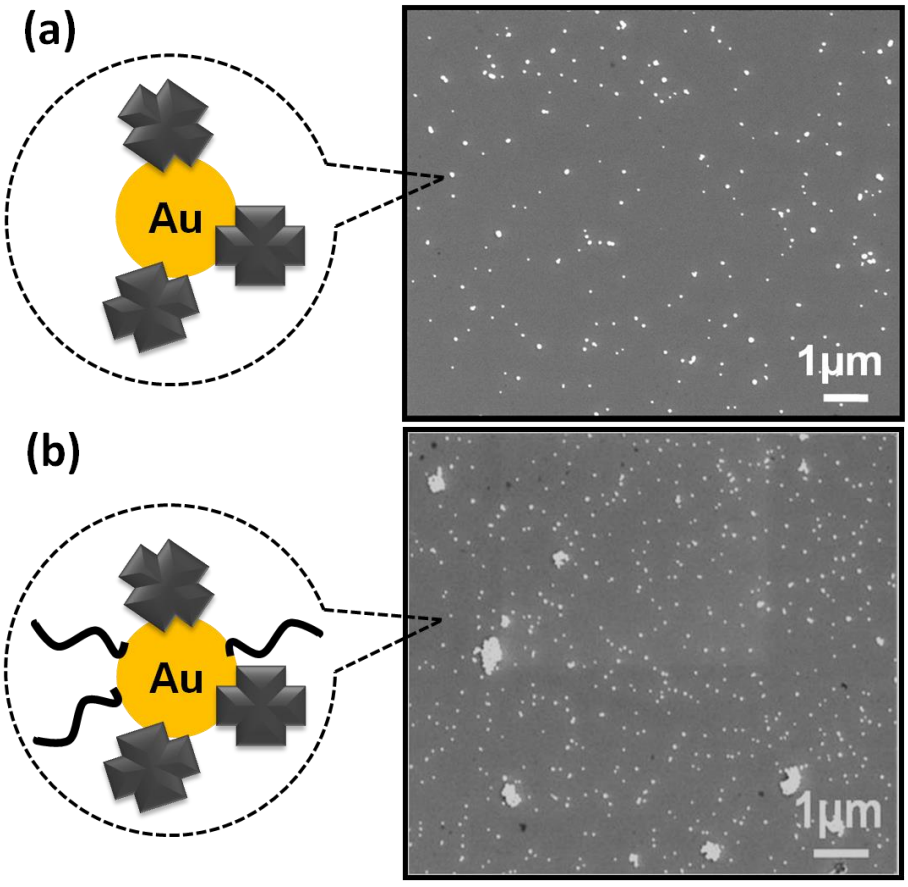

Figure 2.14. SEM images of the surfaces of the sensing plates. FIX and the biotinylated aptamer were immobilized and PEG-*b*-PAAc was attached as a blocking material. (a) SA-GNPs were attached on them. (b) N6-PEG-coated SA-GNPs were attached on them.

2.4.6. Selective binding of aptamer to FIX in the presence of other proteins

The author have confirmed above the high sensitivity of the present sensing system to FIX. To provide further information on the selectivity of the present system, sensing experiments were carried out in the presence of other proteins. The human blood clotting cascade involves clotting factors other than FIX, as well as major additional components such as albumin. Therefore, the author studied the reaction with the complex mixture of FIX containing FXIa and FVIIa, or albumin. FXIa is involved in the cleavage of FIX in the intrinsic clotting pathway, and FVIIa plays an important role in the cleavage of FIX during the extrinsic clotting pathway.[29] These components of human plasma are present in different quantities: FIX, 3–5 μg/mL;[32] FVIIa, 3.6 ng/mL;[33] FXI, 3–6 μg/mL;[34] and albumin, 45 mg/mL.[35] If it can detect FIX selectively among these activation factors, it is anticipated that we will be able to precisely determine blood activation level. Albumin is one of the major components of blood protein (45 mg/mL; 50–70% of blood protein). It is therefore important to confirm that FIX can be detected in such a large excess of albumin. In the mixture containing human clotting proteins (FIX, FXIa, and FVIIa), at levels similar to those in human blood, the author could find the specific interaction of anti-FIX aptamer with dose-dependent FIX (Figure 2.15). Titrations were performed with concentrations lower than the saturation levels (5 pg/mL-55 ng/mL) from the above experiments using PEG-*b*-PAAc and N6-PEG. We observed a similar detection limit (5 pg/mL) to that shown in the above experiments with a pure sample containing only FIX (Figure 2.16). This clearly indicates that the other clotting factors do not interfere with the detection of FIX using the EFC-WM sensor. The detection experiments were also carried out in the presence of albumin. As stated above, the concentration of albumin is quite high (670 μM; 45 mg/mL) compared to FIX (~3–5 μg/mL) in human blood; a ratio of ~8400:1. Considering the diluted blood sample, we used 5.6 mg/mL of albumin and 0.5 ng/mL of FIX, which represents the same ratio (8400:1). In the presence of 5.6 mg/mL of albumin, FIX detection to be suitable for normal blood sample analyses was carried out by the present waveguide-mode sensor system.

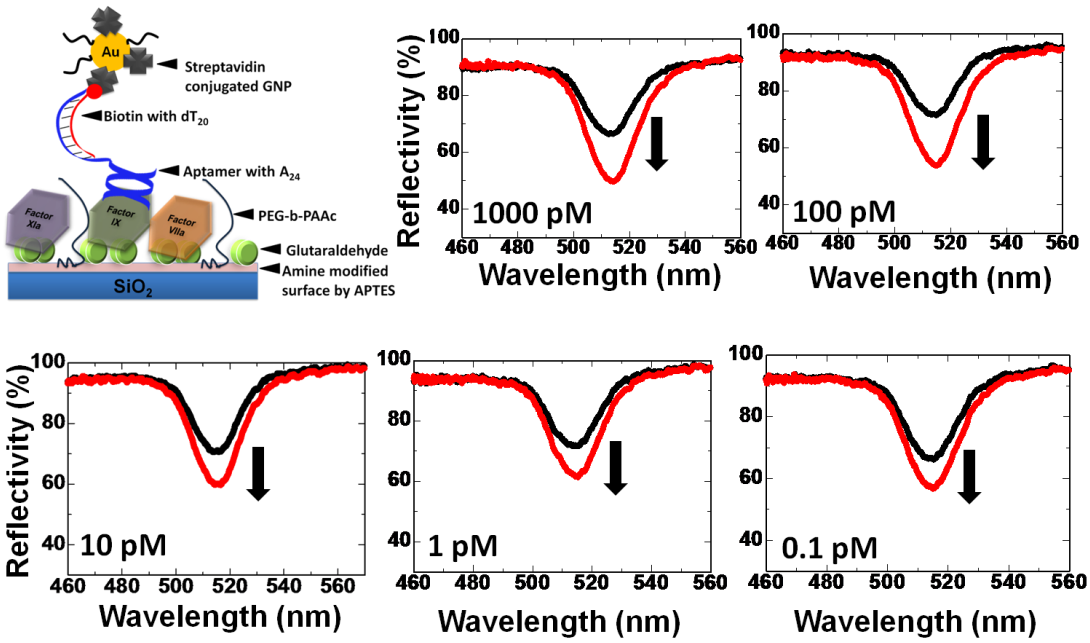

Figure 2.15. Selective binding of aptamer with FIX in the presence of other proteins. The mixture of FIX, FXIa, FVIIa. Kept FXIa (6 µg/mL) and FVIIa (8.4 ng/mL) concentrations as constant and titrated with different concentrations of FIX. Black and red spectrums indicate only buffer and attachment of streptavidin conjugated GNP, respectively. Arrows indicate the direction of changes in the spectrum.

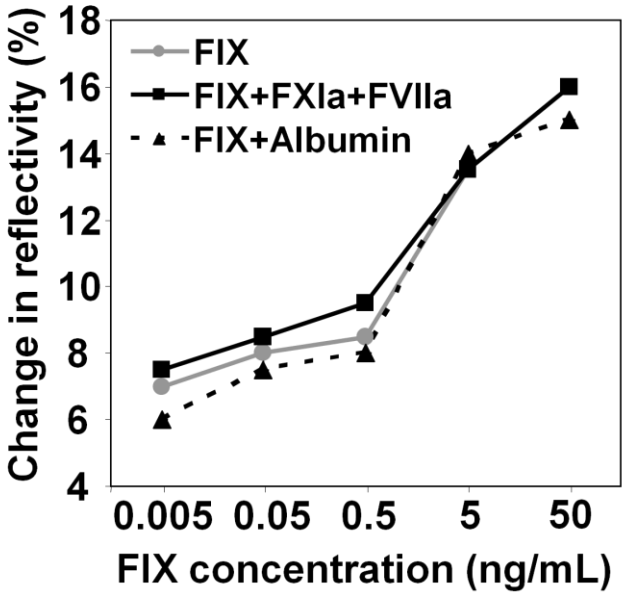

Figure 2.16. Selective binding of aptamer with FIX in the presence of FXIa and FVIIa or albumin. Titrations of different FIX concentrations against constant aptamer and other components are shown by graphical representation. FIX concentrations lower than saturation levels of previous experiments were used.

As can be seen in figure 2.16, 0.5 ng/mL of FIX in 5.6 mg/mL of albumin can be detected. In addition, the detection signal was clearly observed up to a level of 5 pg/mL (see Figure 2.17), which is 2 orders of magnitude lower than that of the normal level of FIX in blood.

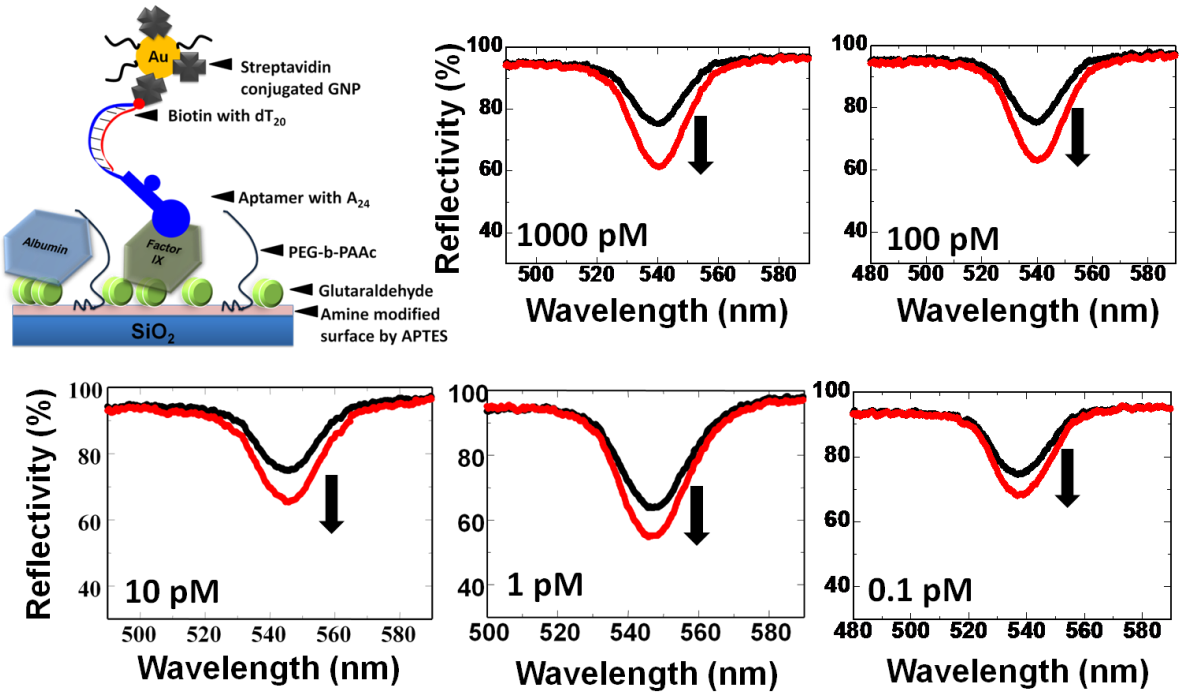

Figure 2.17. Spectra of selective binding of aptamer with FIX from the mixture of FIX and albumin. Albumin concentration was kept as 84 nM and titrated against different concentrations of FIX. Black and red spectrums indicate only buffer and attachment of streptavidin conjugated GNP, respectively. Arrows indicate the direction of changes in the spectrum.

It is also confirmed that the detection limit is the same as that without albumin, as shown in figure 2.16. At present, an aptamer generated against FIXa is undergoing phase 2 clinical trials. Owing to its high specificity against FIXa in blood samples, this aptamer is injected into patients via percutaneous coronary intervention.[36] FIX-aptamer also shown to work well with human plasma containing FIX and FIX-deficient plasma spiked with FIXa,[29] both studies corroborates our results for the FIX in mixed protein samples. The detection system demonstrated in the present investigation, which is resistant to biofouling, would be useful in determining the abundance of FIX in blood samples containing multiple proteins.

2.5. Conclusions

The author has designed a new biosensing system for detecting human coagulation FIX by using its aptamer and GNPs and a waveguide sensor. The Glu-modified sensor chip surface was brought into contact with the FIX sample, and was subsequently blocked using PEG-*b*-PAAc. This blocking treatment completely prevents non-specific binding on the sensor surface. It is interesting to note that coating of SA-GNPs by N6-PEG improved the detection limit to 0.1 pM. The higher sensitivity arises from the crowding effect of N6-PEG on the SA-GNPs, which occupy a certain number of the active biotin-binding sites on the streptavidin. Based on these results, it is concluded that PEG-*b*-PAAc and N6-PEG may be the ideal blocking agents for use in the development of an aptamer-based sensing system (aptasensor) with higher specificity. An FIX detection limit of 0.1 pM was attained even in the presence of other coagulation factors or a realistic albumin concentration. The strategy developed in this study by using an anti-FIX aptamer to detect minute amounts of FIX in a mixed sample (which represents blood serum) is highly recommended for finding clotting deficiencies in human samples.

2.6. References

1. Nagasaki, Y., *Poly. J.* **2011**, 43, 949-958.
2. Hermanson, G.T., Bioconjugate Techniques 2nd Edn. Academic Press, Waltham. **2008**.
3. Otsuka, H., Nagasaki Y., Kataoka, K., *Biomacromolecules* **2000**, 1, 39-48.
4. Nagasaki, Y., Kobayashi, H., Katsuyama, Y., Jomura T., Sakura, T., *J. Colloid. Interface Sci.* **2007**, 309, 524-530.
5. Kamimura, M., Miyamoto, D., Saito, Y., Soga K., Nagasaki, Y., *Langmuir* **2008**, 24, 8864-8870.
6. Yuan, X., Yoshimoto K., Nagasaki, Y., *Anal. Chem*. **2009**, 81,1549-1556.
7. Yoshimoto, K., Nozawa, M., Matsumoto, S., Echigo, T., Nemoto, S., Hatta T., Nagasaki, Y., *Langmuir* **2009**, 25, 12243-12249.
8. Yoshimoto, K., Nishio, M., Sugasawa H., Nagasaki, Y., *J. Am. Chem. Soc.* **2010**, 132, 7982-7989.
9. Uchida, K., Otsuka, H., Kaneko, M., Kataoka K., Nagasaki, Y., *Anal. Chem.* **2005**, 77,1075-1080.

10. Nagasaki, Y., *Chem. Lett.* **2008**, 37, 564-569.
11. Miyamoto, D., Oishi, M., Kojima, K., Yoshimoto K., Nagasaki, Y., *Langmuir* **2008**, 24, 5010-5017.
12. Fujimaki, M., Rockstuhl, C., Wang, X., Awazu, K., Tominaga, J., Koganezawa, Y., Ohki Y., Komatsubara, T., *Opt. Exp.* **2008**, 16, 6408-6416.
13. Lukosz, W., *Biosens. Bioelectron*. **1991**, 6, 215-225.
14. Schlottig, F., Textor, M., Georgi U., Roewer, G., J*. Mater. Sci. Lett*. **1999**, 18, 599-601.
15. Kumar, P., Choithani J., Gupta, K.C., *Nucleic Acids Res.* **2004**, 32, e80.
16. Tang, C.S., Schmutz, P., Petronis, S., Textor, M., Keller B., Vörös, J., *Biotechnol. Bioeng*. **2005**, 91, 285-295.
17. Liu, H., Venkataraman, N.V., Bauert, T.E., Textor M., Xiao, S., *J. Phy. Chem. A* **2008**,112,12372-12377.
18. Rong, G., Najmaie, A., Sipe J.E., Weiss, S.M., *Biosens. Bioelectron.* **2008**, 23,1572-1576.
19. Gopinath, S.C.B., Awazu, K., Tominaga J., Kumar, P.K.R., *ACS Nano* **2008**, 2, 1885-1895.
20. Gonçalves, D., Prazeres, D.M.F., Chu V., Conde, J.P., *Biosens. Bioelectron*. **2008**, 24, 545-551.
21. Bolduc, O.R., Live, L.S., Masson, J., *Talanta* **2009**,77,1680-1687.
22. Fujimaki, M., Nomura, K., Sato, K., Kato, T., Gopinath, S.C.B., Wang, X., Awazu K., Ohki, Y., *Opt. Exp*. **2010**, 18, 15732-15740.
23. Chin, C.D., Laksanasopin, T., Cheung, Y.K., Steinmiller, D., Linder, V., Parsa, H., Wang, J., Moore, H., Rouse R., Umviligihozo, G., Karita, E., Mwambarangwe, L., Braunstein, S.L., van de Wijgert, J., Sahabo, R., Justman, J.E. El-Sadr, W., Sia, S.K., *Nature Med.* **2011***,* 17, 1015-1019.
24. Kretschmann, E., *Z Physik* **1971**, 241, 313-337.
25. Schmitt, K., Hoffmann, C., Eds. Zourob, M. & Lakhtakia, A., Optical Guided-wave Chemical and Biosensors I, Springer Series on Chemical Sensors and Biosensors 7, Springer-Verlag, Berlin Heidelberg, **2010**, 21-54.
26. Gopinath, S.C.B., Awazu, K., Fujimaki, M., Sugimoto, K., Ohki, Y., Komatsubara, T., Tominaga, J., Gupta, K.C. and Kumar, P.K.R. *Anal. Chem.* **2008**, 80, 6602-6609.
27. Fujimaki, M., Nomura, K., Sato, K., Kato, T., Gopinath, S.C.B., Wang, X., Awazu, K., Ohki, Y. *Opt. Exp.* **2010**, 18, 15732-15740.
28. Rusconi, C.P., Scardino, D., Layzer, J., Pitoc, G.A., Ortel, T.L., Monroe, D., Sullenger, B.A., *Nature* **2002**, 419, 90-94.
29. Gopinath, S.C.B., Shikamoto, Y., Mizuno H., Kumar, P.K.R., *Thromb. Haemost.* **2006**, 95, 767-771.
30. Citartan, M., Tan, S., Tang, T., *World J. Microbiol. Biotechnol.* **2011**, 1, 105-111.

31. Duan, X., Li, Y., Rajan, N.K., Routenberg, D.A., Modis Y., Reed, M.A. *Nat. Nanotechnol.* **2012***,* 7, 401-407.
32. Halkier, T., In.: Mechanisms of Blood coagulation, Fibrinolysis and the complement system. Halkier, T., Wooley, P., Ed.; Cambridge University Press: Cambridge, U.K., 1992; p25.
33. Morrissey, J.H. Macik, B.G. Neuenschwander P.F. and Comp, P.C. *Blood* 1993, 81, 734-744.
34. Wuillemin, W.A., Minnema, M., Meijers, J.C.M., Roem, D., Eerenberg, A.J.M., Nuijens, J.H., Cate H.T., Hack, C.E., *Blood* **1995**, 85, 1517-1526.
35. Baker, M.E., *J. Endocrinol.* **2002**,175, 121-127.
36. Cohen, M.G., Purdy, D.A., Rossi, J.S., Grinfeld, L.R., Myles, S.K., Aberle, L.H., Greenbaum, A.B., Fry, E., Chan, M.Y., Tonkens, R.M., Zelenkofske, S., Alexander, J.H., Harrington, R.A., Rusconi C.P., Becker, R.C. *Circulation* **2010**,122, 614-622.

Chapter 3

Co-immobilization of PEG-b-PAMA and N6-PEG Promotes Non-biofouling on Au Surface of Surface Plasmon Resonance Biosensor for Detection of FIX in Human Plasma

3.1. Abstract

Reporting clinically relevant biomolecular interactions is mandatory in the field of medical diagnosis. The major prerequisite of sensors includes measuring the specific target in a sample containing mixture of compounds, without compromising the convenience and sensitivity. On the other hand, development of surface functionalization chemistries having higher non-fouling is important. In this stream-line, using Surface Plasmon Resonance (SPR) coupled with the blocking polymers, poly(ethylene glycol)-b-poly[2-(N,N-dimethylamino)ethyl methacrylate] (PEG-*b*-PAMA), and pentaethylenehexamine-terminated poly(ethylene glycol) (N6-PEG) a detection strategy was generated for the interaction of aptamer and human coagulating factor IX protein (FIX) because its presence is extremely low *in vivo* and important. Initially gold (Au) sensor chip of SPR was modified with PEG-*b*-PAMA followed by SH-dT_{20} and duplexed with anti-factor aptamer extended with A_{24}. Further, N6-PEG was co-immobilized on sensing surface to quench the bio-fouling completely. On this dual tethered PEGylated-surface, the author determined the dissociation constant as 37±10 pM for FIX and aptamer interaction and could reach the sensitivity to 800 fM with aptamer-FIX-antibody sandwich pattern detected by GNP-conjugated anti-mouse antibody. The author could detect FIX with the abundance of albumin. Further, to mimic real detection of FIX in the clinical sample, the author demonstrated the experiments evidence with human plasma instead of FIX. Higher-sensitivity was attained due to dual polymers immobilized on Au surface and it can be a common strategy for any aptamer-protein interactions. Selective binding of the aptamer in the human blood serum-shown here, makes suitability of present strategy for detecting of clinically relevant samples.

3.2. Introduction

Biomolecular recognition is considered as mandatory to convey the importance of biomolecules to understand the events of disease and gene regulations. First reported biosensor was in 1962 having signal recognition elements and transducers, as the basic for sensor development.[1]

After this initiation, various sensors have been proposed to report biomolecular interactions, operate with principles designed for surface plasmon.[2] Among different sensing systems, Surface Plasmon Resonance (SPR) and other sensors mimics SPR dominates as a major in label-free or labeled ways of detection.[3] However, a way of detection without chemical tags is highly welcome for scalable biosensor technology with real-time monitoring with compromised sensitivity. Even though, the sensitivity varies with different systems, sensitivity is the prime determining factor for the quality of the succeeded sensors.[4] Different surface functionalization chemistries with suitable probes have been proposed to improve the sensing system. In a very early stage of sensor development, antibody was used as the probe and in 1967 first immobilized antibody solid surface was proposed by Catt and Niall[5] and later an advanced methods such as Enzyme linked Immunosorbent Assay (ELISA) was introduced followed by several antibody sensing strategies on solid surfaces were established.[6,7] Even though antibodies are potential molecule for the sensor developments in the past several decades, in 1990 an alternate molecules to substitute the antibodies was developed called `aptamer` or 'chemical antibody'. A strategy called Systemic Evolution of Ligands by Exponential Enrichment (SELEX) was introduced to generate the aptamers by three independent researchers, to find the selective molecules from the randomized molecules.[8-10] Aptamers are having the potential characteristics and behave equal to the antibodies. Combination of antibody and aptamer sensing strategy have been proposed as these molecules could complement each other.[11]

Aptamers or antibodies immobilized solid surfaces have a lower antigen capturing efficiency compared with the condition under solution due to random orientations and steric hindrances by interaction with the solid surface.[12-14] To fabricate an efficient solid-surface sensor, the proper immobilization of probe or receptor molecule on the surface of sensor is a crucial step and correctly oriented higher density immobilization would leads an improved level of detections.[14] Right orientation of biomolecules on the solid surface was succeed with the strategies of co-immobilization

of inert materials such as polymers.[15] Poly(ethylene glycol) (PEG) is one of the popular polymers, shown to have non-fouling due to their flexible nature, play an important role in the fields of biology.[16-21] PEG-*b*-polymers modified surfaces are highly efficient in reducing protein adsorption from mixture of sample, such as blood thereby improving the biocompatibility.[22,23]

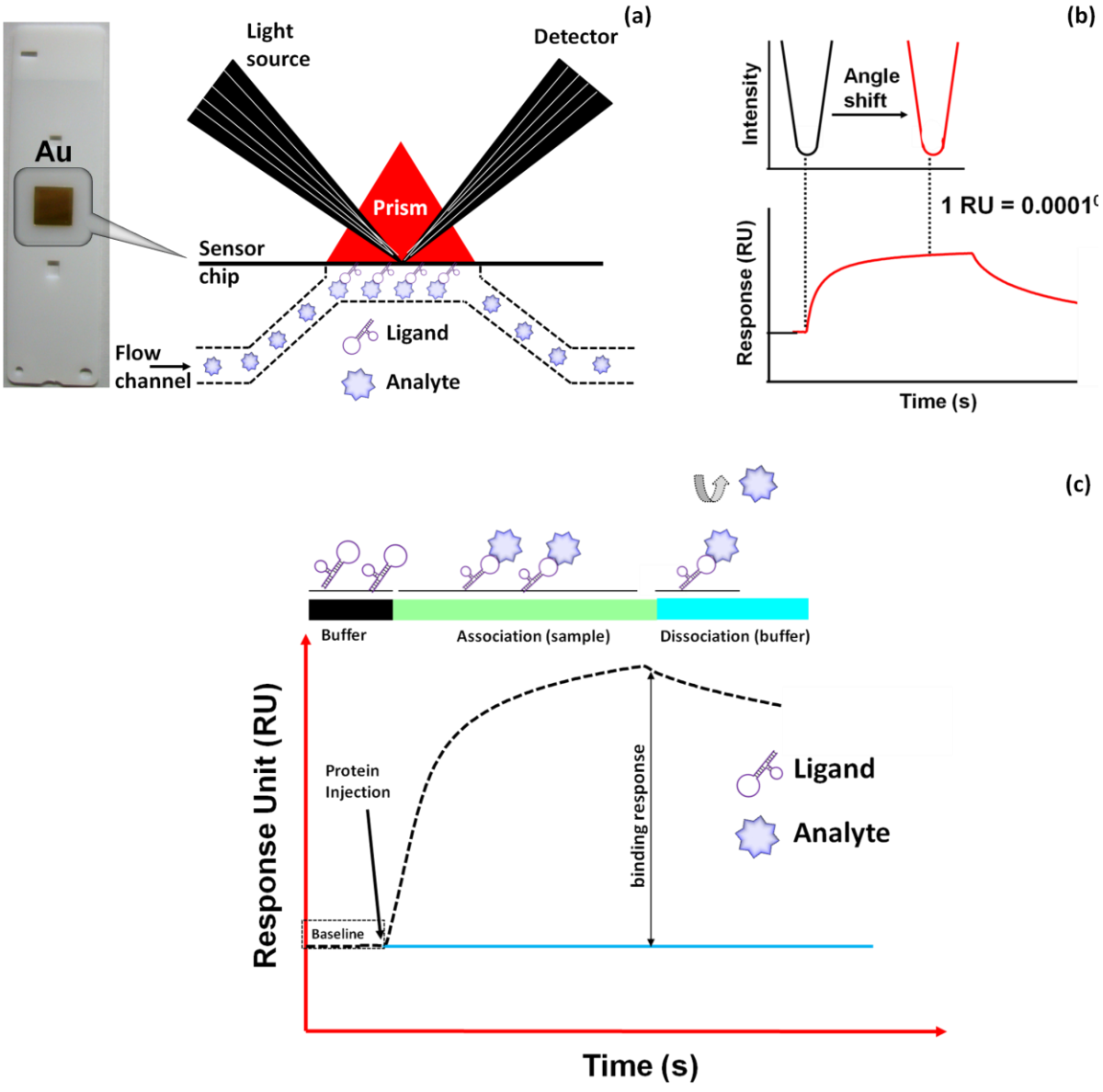

Figure 3.1. Setup in Surface Plasmon Resonance. (a) Principle in SPR for ligand and analyte interaction. The sensing surface (Au) used in SPR-Biacore is shown. (b) Typical angular changes in SPR, upon the complex formation of ligand and analyte. (c) Association and dissociation process in SPR for ligand and analyte interactions.

Natural polymers such as Bovine Serum Albumin (BSA) and Casein may not help in these aspects as it contains IgG that may cause an obstacle to antigen and cross-react with secondary antibodies.[24] PEG-based polymers have driven to overcome this issue, can synthesize chemically with varied lengths to generate high performance sensors.[15,25-28] Densely packed PEG tethered-chain surfaces, having the combination of long and short PEG dual chains greatly reduces non-specific adsorption onto the sensing surface.[19,29-32]

On the other hand, among different reported solid sensing surfaces, gold (Au) is one of the preferred metals for the sensing due to easy water dispersal, compatibility with surface functionalization, biological non-reactivity, and ability to be tailored with uniform and different nano-sizes.[33-37] In this report, a combination of Au surface and PEG-polymers were used to develop the higher sensing system with the assistance of a SPR-based Biacore system. SPR is known as the excitation of surface plasmon by monochromatic waves on the metal coated surface surrounded by biological fluid environment and the excitation of surface plasmon by light is denoted as a SPR. Absorption of molecule on the receptor layer of biosensor changes the refractive index of the layer, reporting the event of binding (Figure 3.1a-c). Using a SPR, the strategy with sandwich pattern of aptamer- FIX-antibody was performed to demonstrate the applications of PEG-*b*-polymers, namely, PEG-*b*-poly[2-(N,N-dimethylamino)ethyl methacrylate] (PEG-*b*-PAMA) and pentaethylenehexamine-terminated PEG (N6-PEG).

The biological importance of FIX was demonstrated in Hemophilia B (Christmas disease), when the FIX concentration in plasma gets abnormal from the normal level which is around 5 µg/mL (87 nM). The human plasma has clotting factors other than FIX, as well as major additional components such as albumin (45 mg/mL). It is therefore important to confirm that FIX can be detected

in such a large excess of albumin. If we can detect FIX selectively among additional components, it is anticipated that we will be able to precisely determine the active level of FIX. In this study, the author demonstrated the detection of FIX with sensing strategy as follows: (i) initially Au sensor chip of SPR modified with PEG-*b*-PAMA followed by SH-dT_{20}; (ii) complementation of aptamer-A_{24} with SH-dT_{20} (iii) unreacted Au surface was blocked by N6-PEG (iv) FIX was allowed to interact with aptamer (v) anti-FIX mouse IgG passed on the FIX modified surface (vi) anti-mouse IgG antibody conjugated-gold nanoparticle (GNP) was allowed to interact with anti-FIX antibody (vii) interaction was measured by SPR.

3.3. Experimental section

3.3.1. Reagents and biomolecules

Anti-mouse IgG (H+L) - 40nm GNP Conjugate from Cytodiagnostics, All oligos are commercially synthesized from Tsukuba Oligo company. TaKaRa Ex Taq, DuraScribe® T7 Transcription Kit, 3-mercaptopropionic acid, Factor IX, Monoclonal Anti-Factor IX antibody produced in mouse, Human serum and BSA from Sigma Aldrich, St. Louis, USA. Sensor chip from GE healthcare, Tokyo, Japan. N6-PEG was kindly provided by JSR (Tokyo, Japan). Synthesis of PEG-*b*-PAMA is outlined by Miyamoto *et al.* and Horiguchi *et al*.[38,39] All reagents were stored according to the suppliers' recommendations.

3.3.2. Western blot analysis

The specificity of the antibody for the FIX was analyzed by standard blotting assays with an appropriate antibody. In brief, for western blot analyses, FIX was separated by sodium dodecyl sulfate (SDS)-polyacrylamide gel electrophoresis and transferred to polyvinylidene difluoride (PVDF) membrane. After immobilization of the protein, the membrane was blocked with 3% nonfat milk in Tris-buffered saline (TBS) at room temperature for 1 h and then treated with a 1:10,000 dilution of the

primary antibody (anti-FIX) at 4°C overnight. After removal of unbound primary antibody by washing, the membrane was incubated for 1 h with horseradish peroxidase (HRP)-conjugated goat anti-mouse immunoglobulin G (secondary antibody). The immunocomplexes thus formed were visualized by staining with ECL-plus western blotting detection solution. The specificity of primary antibody interactions with secondary antibody was analyzed by a standard dot-blotting method using different dilutions of primary antibody, and immunocomplexes were identified using a 1:1000 dilution of secondary antibody, followed by ECL-plus western blotting detection.

3.3.3. Enzymatic synthesis of aptamer

A stable 33-mer (2′-fluoro-modified) RNA-aptamer (FIX-aptamer), which was previously reported by Rusconi et al.[40] was prepared and its ability to bind FIX or FIXa was verified.[40,41] Detailed the preparation of FIX aptamer by *in vitro* transcription is in chapter 2.

3.3.4. Interactive analyses of aptamer and FIX

Initially Au sensing surface of SPR was modified with PEG-*b*-PAMA followed by SH-dT_{20} and duplexed with FIX-aptamer extended with A_{24}. Different concentrations of FIX (0.8 pM to 80 nM) were injected to determine the dissociation constant and the limit of detection. On the FIX immobilized surface anti-FIX mouse antibody (FIX-antibody) followed by GNP-conjugated anti-mouse IgG (mouse IgG-GNP) was passed. A four line Biacore system (Biacore 3000) used for all the experiments. Among these, one flow channel was always used for control experiment. Flow rates carried out are as follows, PEG-*b*-PAMA (10 µL/min, 300 µl), SH-dT_{20}, Aptamer-A_{24} (2 µL/min, 20 µL), N6-PEG (10 µL/min, 300 µL), FIX, FIX antibody, mouse IgG-GNP (10 µL/min, 50 µL). Immobilized aptamer was regenerated by 10 mM NaOH (60 µL/min,5 µL). All the measurements were carried out at 25º C. To find the saturated concentration of each biomolecule for the strategy above explained, the author titrated the optimal biomolecule concentration. For that, first different concentrations of PEG-*b*-

PAMA (2 mg/mL to 50 mg/mL) were injected on the Au surfaces. Then different concentrations (1 µM to 5 µM) of SH-dT_{20} were injected on the optimized PEG-*b*-PAMA immobilized surfaces. Similarly, we also titrated the aptamer concentrations from 500 nM to 1000 nM on the optimized SH-dT_{20} modified surfaces. FIX-antibody titration (25 nM to 200 nM) was also carried out on the FIX (200 nM) immobilized surfaces.

3.3.5. Interactive analyses of antibody and FIX

The Au surface modified with COOH, using 3-mercaptopropionic acid to immobilize the FIX antibody. Before that initially the author did pH scouting on surface modified with COOH to immobilize the FIX antibody. 2 nM of FIX-antibody diluted individually with different pH (4, 4.5, 5.0, and 5.5) and passed directly on the COOH modified surfaces. With the suitable pH, the antibody was immobilized on the COOH modified Au surfaces after activated by 100 mM *N*-hydroxysuccinimide (NHS) and *N*-ethtyl-*N'*-(3-dimethylaminopropyl)carbodiimde hydrochloride (EDC). Then, remaining free COOH-surfaces were blocked by 10 mg/mL of N6-PEG or 1 M ethanolamine. Different concentrations of FIX (30 nM to 240 nM) were injected on the FIX-antibody immobilized surfaces. For the comparison of our surface modification the same experiment was done with the commercial CM5 chip.

3.3.6. Dissociation constant of FIX-aptamer and FIX-antibody against FIX

To find the dissociation (Kd) value of FIX and aptamer, different concentration of FIX (15 nM to 120 nM) on the constant (500 nM) aptamer injected immobilized surfaces. And also to check the FIX-antibody dissociation constant, the author injected different concentrations of FIX (30 nM to 240 nM) on the constant FIX-antibody (200 nM) immobilized surfaces. Kd value is calculated using the BIA-Evaluation software by association and dissociation of FIX on aptamer and antibody immobilized surfaces. The rate of association was measured from the forward reaction, and the dissociation rate was measured from the reverse reaction. The equilibrium dissociation rate constant *(K*d) was

calculated by *k*d/*k*a, (*K*d- equilibrium dissociation constant; *k*d - dissociation rate; *k*a - association rate).

3.3.7. Sandwich assay

To detect the FIX here the author performed two kinds of sandwich assay, such as aptamer-FIX-antibody (200 nM antibody was passed on the aptamer-FIX immobilized surfaces) and antibody-FIX-aptamer (500 nM aptamer was passed on the antibody-FIX immobilized surfaces). Different binding sites of aptamer and antibody on FIX was confirmed by SPR and gel-shift assay. For SPR, on the aptamer and FIX (120 nM) immobilized surface, different concentrations (25 to 200 nM) of antibody were passed (10 µL/min, 50 µL). For the gel-shift assay, the author used the native polyacrylamide gel electrophoresis (Native-PAGE). Before loading on the gel, aptamer (0.3 µg) was denatured at at 90ºC for 2 min and cooled to room temperature then pre-mix was made with different ratios of FIX (1:3, 1:6 and 1:9) in 10 mM Hepes-KOH (pH 7.4) buffer containing, 150 mM NaCl and 2 mM $CaCl_2$. $CaCl_2$ was added after the denaturing step. Similarly, aptamer:FIX:antibody pre-mix was made with different ratios (1:3:6, 1:3:12, and 1:3:24). After incubation at room temperature for 10 min, all mixes were resolved on 10% Native-PAGE. Control lane was loaded with only the denatured aptamer. Gel was run with 150 V for 1 hr and stained with ethidium bromide. After that gel was detained with ddH_2O and image was photographed.

3.3.8. Limit of detection of FIX in the presence of albumin or human plasma

To check the limit of detection of FIX the author titrated with the FIX concentrations from 0.8 pM to 80 nM on the FIX-aptamer (500 nM) immobilized surfaces followed by the constant FIX-antibody (200 nM), and mouse IgG-GNP (0.1 OD). Control experiments were carried out with complementary of FIX- aptamer. Limit of detection is calculated with the value 3 times higher resonance changes than the control experiment.. For selective binding which mimics a similar situation in the blood samples, experiments with mixed albumin was carried out. Different concentrations of FIX (from 0.8 pM to 8000

pM),mixed with constant higher concentration of albumin (45 mg/mL) passed on the FIX-aptamer immobilized surface. Then constant FIX-antibody (200 nM) and mouse IgG-GNP (0.1 OD) were injected. To detect the FIX in the human plasma, instead of FIX, the author injected different diluted human plasma from 1:10 to 1:1280, with half serial dilutions. All other surface chemical modifications and detection strategies were the same as those described above.

3.4. Results and Discussion

3.4.1. PEG-*b*-PAMA assisted immobilization of Aptamer on Au surface

Prior to check the interaction of aptamer and FIX, preliminary assessment was performed by immobilizing PEG-*b*-PAMA on Au surface at different pH of acidic (4.0), neutral (7.4) and alkali (9.0). The responses obtained by SPR were similar with all the above pH conditions, indicates the stability of PEG-*b*-PAMA under these conditions. Similar uneffectiveness of varied pH conditions was reported by Yoshimoto *et al*.[42] It was reported that adsorption of PEG-*b*-PAMA on the Au surface was not affected by strong ionic condition.[42,43] Due to ideal condition with the SPR system recommended by manufacturer, neutral condition (pH 7.4) was desired for further experiments. At this pH the response was reached (1200 RU) with 6 mg/mL of PEG-*b*-PAMA reconstructed surface and the response will increase further to only a few hundreds upon increasing the concentration to 12, 25, and 50 mg/mL. The saturation level was attained at PEG-*b*-PAMA concentration of 6 mg/mL. PEG-*b*-PAMA attachment on Au was occurred through the reaction of the lone pair of the amino groups of the PAMA chain, having a strong affinity to the Au atoms.[39] The polyamine segment PEG-*b*-PAMA interacts with a Au surface via co-ordination of nitrogen atom.[43] After attach the PEG-*b*-PAMA, the author analysed the immobilization of thiolated-DNA oligo (SH-dT_{20}) on the PEG-*b*-PAMA modified Au surface, in order to make the duplex with the aptamer to be analyzed (Figure 3.2a). Clear response (600 RU) was observed with 1 µM level. The response was increased further when the concentration of SH-dT_{20} was increased to 2 µM (900), at the concentration of 3 µM (980) higher immobilization of SH-dT_{20} on

PEG-*b*-PAMA surface was attached with the saturation level. Whereas, when the PEG-*b*-PAMA was neglected from the sensing surface, lesser SH-dT_{20} was bound even at this concentration (Figure 3.2b). Inclusion of PEG-*b*-PAMA saturated with 3 µM of SH-dT_{20} and promotes the proper attachment due to the cationic charge of the PAMA segment on the periphery of the Au surface.[39]

Previously, it was reported that PEG-*b*-PAMA co-immobilized surface with SH-ssDNA supports the proper duplex formation and behave efficiently.[44-46] Yoshimoto et al.[45] have found the role of PEG-*b*-PAMA on Au surface for the immobilization of SH-DNA and it would be stronger even under stringent aqueous condition. Sulfanyl-group with single strand DNA has strong interaction on Au surface was reported to be potential when co-immobilized with PEG and the increment until 5 folds compared to the baregold.[45]

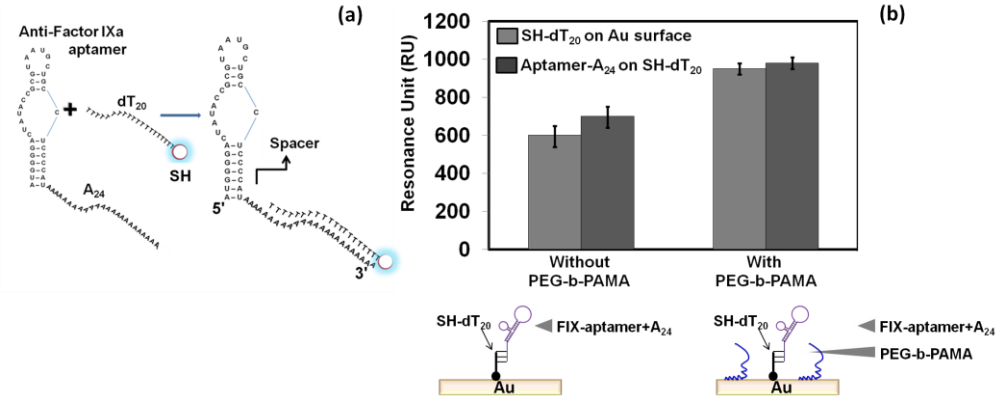

Figure 3.2. Evaluation of immobilization of SH-dT_{20} and aptamer-A_{24} duplex formation on Au surface. (a) Schematic for SH-dT_{20} and aptamer-A_{24} duplex. (b) analyses of SH-dT_{20} and aptamer-A_{24} in the presence and absence of PEG-*b*-PAMA. Tested with 3 µM of SH-dT_{20} and 500 nM of aptamer-A_{24}. Cartoon as inset illustrates the strategies.

With this ideal situation, a stable FIX-aptamer (2' fluoro-modified) extended with A_{24} (20 bases for complementation and 4 bases for spacer), was passed. With the injection of FIX-aptamer, the author could notice the proper duplex of aptamer on the SH-dT_{20} with nicely displayed

sensogram to 900 RU, with the concentration of 500 nM. The aptamer-A_{24} interaction with the SH-dT_{20} noticed with higher response on the PEG-*b*-PAMA modified surfaces compared to the surface free from PEG-*b*-PAMA (Figure 3.2b). The optimal PEG chain density on the surface might improve the orientation of the immobilized SH-dT_{20} resulting in an improvement in the aptamer immobilization. A suitable density of surrounding PEG chains prevented the immobolized aptamer from lying down or nonspecically bind on the Au surface, and improve the conjucation efficacy with the FIX. This concentration (500 nM) against the saturated level of SH-dT_{20} with 3 µM is in the ratio of 6:1 (aptamer: SH-dT_{20}). The responses of sensogram at these two concentrations are same even the ratio are different, this might be due to difference in the size of these two molecules.

3.4.2. Co-immobilization of PEG-*b*-PAMA and N6-PEG promotes non-biofouling on Au surface for detection of FIX

After aptamer immobilization the remaining Au surface was masked by BSA with higher concentration (45 mg/mL). On this BSA masked surface the author injected by different concentrations of FIX in the HEPES buffer containing calcium ions.

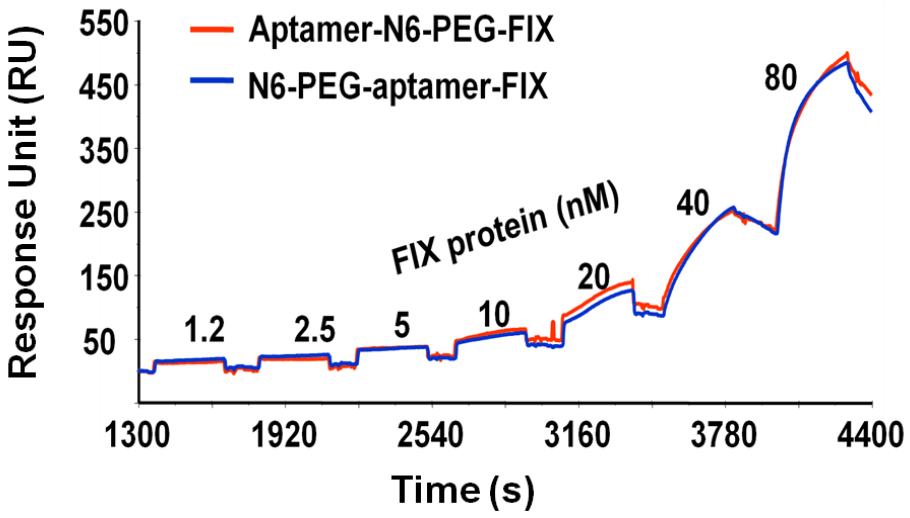

Figure 3.3. Determination of stability of aptamer upon N6-PEG attachment. Immobilization of FIX on the Aptamer-N6-PEG modified surface (Red) and N6-PEG-aptamer modified surfaces (blue).

Inclusion of calcium ions to the reaction mix mimics the physiological conditions under which blood is enriched with calcium. In the absence of calcium ion aptamer could not interact with FIX [40,47]. Even though, with the assistance of BSA, the author could observe the specific interaction of aptamer and FIX, there was non-specificity still exists. Efficiency of BSA blocking is might be less, due to acidic nature of BSA.[48] Further, BSA blocked surface has negative charge and compete with the interactions of negatively charged protein to be analysed and also mask the preloaded antibody from the complex formation.[48] To overcome this issue, the author used N6-PEG blocking instead of BSA after aptamer immobilization. N6-PEG (6 kDa) has 6 amino groups at one end of the chain to interact with Au surface. N6-PEG has eletrostatically attractive force and this effect is three times higher than PEG with mono-amine end.[15] The coordination of the lone pair of the amino groups to the Au surface is involved in this reaction makes Au-surface is long-term stable than a common Au-S linkage.[15,30,49,50]

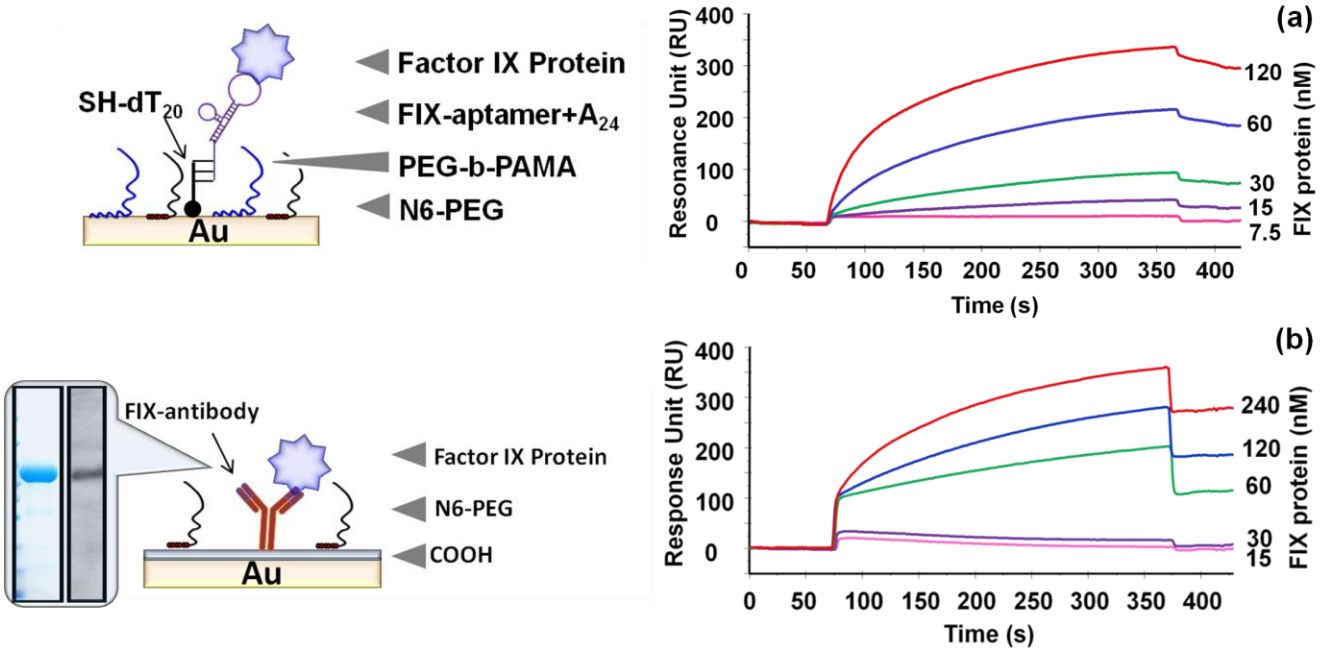

Figure 3.4. Determination of dissociation constant. (a) FIX-aptamer interaction. FIX with different concentrations (7.5 to 120 nM) were passed on the FIX aptamer immobilized surface. (b) FIX-antibody interaction. FIX with different concentrations (15 to 240 nM) were passed on the FIX antibody immobilized surface. Samples were injected at the flow rate of 10 µl/min. All experiments were performed with 10 mM HEPES buffer (pH 7.4) containing 150 mM NaCl and 2 mM $CaCl_2$. Figure inset is shown for purity of FIX on SDS-PAGE and FIX-antibody specificity by western blot analysis.

To determine the strength of the attached N6-PEG the author tested with two kinds of experiments, in one set-up after attach aptamer, N6-PEG was passed and in other case, it is vise-versa (passed N6-PEG then aptamer). In both cases, the author could find the same kind of responses, even with the consequent injections of FIX with different concentrations (Figure 3.3). These increments with N6-PEG indicate the specificity occurred with the assistance of PEG-*b*-PAMA and N6-PEG for aptamer and FIX interactions. Previously, higher increment in the S/N with N6-PEG was reported compared with BSA as the blocking agent.[30] Moreover, the isoelectric point (pI) of BSA (4.7) is lower than the experimental condition performed (pH 7.4), as stated by Nagasaki.[15]

3.4.3. Dual polymers-assisted interaction - Determination of dissociation constant of aptamer and FIX

To access the dissociation constant of FIX and FIX-aptamer interaction in the presence of PEG-*b*-polymers, the author performed the experiments with different combinations of PEG-*b*-polymers and compared BSA blocked Au surface. These combinations include, only BSA, only N6-PEG, only PEG-*b*-PAMA, PEG-*b*-PAMA with BSA and PEG-*b*-PAMA with N6-PEG. Based on the responses of lower concentrations (15 to 120 nM) of FIX obtained, (Figure 3.4a) evaluation was done using the Biacore Evaluation software, and were fitted with a 1:1 binding model (for the interaction between aptamer and FIX according to the equation A+B=AB). The lowest dissociation constant (Kd) (highest sensitive) for aptamer and FIX interaction was 37±10 pM with the combinations of PEG-b-PAMA and N6-PEG. However, in other cases for the same interaction, Kds were 684±15 pM (only BSA), 278±8 pM (only N6-PEG), 142±5 pM (only PEG-*b*-PAMA) and 80±7 pM (PEG-*b*-PAMA and BSA) (Table 3.1). Based on the comparison between these results, it seems the association rate is nearly same in all the cases, whereas there were changes in dissociation rates, indicate difference in the stability of the biomolecular attachment in the presence PEG-*b*-polymers.

Blocking agent	Association constant $K_a(M^{-1}S^{-1})$	Dissociation constant $K_d(S^{-1})$	Equilibrium constant $K_D(M)$
BSA	4.16×10^{4}	2.85×10^{-5}	$6.84 \pm 1.5 \times 10^{-10}$
N6-PEG	2.8×10^{4}	1.26×10^{-5}	$4.5 \pm 0.8 \times 10^{-10}$
PEG-*b*-PAMA	2.44×10^{4}	3.46×10^{-6}	$1.42 \pm 0.5 \times 10^{-10}$
PEG-*b*-PAMA & BSA	3.86×10^{4}	3.13×10^{-6}	$8.1 \pm 0.7 \times 10^{-11}$
PEG-*b*-PAMA & N6-PEG	3.4×10^{4}	1.26×10^{-6}	$3.7 \pm 1.0 \times 10^{-11}$

Table 3.1. Kinetic parameters for the interaction of aptamer and FIX in the presence of different combinations of PEG-*b*-polymers

Among these choices, a dual PEG-polymer (PEG-*b*-PAMA with N6-PEG) has shown higher responses, makes the clear appealing application of PEG-*b*-PAMA, which made the proper construction on the sensing surface. On the other hand N6-PEG improved the non-fouling and completely controlled the bio-fouling. Previously, it was proved that the K_D of FIX and aptamer is 580 pM by filter binding assay.[40] In this study, PEG-*b*-PAMA with N6-PEG polymers are drastically reduce the back-ground noice and improve the sensitivity and specificity. Higher molecular weight blocking agents [BSA (66 kDa), casein (>20 kDa) and gelatin (>100 kDa)] causes interference with molecular recognition site, whereas polymers are having lower molecular weights (~10 kDa).[15]

3.4.4. Determination of dissociation constant of antibody and FIX on the N6-PEG modified COOH surface

To compare the interactions of aptamer and FIX, the author also evaluated the Kd of FIX-aptamer, FIX-antibody interaction on COOH modified Au surface and the commercially availed CM5 chip. The author could observe the specific binding of FIX to the antibody on the Au surface in dose-dependent manner with N6-PEG or ethanolamine as a blocking (Figure 3.4b). It was also noticed the binding of FIX even in the absence of antibody when ethanolamine used as a blocking. (Figure 3.5a). Ethanolamine is considered as one of the believable blocking for the COOH modified surfaces, but still some of the active group on the COOH surface gives non-specificity with FIX, because amine in the

protein easily bind on the COOH surface. To avoid these nonspecific bindings one way is to block the remaining COOH on the surfaces. Here, the author used N6-PEG instead of ethanolamine and it was found that complete quenching of nonspecific binding of FIX by the strong interaction of amine groups in the N6-PEG with COOH surfaces and gradually increase the specific response with different concentrations of FIX on FIX-antibody (Figures 3.4b & 3.5b). N6-PEG not only suppresses the bio-fouling as shown in the figure and also increases the responses compared with ethanolamine blocked surface. The author found that N6-PEG is the suitable blocking agent for Au surface, and also its very effective on COOH modified surfaces. When different concentrations of FIX was injected on the FIX-antibody hybridized N6-PEG surfaces the author could see the clear increment with increasing concentration of FIX and the K_D for specific interaction of FIX and antibody were determined as 48±12 nM (Figure 3.4b). It is interesting to note that in both aptamer-FIX and antibody-FIX interactions, N6-PEG played a major role to prevent the bio-fouling. For comparision the author also did the same antibody-FIX using the commercially COOH modified CM5 chip. It was found that the same response increases with FIX and anti-FIX antibody interaction on both N6-PEG and ethanolamine blocked surfaces (Figure 3.6 a,b).

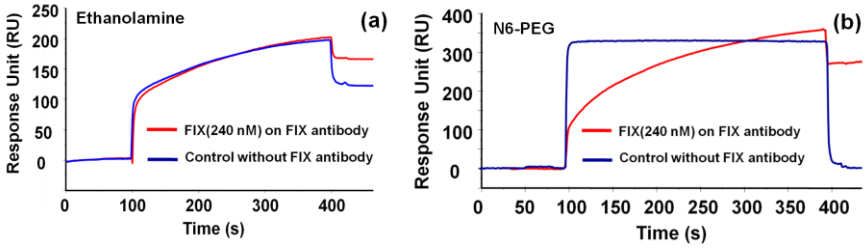

Figure 3.5. Comparative analyses between ethanolamine and N6-PEG for FIX-antibody and FIX interaction. SPR analyses for the specific and non-specific interaction in the presence of (a) ethanolamine and (b) N6-PEG.

The k_D was found as 25±15 nM, which is very close to N6-PEG modified surface (Table 3.2). However, it can be inferred that N6-PEG modified surface is much cheaper than commercial available CM5 surface.

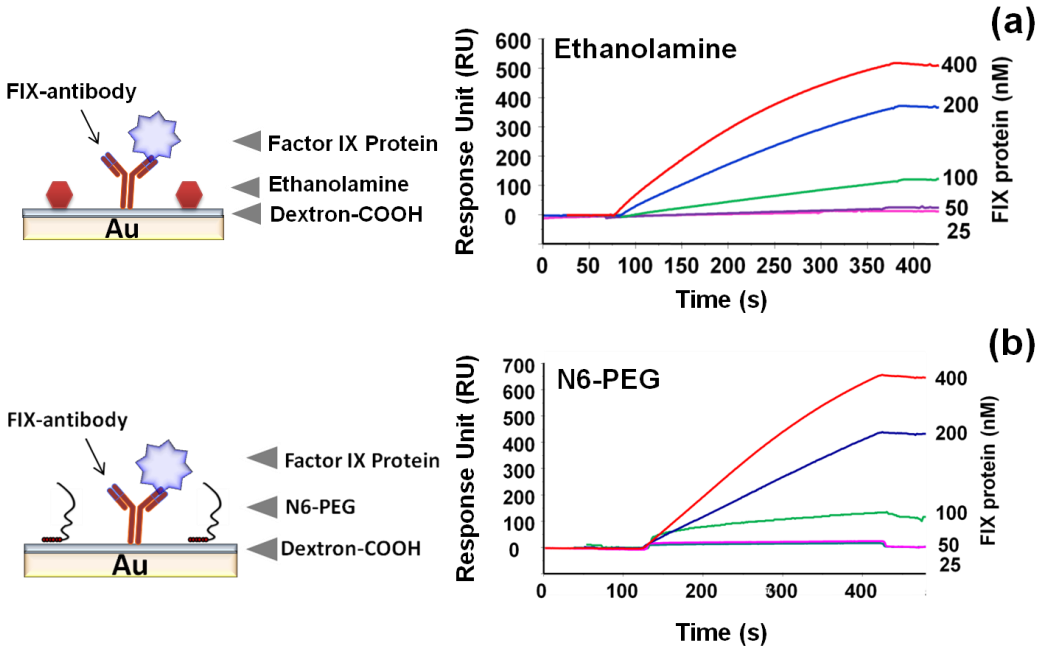

Figure 3.6. Comparative analyses on CM5 chip, between ethanolamine and N6-PEG for FIX-antibody and FIX interaction (a) SPR analyses in the presence of ethanolamine. (b) SPR analyses in the presence of N6-PEG. Cartoon illustrates the complex formation on the Au surface Samples were injected at the flow rate of 10 µL/min. All experiments were performed with 10 mM HEPES buffer (pH 7.4) containing 150 mM NaCl and 2 mM $CaCl_2$.

Sensing surface	Association constant K_a ($M^{-1}s^{-1}$)	Dissociation constant K_d (s^{-1})	Equilibrium constant K_d (M)
Au	1.15×10^{4}	5.63×10^{-4}	$48 \pm 12 \times 10^{-9}$
CM5	2.4×10^{2}	6.14×10^{-6}	$25 \pm 15 \times 10^{-9}$

Table 3.2. Kinetic parameters for the interaction of FIX-antibody and FIX in the presence of or N6-PEG.

3.4.5. Aptamer-FIX-antibody sandwich on PEGylated Au surface

Based on the above study with FIX interactions with two different probes (aptamer and antibody), the author designed the sandwich pattern on the aptamer-FIX immobilized surface by interacting with FIX- antibody. In the past, aptamer-antigen-antibody sandwich assays have been considered to obtain a higher sensitive.[11] When make the sandwich assay, the key issue is the availability of two different binding sites on the target protein (FIX) for different probes (aptamer and antibody). To make

sure about this issue, the author carried out confirmations with two kinds of experiment by SPR and gel-mobility shift. When pass the antibody on the aptamer-FIX immobilized surface of SPR, the author could see the concentration dependent attachment of anti-FIX antibody (Figure 3.7a).

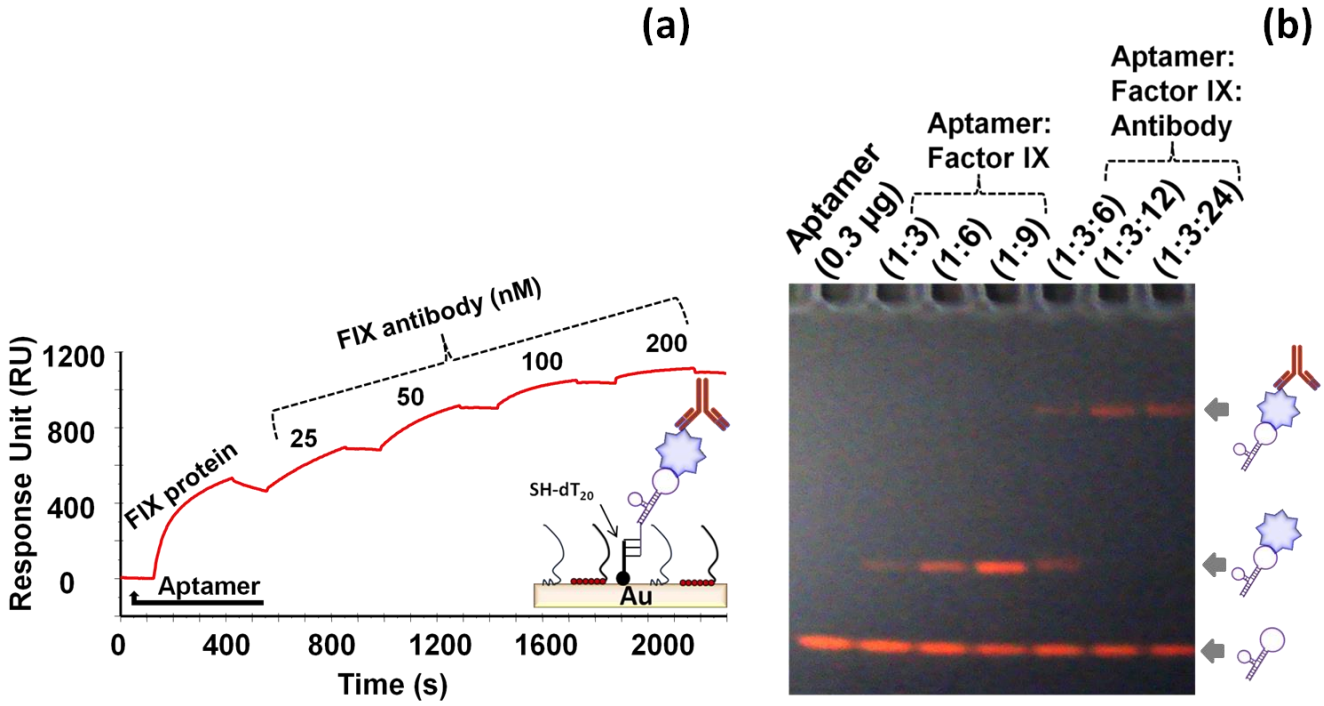

Figure 3.7. Analyses of sandwich formation with aptamer-FIX-antibody. (a) SPR analyses for the complex formation of aptamer-FIX-antibody on surface modified by PEG-polymers. After immobilization of aptamer (500 nM) and blocking with N6-PEG on Au surface FIX (200 nM) was attached. On the FIX immobilized surface different concentrations of anti-FIX antibody were passed. Figure inset is cartoon for this complex. Samples were injected at the flow rate of 10 µl/min. (b) Native-PAGE for the complex of aptamer-FIX-antibody. Shift and super-shifts were shown with aptamer-FIX and aptamer-FIX-antibody complexes. All experiments were performed with 10 mM HEPES buffer (pH 7.4) containing 150 mM NaCl and 2 mM $CaCl_2$.

This results confirm that the formation of sandwich pattern of aptamer-FIX-antibody on the sensing surface. Similarly, it was also evaluated the sandwich formation on the electrophoresis analyses by resolving different complexes (only aptamer, aptamer-FIX and aptamer-FIX-antibody) on the native-PAGE. The resolved gel-pattern showed a clear shift with aptamer-FIX complex and super-shift with aptamer-FIX-antibody complexes in dose-dependent manner (Figure 3.7b). Previously, by applying

PEG/Antibody co-immobilized magnetic beads combined with a fluorescent system, a sandwich ELISA pattern was developed by our research team to detect alpha-fetoprotein.[30] In several instances aptamers are proposed as equal or better molecule than antibodies, however, both aptamer and antibody can complement each other in sandwich assays.[11]

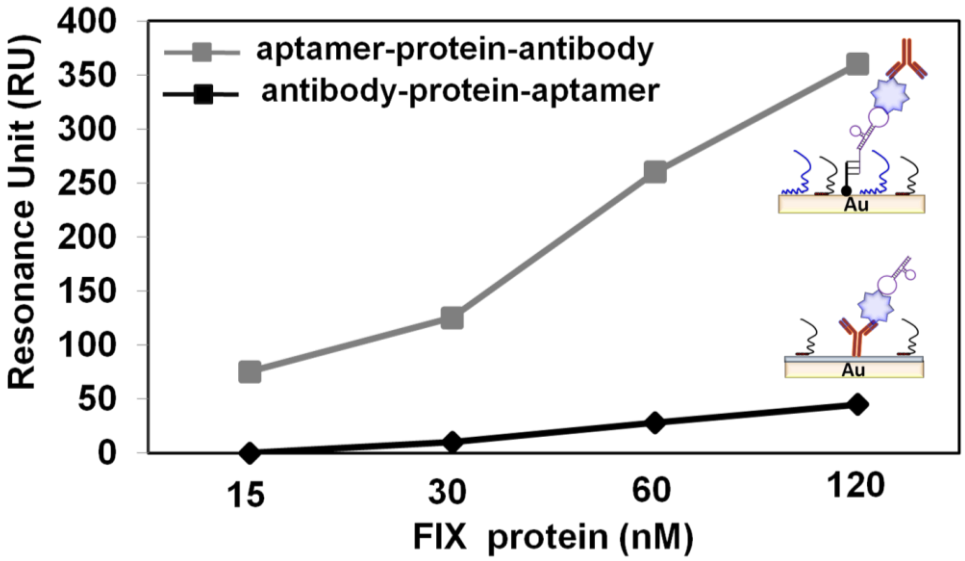

Figure 3.8. Analyses of two different sandwich patterns on PEGylated surface. Aptamer-FIX-antibody and antibody-FIX-aptamer sandwiches were compared. On the aptamer or antibody modified surfaces FIX was injected (from 15 to 120 nM). Figure inset is cartoon for this complex. Samples were injected at the flow rate of 10 µL/min.

The author also compared two different sandwich types, namely, aptamer-FIX-antibody and antibody-FIX-aptamer on the dual polymer (PEG-*b*-PAMA and N6-PEG) immobilized Au surface. With FIX concentration of 120 nM, the response obtained was 350 RU in the case of aptamer-protein-antibody sandwich pattern. Whereas, under similar condition only the response of 50 RU was obtained by antibody-FIX-aptamer strategy, showing about 7 folds lesser efficiency with antibody-FIX-aptamer sandwich. Similarly, with the injection of different FIX concentrations (15 to 120 nM), the aptamer-FIX-antibody strategy has shown the better responses, indicates the higher affinity between aptamer and FIX are suitability of aptamer-FIX-antibody strategy (Figure 3.8).

3.4.6. Sensitive detection using mouse-IgG-GNP on PEG-*b*-PAMA and N6-PEG co-immobilized Au surface for detection of FIX in mixed sample

Based on the above sandwich pattern, the author formulated a strategy with mouse IgG-GNP for higher sensitivity on the FIX antibody. Before check the sensitivity assisted with mouse IgG-GNP, the author evaluted the necessary amount of N6-PEG to block the Au surface and to reduce the non-specificity of mouse IgG-GNP on the sensing surfaces. For that, the author did the control experiment with different concentration of N6-PEG from 0 to 5 mg/mL of N6-PEG on the sensing surface in the absence of FIX. On the N6-PEG immobilized surface, mouse IgG-GNP did not show Non-specific binding, whereas in the absence of N6-PEG there was non-specificity. With increase in the N6-PEG concentration, the non-specificity decreased concomitantly, at the concentration with 5mg/mL N6-PEG, complete abolish in the nonspecific binding was occurred (Figure 3.9).

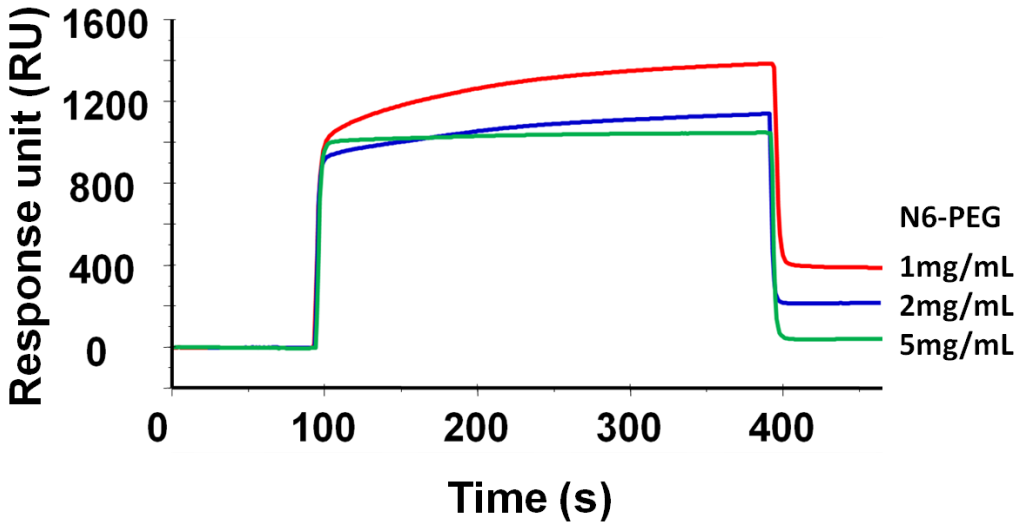

Figure 3.9. Analyses of non-specific attachment of mouse-IgG-GNP on N6-PEG modified surface. Different concentrations (1, 2 and 5 mg/mL) of N6-PEG were tested. Samples were injected at the flow rate of 10 µL/min.

This optimized concentration (5 mg/mL) of N6-PEG was used for further experiments with mouse IgG-GNP. The strategy to detect the FIX assisted with mouse IgG-GNP is shown in Figure 3.10a. With this strategy, the author performed the experiments on SPR with different combinations of

blocking agents (only BSA, only N6-PEG, only PEG-*b*-PAMA, PEG-*b*-PAMA with BSA and PEG-*b*-PAMA with N6-PEG) and injected FIX. When the author injected 80 nM of FIX, a dual PEG-polymer (PEG-*b*-PAMA with N6-PEG) was shown to be with higher display of responses (Figure 3.10b). The author could observe 3 fold higher responses in the presence PEG-*b*-PAMA and N6-PEG compared with BSA as a blocking. Moreover, almost no non-specific attachment of mouse IgG-GNP was noticed on this surface. With this dual polymer surface construction, we determined the limit of detection of FIX as 800 fM with the response of about 200 RU. With increasing the FIX concentration, the author could observe the clear increment in the responses (Figure 3.11).

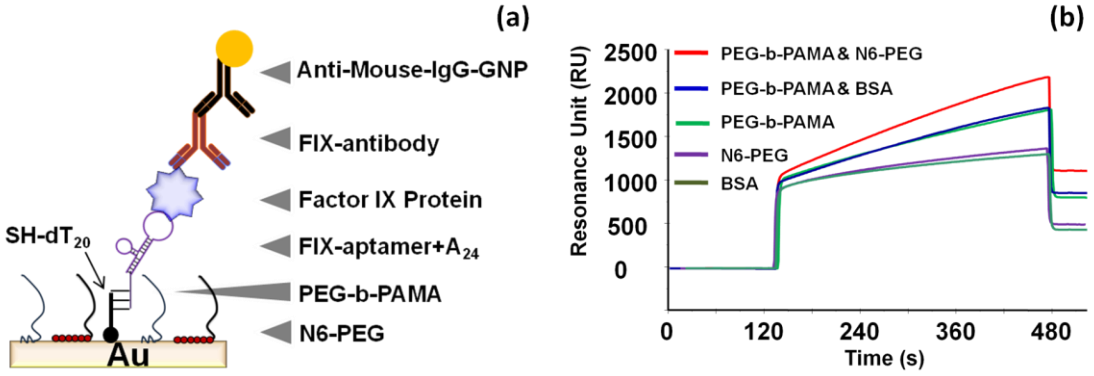

Figure 3.10. Detection of FIX by mouse-IgG-GNP. a) Schematic of chemical surface modifications on the Au surface of the SPR-sensing surface for aptamer and FIX interactions. (b) Determination of the binding of FIX for the interactions of aptamer on Au surface with different surface modifications. 80 nM of FIX was injected on the different surface modifications followed by FIX antibody and analyzed by mouse IgG-GNP.

The biological importance of FIX was demonstrated in Hemophilia B (Christmas disease), when the FIX concentration in plasma gets abnormal from the normal level which is around 5 µg/mL (87 nM). This plasma sample containing albumin as the major protein with other clotting factors in addition to FIX. If one can detect FIX selectively among these activation major proteins, it is anticipated that the author will be able to precisely determine active level of FIX. Human blood serum containing albumin to the level of ~45 mg/mL (~55%) and glubulin to the level of ~25 mg/mL

(~38%).[24,47] To check the selective binding of FIX in the presence of albumin, the author performed the experiment using FIX mixed with high concentration of albumin (45 mg/mL), and with this real albumin concentration in serum the author could detect FIX at 80 pM (Figure 3.11).

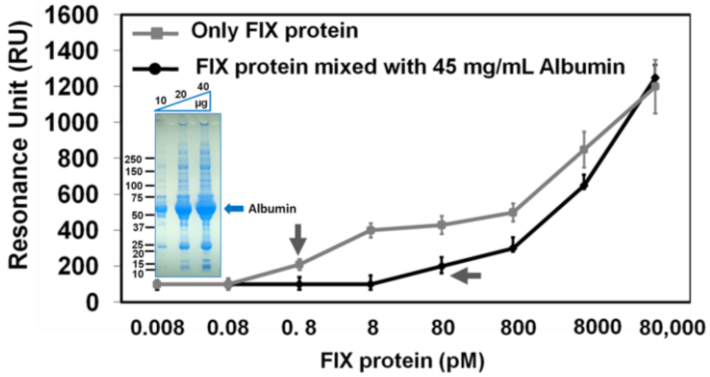

Figure 3.11. Limit of detection of FIX in the presence or absence of albumin. FIX (from 0.008 to 80,000 pM) only or mixed with 45 mg/mL of albumin passed on the FIX aptamer immobilized surfaces followed by FIX antibody and detected by mouse IgG-GNP. Samples were injected at the flow rate of 10 µL/min. All experiments were performed with 10 mM HEPES buffer (pH 7.4) containing 150 mM NaCl and 2 mM $CaCl_2$. Detection limits are indicated by arrows. Figure inset shows the abundance of albumin in human plasma.

The attained higher sensitivity with sandwich pattern detected by mouse IgG-GNP, was due to PEG-*b*-PAMA and N6-PEG immobilized Au surface, can be used as the common strategy for any aptamer-FIX interactions. Further, SH-dT_{20} and aptamer-A_{24} duplex could be regenerated by injecting 10 mM NaOH, on the sensing surface (Figure 3.12). The author detected FIX with the abundance of albumin which mimics physiological condition makes suitability of present strategy for detecting FIX deficiency in human blood samples.

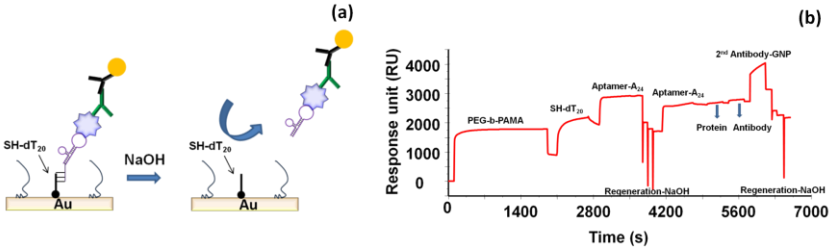

Figure 3.12. Regeneration on the sensing surface. (a) cartoon illustrates the regeneration process. (b) Regeneration by SPR. Regeneration was performed by 10 mM NaOH, injected at the flow rate of 60 µl/min, for 2 x 5 sec. Performed with 10 mM HEPES buffer (pH 7.4) containing 150 mM NaCl.

3.4.7. Detection of FIX in human plasma on co-immobilized PEG-*b*-PAMA and N6-PEG modified Au surface

Human blood serum also containing other clotting factors including FIX involved in the human clotting system and participates in the cleavage in the intrinsic and the extrinsic clotting pathways[41], in addition to albumin and globulin. To confirm the above results with further step, the author directly used human plasma and evaluated the existing FIX using the designed strategy with mouse IgG-GNP. The author evaluated the serially diluted human plasma from 1:10 to 1:1280 which are equivalent to the dilutions from 8 nM to 0.062 nM of FIX. Upon injection, the author could observe the clear changes in the sensogram from the diltution of 1:160 which is equivalent to 500 pM of FIX With this concentration the changes in the sensorgram was 250 RU (Figure 3.13 a,b).

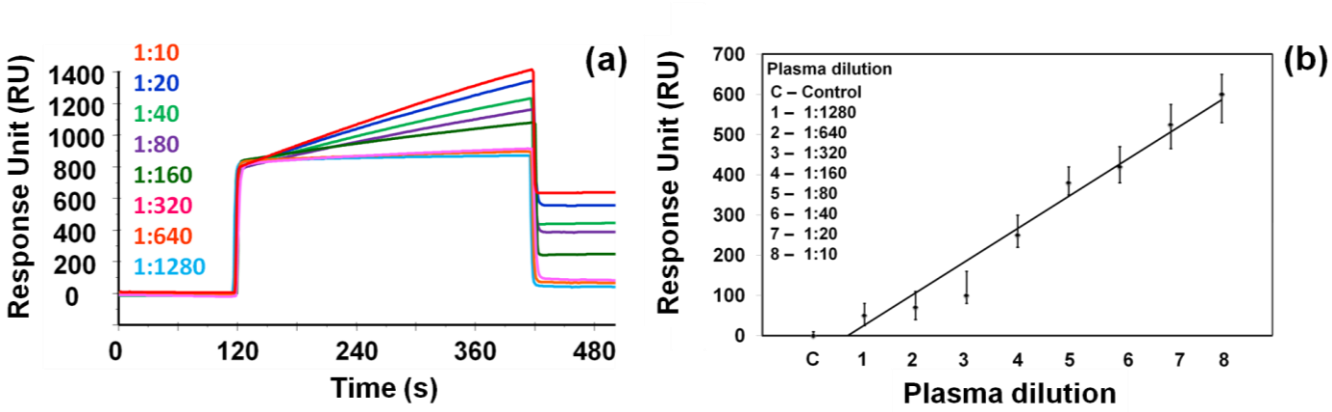

Figure 3.13. Detection limit of FIX in human plasma. (a) SPR analysis. Human plasma with dilution from 10 to 1280 injected on the FIX aptamer immobilized surfaces (Instead of FIX protein) followed by FIX antibody and analyzed by mouse-IgG-GNP. (b) Graphical representation of analyses of aptamer against different dilutions of human plasma containing FIX by SPR. The real concentrations are indicated. Samples were injected at the flow rate of 10 µl/min. All experiments were performed with 10 mM HEPES buffer (pH 7.4) containing 150 mM NaCl and 2 mM $CaCl_2$. Samples were injected at the flow rate of 10 µL/min.

Specific interactions of aptamer and FIX were further evaluated using complementary aptamer sequence and no binding was noticed both by gel-shift assay and SPR analyses (Figure 3.14).

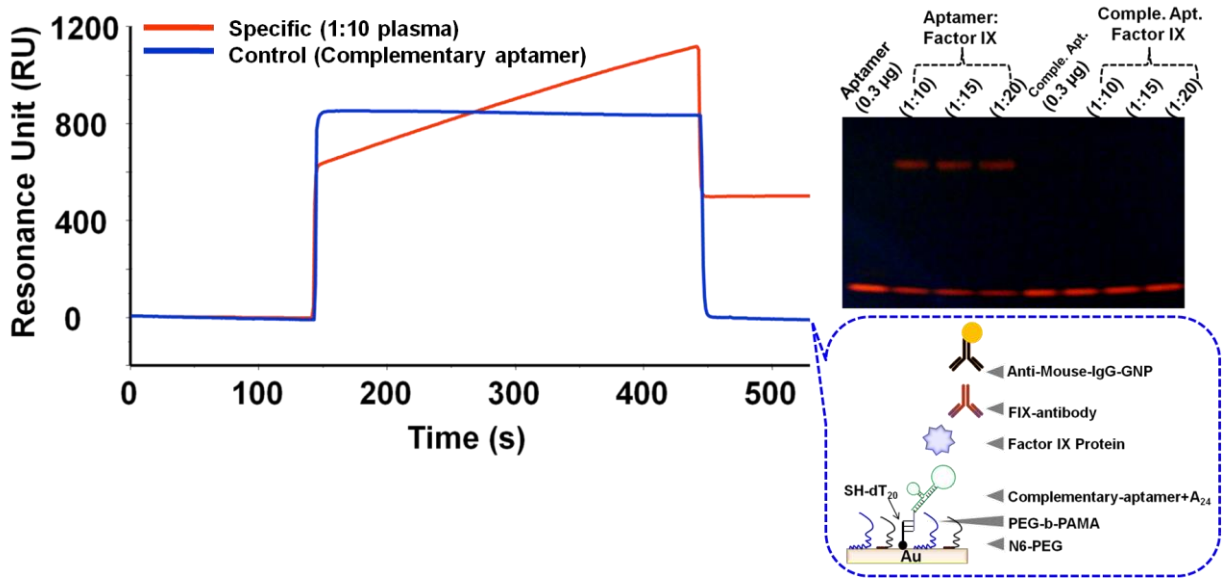

Figure 3.14. Analyses of FIX in human plasma. Human plasma with dilution 1:10 was injected on the FIX aptamer immobilized surfaces (Instead of FIX protein) followed by FIX antibody and detected by mouse –IgG GNP. Control experiment was done with complementary of FIX aptamer. Figure inset is cartoon for control experiment. Samples were injected at the flow rate of 10 µl/min. Native-PAGE for the specific aptamer-FIX and complementary aptamer-FIX complexes is shown by gel-shift assay. Shift and super-shifts were shown with aptamer-FIX. All experiments were performed with 10 mM HEPES buffer (pH 7.4) containing 150 mM NaCl and 2 mM $CaCl_{2.}$

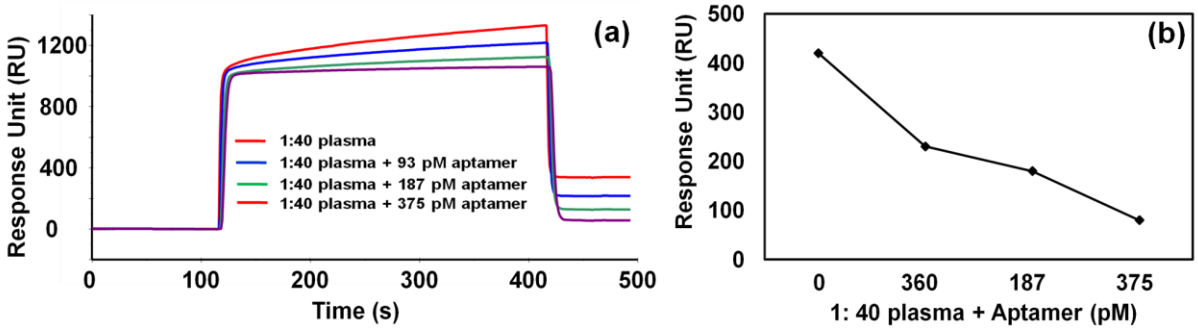

Figure 3.15. Confirmation of FIX and aptamer interaction. (a) Analyses of FIX in plasma with pre-mixed aptamer. After immobilization of aptamer and blocking with N6-PEG on Au surface, plasma containing FIX (1:40 dilution) was premixed with different concentrations of specific aptamer (0 to 375pM) without poly-A tail. Samples were injected at the flow rate of 10 µL/min. All experiments were performed with 10 mM HEPES buffer (pH 7.4) containing 150 mM NaCl and 2 mM $CaCl_{2.}$ (b) Graphical representation of analyses of aptamer against constant (1:40 dilution) human plasma mixed with different concentration of aptamer without poly-A tail.

Similarly, pre-mix of specific aptamer without poly-A tail (cannot make a duplex with SH-dT_{20}) and FIX, causes reduction in the binding with increasing concentration of pre-mixed aptamer (Figure 3.15). Results obtained with human plasma using the designed strategy here indicate its suitability to analyse the deficiency level of FIX in human blood samples.

3.5. Conclusions

In this study, using dual PEG-block polymers (PEG-*b*-PAMA and N6-PEG) co-immobilized Au sensing surface of SPR, the detection strategy using was formulated for the detection of FIX with the assistance of FIX-aptamer and FIX-antibody as the sandwich pattern. The detection was performed with mouse IgG-GNP. PEG-*b*-PAMA treated Au surface promoted the proper orientation of thiolated DNA oligos on the Au surface with higher number of molecules. Co-immobilization of N6-PEG with PEG-*b*-PAMA completely abolished the bio-fouling, whereas BSA and ethanolamine have shown higher non-specificity. With dual polymers construction the limit of detection was attained to 800 fM, further, the selective FIX detection was shown with albumin containing sample. In addition, the concrete of the present polymer assisted detection strategy was proved by detecting FIX in human plasma, to be opted for the detection of clinically relevant samples.

3.6. References

1. Li, Y., Schluesener, H.J., Xu, S., *Gold Bulletin* **2010**, 43, 29-41.
2. Guo, X., *J. Biophotonics*. **2012**, 5, 483-501.
3. Homola, J., Yee, S.S., Gauglitz, G., *Sens. Actuators B Chemical* **1999**, 54, 3–15.
4. Jing, M., Bowser, M.T., *Anal. Chim. Acta* **2011**, 686, 9–18.
5. Catt, K., Niall, H.D., *Nature* **1967**, 213, 825–827.
6. Engvall, E., Permann, P., *Immunochemistry* **1971**, 8, 871–874.
7. Hock, B., *Analytica Chimica Acta* **1997**, 347,177–186.
8. Tuerk, C.; Gold, L., *Science* **1990**, 249, 505–510.
9. Ellington, A.D., Szostak, J.W., *Nature* **1990**, 346, 818–822.

10. Robertson, D.L., Joyce, G.F., *Nature* **1990**, 344, 467–468.
11. Kim, S., Lee, J., Lee, S.J., Lee, H.J., *Talanta* **2010**, 81, 1755-1759,
12. Kanno, S., Yanagida, Y., Haruyama, T., Kobatake, E., Aizawa, M., *J. Biotechnol.* **2000**, 76, 207-214.
13. Lu, B., Smyth, M.R., O`Kennedy, R., *Analyst* **1996**, 121, 29R.
14. Kumar, S., Ch, R., Rath, D., Panda. S., *Mater. Sci. Engg. C.* **2011**, 31, 370-376.
15. Nagasaki, Y. *Poly. J.* **2011**, 43, 949-958,
16. Oishi, M., Sasaki, S., Nagasaki, Y., Kataoka, K., *Biomacromolecules* **2003**, 4, 1426-1432.
17. Oishi, M., Nagasaki, Y., Itaka, K., Nishiyama, N., Kataoka, K., *J. Am. Chem. Soc.* **2005**, 127, 1624-1625.
18. Oishi, M., Ikeo, S., Nagasaki, Y., *Poly. J.* **2007**, 39, 239-244.
19. Yuan, X., Yoshimoto, K., Nagasaki, Y., *Anal. Chem*. **2009**, 81, 1549–1556.
20. Trubetskoy, V.S., *Adv. Drug Deliv. Rev.* **1999**, 37, 81-88.
21. Otsuka, H., Y. Nagasaki, K. Kataoka, *Adv. Drug Deliv. Rev.* **2003**, 55, 403-419.
22. Kenausis, G. L., Vörös, J., Elbert, D. L., Huang, N. P., Hofer, R., Ruiz-Taylor, L., Textor, M., Hubbell, J. A., Spencer, N. D., *J. Phys. Chem. B* **2000**, 104, 3298–3309.
23. Langer, R., Vacanti, J. P., *Science* **1993**, 260, 920–926.
24. Baker, M E., *J. Endocrinol.* **2002**, 175, 121–127.
25. Bailey, F.E.J.V.K., Marcel Dekker Inc., New York, **1990**.
26. Malmsten, M., Emoto, K., Van Alstine, J.M., J*. Colloid Interface Sci.* **1998**, 202, 507-517.
27. Otsuka, H., Nagasaki, Y., Kataoka, K., *Langmuir* **2004**, 20, 11285-11287.
28. Satomi, T., Nagasaki, Y., Kobayashi, H., Otsuka, H., Kataoka, K., *Langmuir* **2007**, 23, 6698-6703.
29. Uchida, K., Otsuka, H., Kaneko, M., Kataoka, K., Nagasaki, Y., *Anal. Chem.* **2005**, 77, 1075–1080.
30. Nagasaki, Y., Kobayashi, H., Katsuyama, Y., Jomura, T., Sakura, T., *J.Colloid Interface Sci.* **2007**, 309, 524-530.
31. Kamimura, M., Miyamoto, D., Saito, Y., Soga, K., Nagasaki, Y. *Langmuir* **2008**, 24, 8864-8870,
32. Yoshimoto, K., Nishio, M., Sugasawa, H., Nagasaki, Y., *J. Am. Chem. Soc.* **2010**, 132, 7982–7989.
33. Lim, Z., Li, J., Ng, C., Yung, L.L., Bay, B., *Acta Pharmacol. Sinica* **2011**, 32,983-990.
34. Iliuk, A.B.,Hu,L.,Tao,W.A., *Anal. Chem. 2011*, 83, 4440–4452.
35. Upadhyayula, V.K., *Analytica Chimca Acta* **2012**, 715, 1–18.
36. Guirgis, B.S., Sá E Cunha, C., Gomes, I., Cavadas, M., Silva, I., Doria, G., Blatch, G.L., Baptista, P.V., Pereria, E., Azzazy, H.M., Mota, M.M., Prudencio, M., Franco, R., *Anal. Bioanal. Chem.* **2012**, 402,1019-1027.
37. Zanoli, L.M., D′Agata, R.,Spoto,G., *Anal. Bioanal. Chem.* **2012**, 402, 1759–1771.
38. Miyamoto, D., Oishi, M., Kojima, K., Yoshimoto K., Nagasaki, Y., *Langmuir,* **2008**, 24, 5010-5017.

39. Horiguchi, Y., Miyachi, S., Nagasaki, Y., *Langmuir* 2013, **29**, 7369–7376.
40. Rusconi, C.P., Scardino, D., Layzer, J., Pitoc, G.A., Ortel, T.L., Monroe, D., Sullenger, B.A. *Nature* **2002**, 419, 90-94.
41. Gopinath, S.C.B., Shikamoto, Y., Mizuno H., Kumar, P.K.R., *Thromb. Haemostasis* **2006**, 95, 767-771.
42. Yoshimoto, K., Nozawa, M., Matsumoto, S., Echigo, T., Nemoto, S., Hatta, T., Nagasaki, Y., *Langmuir* **2009**, 25, 12243–12249.
43. Nagasaki, Y., *Chem. Lett.* **2008**, 37, 564-569.
44. Hermanson, G.T. Bioconjgate Techniques 2nd edition, Academic Press, Waltham, **2008**.
45. Yoshimoto, K., Matsumoto, S., Asakawa, R., Uchida, K., Ishii, T., and Nagasaki, Y., *Chemi. Lett.* **2007**, 36, 1444-1445.
46. Oishi, M., Kataoka, K., Nagasaki, Y., *Bioconjugate Chem*. **2006**, 17, 677-688.
47. Lakshmipriya, T., Fujimaki, M., Gopinath, S.C.B., Awazu, K., Horiguchi, Y., Nagasaki, Y. *Analyst* 2013,138, 2863-2870.
48. Valle-Delgado, J.J., Molina-Bolivar, J.A., Galisteo-Gonzalez, F., Galvez-Reiz, M.J., Feiler, A., Rutland, M.W. *Langmuir* **2006**, 22, 5108-5114.
49. Furusho, H., Kitano, K., Hamaguchi, S., Nagasaki, Y., *Chem. Mater.* **2009**, 21, 3526–3535.
50. Pong, B.- K., Lee, J.- Y., Trout, B. L., *Langmuir* **2005**, 21, 11599-11603.

Chapter 4

Generation of Anti-influenza Aptamers for Sensing Applications on PEG-b-PAAc/Fluorescent Hybridized Surface of Surface Plasmon Fluorescence Spectroscopy

4.1. Abstract

Systematic evolution of ligands by exponential enrichment (SELEX) is a selection process for identifying high-affinity selective molecules from a randomized combinatorial nucleic acid library against a wide range of target molecules. Using a pool of N25 RNA molecules, the SELEX process was performed against two targets from influenza viruses, namely, intact influenza B/Tokio/53/99 and hemagglutinin of infuluenza B/Jilin/20/2003. The selection processes were evaluated by surface plasmon fluorescence spectroscopy (SPFS), and the result was compared with that obtained by a conventional radioisotope method. Clear discriminations among different selection cycles were displayed by SPFS, indicating that this method can be used as an alternative method of radioisotope labeling. The dissociation constant of the selected aptamers against the targets was in the low nanomolar range. The sensitivity of the selected aptamer against intact influenza B/Tokio/53/99 to detect the influenza virus was low ng/mL level, approximately 250-fold higher sensitivity than that of the commercially obtained antibody. The target-binding sites on the aptamer were predicted by mapping analyses. The selected aptamer could discriminate other influenza strains and the sensitivity of the selected aptamer was further confirmed by gold nanoparticle-based sensing on a waveguide-mode sensor. This finding demonstrates that the selected aptamer would be useful for detecting influenza viruses at an early stage of infection and for the purpose of influenza surveillance.

4.2. Introduction

Systematic evolution of ligands by exponential enrichment (SELEX) was developed by 3 independent researchers in 1990 as an approach to identifying selective molecules among a randomized combinatorial library of about 10^{14} molecules, against organic dyes[1] and T4 DNA polymerase[2] and to alter the cleavage activity of a ribozyme.[3] In the past, this SELEX procedure was also carried out against targets (aptatopes) of different sizes, ranging from small ligands to the entire cell, such as, membrane proteins, human cells and whole viruses.[4-7] The SELEX process involves 3

vital steps, that is, target binding with the library of molecules, separation of the ligand-aptamer complex, and regeneration of bound molecules. The success of the SELEX process is mainly determined by the separation of target-bound molecules from unbound molecules. After successive selection rounds, usually 5–14 cycles, high-affinity molecules are obtained. The high-affinity selective molecules obtained after several iterative rounds of SELEX are called "aptamers".[8] Nucleic acid libraries involved in the aptamer selection process can be either DNA or RNA. An RNA library usually gives a higher success rate than a DNA library because of the availability of diverse stem-loop secondary structures. Due to advantage of diverse possibilies with versatile structures, RNA will yield high affinitity aptamers. Usually, loop regions of the secondary structures of the aptamers contact the target molecules through the process of "induced fit".[9] In this study, we chose 2 targets from influenza B viruses for aptamer selection. One is intact influenza B/Tokio/53/99 (Tokio-virus) and the other is hemagglutinin (HA) of influenza B Jilin/20/2003 (Jilin-HA), which belong to the Yamagata and Victoria lineages, respectively.

Influenza is an infectious disease that spreads worldwide with seasonal epidemics, and the emergence of different strains because of transmission among them has resulted in deaths.[10,11] There are three major classes (A, B and C) of influenza viruses and influenza A and B are circulating with human population. Influenza virus has a diameter of about 100 nm, one of the surface proteins of influenza, HA play a important role in the infection with host cells through the sialic acids (Figure 4.1). Influenza B has the Victoria and Yamagata lineages, and several strains have arisen from these types.[12] Generating the molecules that can distinguish the closely related viruses with higher specificity is a vital issue, especially for global influenza surveillance systems. With respect to pandemic surveillance, the primary goals are to establish detection systems for identifying new influenza strains that are different from other existing viruses. Current conventional detection systems for influenza viruses mainly rely on immunoassays, which use antibodies as the probe.

Immunochromatography test is presently in use for the identification of influenza viruses and for discrimination between influenza A and B viruses, using antibody-GNP conjugates. Generation of RNA[4] and DNA aptamer[13,14] for influenza viruses has been proven to be useful as an alternate candidate to antibodies. To generate the system for earlier diagnosis, in the present study, new anti-influenza aptamers were generated.

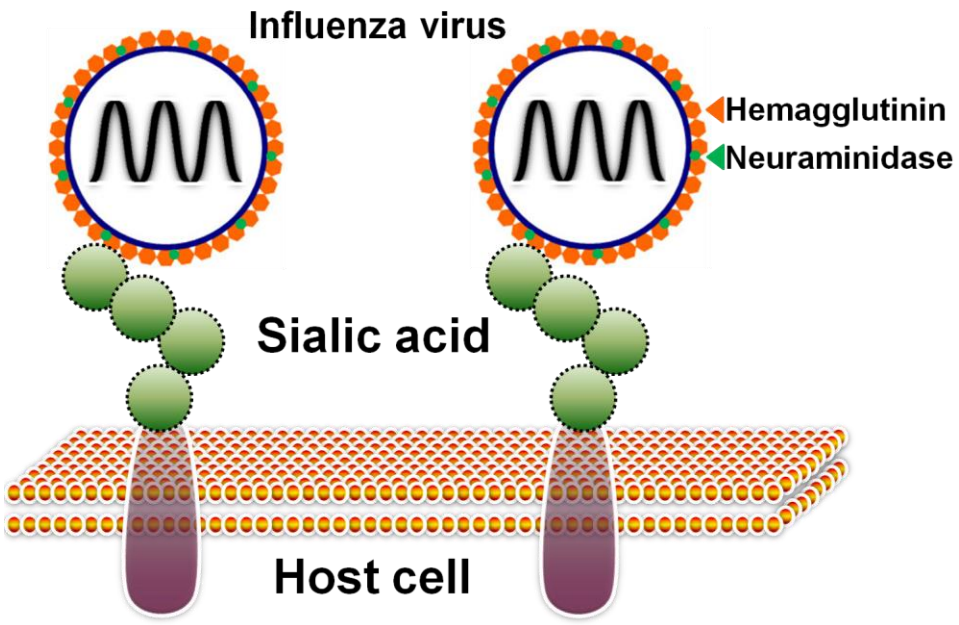

Figure 4.1. Influenza and host cell interaction. Two major proteins (HA and NA) are on the surfaces of influenza virus. Sialic acid mediates the interactions with HA.

The SELEX process can be monitored or evaluated by various methods that mainly involve highly sensitive labeling. The radioisotope labeling method is one of the sensitive methods widely used to evaluate the selection processes, however, the facilities available for this method are limited and there is some safety issues associated with exposure to radioactive materials. Among several of the labeling techniques, fluorescent labeling is considered to be a sensible detection method. In our study, we used SPFS to assess the processes that are involved in the SELEX and for detection of influenza viruses. SPFS involves a combination of fluorescent labeling and enhancement of

fluorescence intensities via electric field enhancement by surface plasmon resonance (SPR), reported using fluorescent material on gold,[15] latex particles[16] and polymers.[17] Biomolecular interactions on the metal surface with a bound fluorescent label in the vicinity of the enhanced electric field has been found to result in appropriate enhancement of output spectral signals.[18] In this study, the author added cyanine (Cy5) to the 5′ end of polyT (dT_{20}) and enabled complementation with the extended 3′ aptamer end with polyA (A_{24}). Cyanine is one of the potential fluorescent compounds effectively used in the oligonucleotide-based sensing.[19] With this strategy, the author could clearly recognize the progression in the SELEX process, and results were supported by the isotope labeling strategy. Detection of targets at low concentrations using the developed aptamers was also demonstrated using gold nanoparticle-based waveguide-mode sensor. Further discrimination studies were carried out by SPFS using different influenza strains.

4.3. Experimental section

4.3.1. Reagents and Biomolecules

3-Aminopropyltriethoxysilane (3-APTES) was purchased from Sigma-Aldrich (Japan). Glutaraldehyde and reverse transcriptase (M-MLV, RNase H+) were procured from Wako Chemicals (Japan). Poly(ethylene glycol)-b-poly(acrylic acid) (PEG-*b*-PAAc) was obtained from General Science Corporation, Japan. Pentaethylenehexamine-terminated PEG (N6-PEG) was provided by JSR (Japan). Dr. GenTLE precipitation carrier, T4 RNA Ligase, and PrimeSTAR Max DNA Polymerase were from Takara Bio Inc., Japan. The Pop-Top Membrane Holder is from Whatman, USA. H3N2 virus (A/Panama/2007/1999), Tokio-virus and Jilin-HA were obtained from Prospec-Tany TechnoGene Ltd. (Israel). Recombinant hemagglutinin from influenza virus H2N2 (A/Japan/305/1957), H5N1 (A/chicken/India/NIV33487/2006), and H1N1 (A/California/07/2009), were from Sino Biological Inc. China. *Escherichia coli* tRNA was obtained from Roche Diagnostics (Germany). Streptavidin-conjugated gold nanoparticles (SA-GNPs) [40 nm; 15 optical density (OD)] were from BioAssay Works

(USA). The shorter oligo (dT_{20}) that was conjugated with cyanine (Cy5) or biotin at the 5′ end and other oligo nucleic acids were synthesized commercially from Tsukuba Oligos, Japan. Horseradish peroxidase-conjugated anti-mouse IgG was obtained from Promega (USA). Clear Blot membrane-P was obtained from ATTO and nitrocellulose membranes were from Millipore (USA). The ECL-plus western blotting detection kit was purchased from Amersham (USA). Protein markers were obtained from Bio-Rad Laboratories Inc. (USA). All reagents were stored according to the suppliers' recommendations.

4.3.2. Immunoblot analyses

The specificity of the antibody for the Tokio-virus was analyzed by standard blotting assays as described in chapter 3 with an appropriate anti-influenza B antibody.

4.3.3. Preparation of the initial random library

To generate the RNA library, DNA templates with randomized regions of 25 bases were synthesized commercially. This library was designed with constant 5′ and 3′ primer regions for amplifications. Using the DNA template (5′-GGGAGAATTCCGACCAGAAG–N25–CCTTTCCTCTCTCCTTCCTCTTCT-3′), the library of DNA molecules was initially amplified by polymerase chain reaction (PCR) with 2× PrimeSTAR Max DNA Polymerase (including all dNTPs; dATP, dTTP, dGTP and dCTP), forward (5′-AGTAATACGACTCACTATAGGGAGAATTCCGACCAGAAG-3′) and reverse (5′-AGAAGAGGAAGGAGAGAGGAAAGG-3′) primers. The forward primer had the T7 promoter region (underlined) at the 5′ end in order to generate RNA molecules during transcription. The enzymatically synthesized double-stranded DNAs were ethanol precipitated, and *in vitro* transcription reactions were performed using T7 RNA polymerase. Transcription was carried out at 37°C for 3 h with a Cellscript transcription kit (Epicentre Biotechnologies, USA). The products were treated with 2 units of DNase I

(RNase free) for 20 min at 37°C to remove the residual template DNA, and the reaction was terminated by adding an equal volume of 2× urea buffer (7 M urea, 50 mM ethylenediaminetetraacetic acid [EDTA], and 90 mM Tris-borate containing 0.05% bromophenol blue). Subsequently, the reaction mixtures were heated at 94°C for 2 min and loaded on a 12% polyacrylamide gel containing 7 M urea to fractionate the product. The RNA band was visualized under ultraviolet (UV)-shadow and extracted from the excised gel piece by the crush and soak method. The RNA was ethanol precipitated, dried under vacuum, and redissolved in RNase-free water; the concentration was measured spectrophotometrically at 260 nm.

4.3.4. SELEX process

The SELEX process was carried out using about 10^{14} RNA molecules with central random regions and constant regions at both ends. The SELEX process is shown in Figure 4.2. First-round selection was done with concentrations of 80 and 38 µg/mL for Tokio-virus and Jilin-HA, respectively. Before adding the targets, the RNA library molecules were refolded properly by denaturation at 94ºC for 2 min and cooling to room temperature. The folded RNA molecules were mixed with the targets in the presence of HEPES binding buffer (10 mM 2-[4-(2-hydroxyethyl)piperazin-1-yl]ethanesulfonic acid, pH 7.4, 150 mM NaCl, 5 mM $MgCl_2$) and tRNA (10-fold excess of the initial library concentration) molecules for competition. Magnesium chloride in the HEPES binding buffer maintains the stability of the specific interaction between the target and aptamer. This mixture was incubated at room temperature for 10 min and then passed through the nitrocellulose membrane held on the Pop-Top Membrane Holders. The unbound molecules were discarded by washing with 1 mL of the HEPES binding buffer. The bound molecules that were complexed with the targets and were captured on the membrane were recovered by heating at 94ºC with the H_2O containing 7 M urea. The recovered solutions with RNA molecules were ethanol precipitated using the Dr. GenTLE precipitation carrier. These precipitated molecules were amplified further by a reverse transcription reaction followed by

PCR. Purified molecules were used for the next round of selection, and the processes were repeated

Cycle	Pool RNA (μM)	Competitor tRNA (μM)	Protein μg/mL	PCR cycles	Seperation method	Filter binding (%)
1	8	80	80	8	filter	0
2	4	80	40	10	filter	ND
3	2	40	16	16	plate	ND
4	2	40	16	18	plate	3.7
5	2	120	80	10	filter	ND
6	1	80	16	18	plate	ND
7	1	160	24	12	filter	ND
8	1.5	80	16	16	plate	ND
9	0.75	200	57	12	filter	9
10	0.5	200	57	10	filter	ND
11	1.5	240	28	10	filter	13.5

Table 4.1: Selection cycles with the target Tokio-virus; ND-Not determined

Cycle	Pool RNA (μM)	Competitor tRNA (μM)	Protein μg/mL	PCR cycles	Separation method	Filter binding (%)
1	8	80	38	8	filter	0
2	4	80	24	12	filter	ND
3	2	40	6.6	16	plate	0.5
4	1	120	16	10	filter	ND
5	0.5	60	6.6	18	plate	ND
6	2	120	32	10	filter	ND
7	2	160	24	10	filter	1.5
8	1.5	80	6.6	16	plate	ND
9	0.75	200	24	8	filter	ND
10	0.5	200	24	10	filter	ND
11	1.5	240	12	10	filter	13

Table 4.2: Selection cycles with the target Jilin-HA; ND - Not determined

with different ratios of targets and competitor (tRNA) (Tables 4.1 & 4.2). In addition to the separation strategy using the nitrocellulose membrane, we also used microtiter plate for the separation. Separation of the target and aptamer complex by a nitrocellulose membrane was performed with 1st, 2nd, 5th, 7th, and 9–11th selection cycles for Tokio-virus or 1st, 2nd, 4th, 6th, 7th, and 9–11th selection cycles for Jilin-HA. To remove the molecules that copurified as nonspecific binders during the recovery of aptamer from the filters, prefiltration in the absence of target molecules was done

between each selection cycle. Microtiter plate was used with 3rd, 4th, 6th, and 8th selection cycles for Tokio-virus or 3rd, 5th, and 8th selection cycles for Jilin-HA. In this case, the target was covalently immobilized on the surface of the microtiter plate and blocked with 3% bovine serum albumin (BSA).

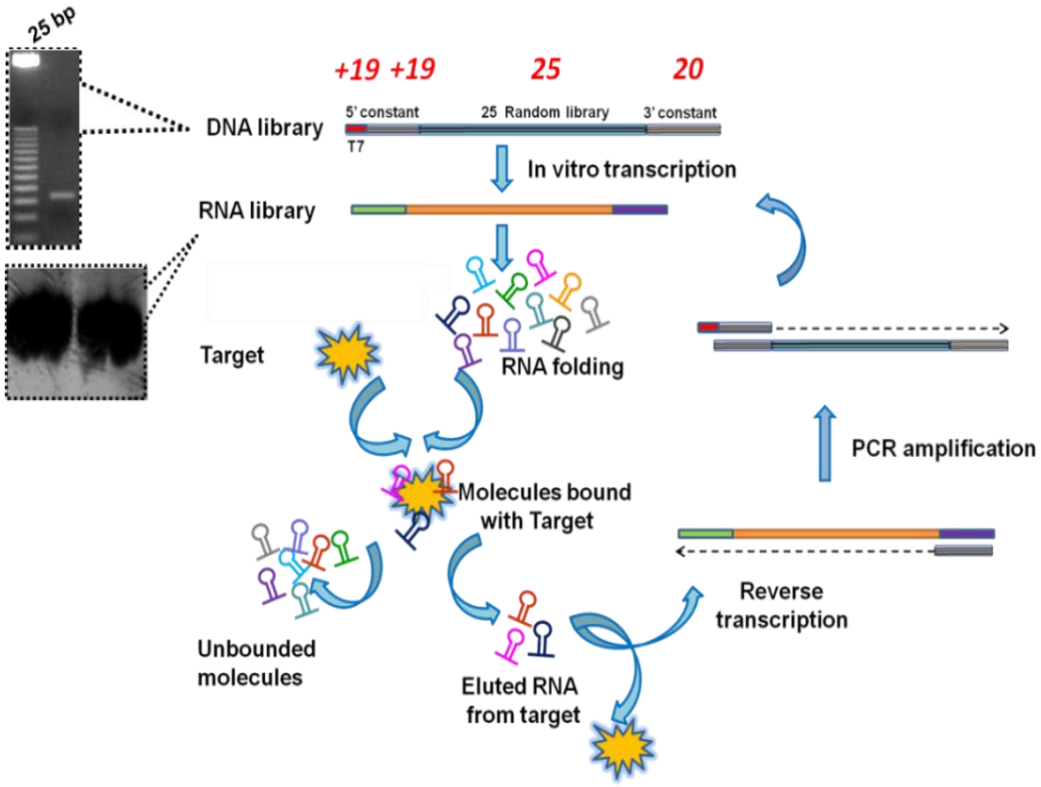

Figure 4.2. Schematic of the systematic evolution of ligands by exponential enrichment (SELEX) process. The steps involved in SELEX include 3 steps: complex formation, separation, and amplification.

The non-specific molecules generated from this separation method were removed by pre-negative selection on the surface of the microtiter plate coated with only BSA. The bound molecules from the microtiter plate were recovered by adding the 90°C HEPES binding buffer (without $MgCl_2$).

4.3.5. Filter-binding assay

To check the selection progress by radioisotope labeling, molecules that were obtained from SELEX were labeled by incorporating α-ATP (P^{32}) in the transcription reaction described in initial random library preparation. The labeled molecules were fractionated on a 12% polyacrylamide gel

containing 7 M urea, and the RNA product was purified as performed in the initial library preparation. Using this pure labeled RNA, interactions were carried out using different ratios of the targets in the HEPES binding buffer in the presence of tRNA as competitor, and each reaction was incubated at room temperature for 10 min and the reaction mixture was filtered on a nitrocellulose membrane fitted on a Pop-Top Membrane Holder. An imaging film was exposed on the membrane for 1 h at room temperature. The exposed film was scanned, and counts were measured on the images of the bound molecule. Based on the count, the bound molecules were calculated using the following formula: binding parcentage of molecules (%) = (count of the labeled molecules bound to protein/count of total labeled molecules used in the reaction) $\times$ 100.

4.3.6. Determination of the dissociation constant

To calculate the dissociation constant (K_d) of the selected aptamer against the targets, we labeled the selected aptamer by using PcP (P^{32}) at the 3′ end. To ligate PcP (P^{32}), an overnight reaction was performed at 4°C with the RNA ligase enzyme. The labeled aptamer was fractionated, purified on the 12% polyacrylamide gel containing 7 M urea, and extracted as detailed in the initial pool preparation. Different concentrations of targets (0 to 51.2 µg/mL) were mixed individually with a constant concentration (40 nM) of unlabeled aptamer. Each reaction also included 400 nM of tRNA for competition and 5 kcpm of PcP (P^{32})-labeled aptamer for detection. These mixtures were incubated in the HEPES binding buffer and incubated for 10 min at room temperature, filtered on a nitrocellulose membrane, and analyzed. The values obtained were used to calculate the K_d by using the GraphPad Prism software (version 2.1) (http://www.graphpad.com/scientific-software/prism/).

4.3.7. Sensing surface preparation and chemical modification

To prepare the sensing surface, Cr, Au, and SiO_2 were deposited on a S-LAH66 glass substrate (Ohara corporation, Japan). The Cr (0.6 nm) and Au (49 nm) layers are deposited by a vapor-

depositon method, while the SiO_2 (20 nm) is deposited by a rf-magnetron sputtering method. The sensing surface was modified by immersion in a 0.5% (v/v) ethanol solution of 3-APTES for 24 h. The 3-APTES reacted with the surface hydroxyl groups of SiO_2 to give an amine group-functionalized substrate that was rinsed with ethanol and dried in a stream of nitrogen gas. The amine-functionalized SiO_2 surface was treated with a 2.5% solution of aqueous glutaraldehyde (Glu) for 3 h at room temperature to form an aldehyde-activated surface. The Glu-activated surface allowed for the covalent attachment of the targets (Tokio-virus or Jilin-HA). PEG-*b*-PAAc with a concentration of 4 mg/mL, was used as the blocking polymer after attaching the targets on the Glu-modified surfaces. Previously, the author reported about the specific biomolecular interaction that completely avoided charge-based binding on Glu-modified rough surface[20] using PEG-*b*-PAAc on SiO_2.[21]

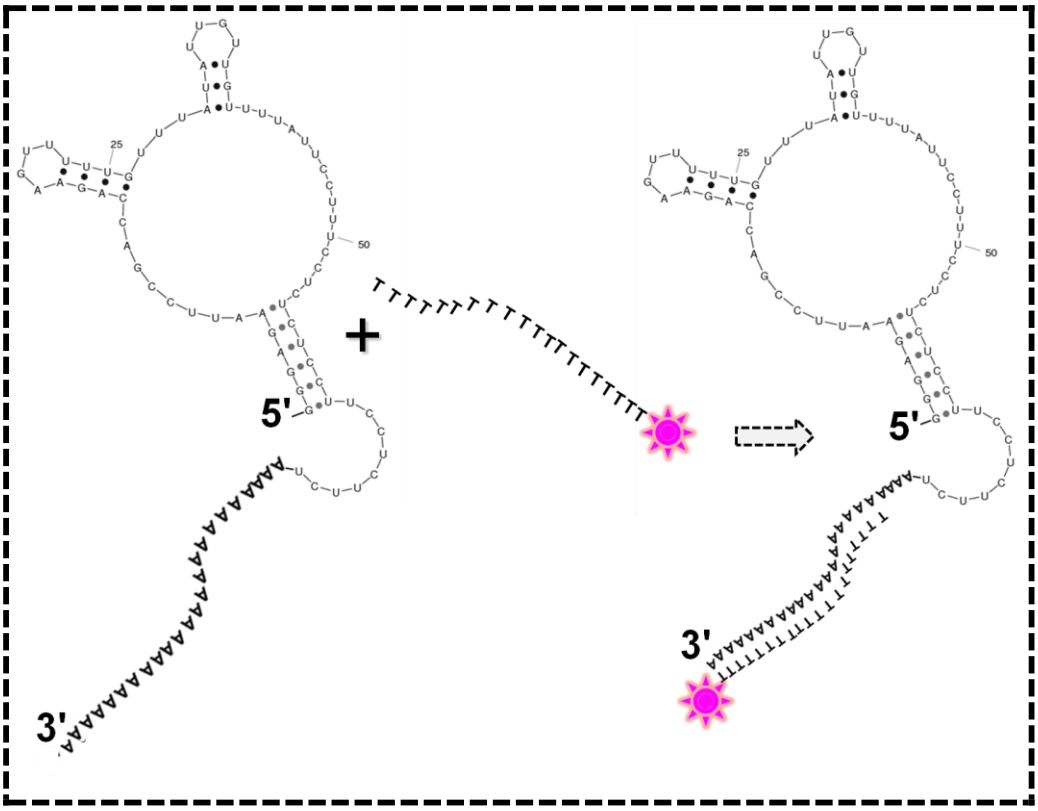

Figure 4.3. Duplex formation between aptamer and Cy5-labeled ssDNA. 3' end of aptamer was extend with poly-A. A spacer was created for efficient duplex formation.

The selected aptamer candidates from the SELEX processes, which were extended with A_{24} at the 3′ end, were permitted to react on the immobilized target. The free end of the aptamer with A_{24} (100 nM) was duplexed with Cy5-conjugated dT_{20} (20 nM) (Figure 4.3).

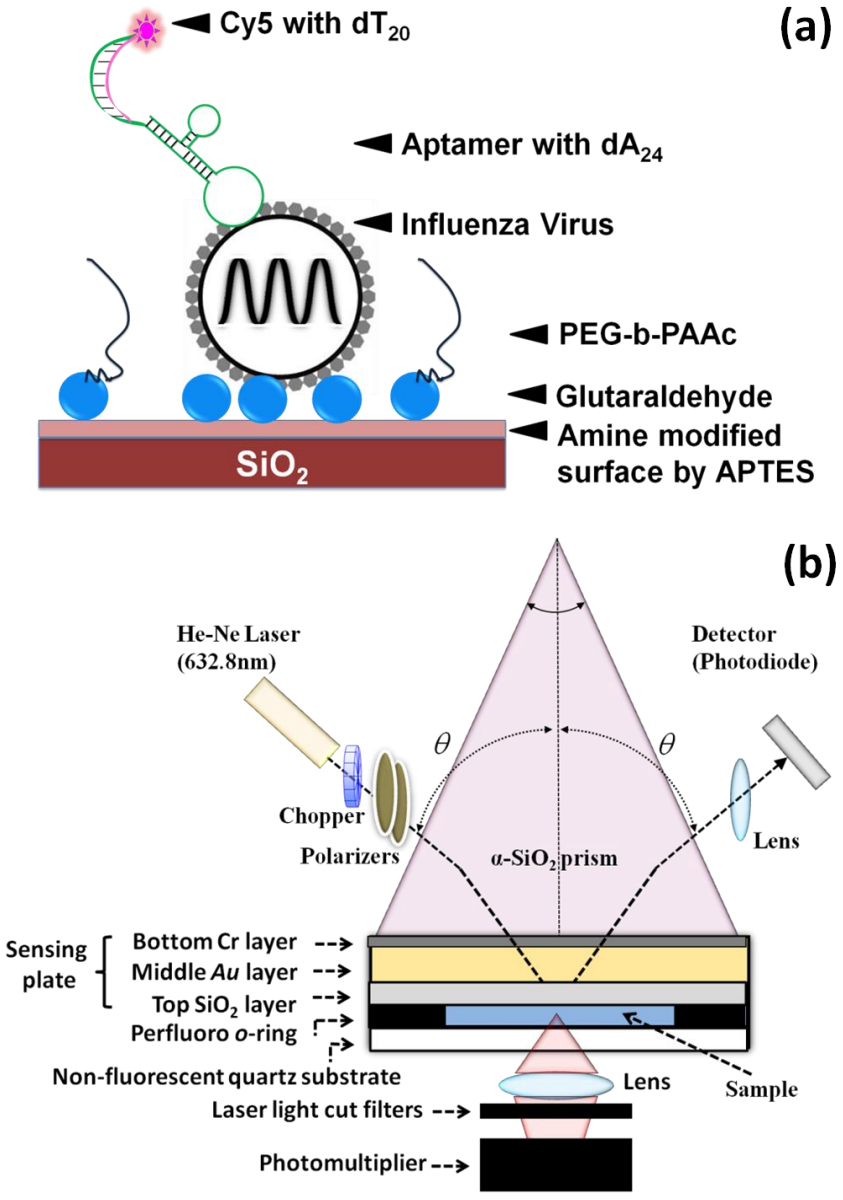

Figure 4.4. Experimental design to detect influenza virus. (a) Schematic of the chemical surface modifications on the SiO_2 layer of the sensing plate for aptamer and target interactions. Glu was attached to the amine-modified surface and was followed by target immobilization. The aptamer ending with A_{24} was attached on the target, and then Cy5 with dT_{20} was allowed to react. (b) Setup for the surface plasmon resonance spectroscopy (SPFS). An He-Ne laser was used as the light source. The sensing plate with the layers of Cr, Au, and SiO_2 was used.

This complex was measured with emission at 670 nm. Biomolecular interactions (Figure 4.4a) were performed with the incubation of 30 min; after each interaction the sensing surface was thoroughly washed 3 times with 450 μL of HEPES binding buffer.

4.3.8. Setup of the SPFS sensor

The molecules selected from the SELEX process was evaluated by SPFS according to the scheme shown in figure 4.4b. The beam of a He-Ne laser (632.8 nm) was used and it passes through a chopper that is connected to a lockin amplifier. The modulated beam then passes through two polarizers, by which the intensity and the plane of polarization of the laser can be adjusted. P-polaraization was selected for the excitation of surface plasmon resonance. A programmable shutter was installed to constantly block the laser, thus minimizing the photobleaching effect of the fluorescent dyes. The perfluoro "O" ring was mounted between non-fluorescent quartz glass substrate and the sensing chip to inject the sample. The prism was coupled to the substrate of the sensing plate. The "O" ring was connected with an inlet and outlet for liquid exchange. Approximately 450 μL of the sample was injected. The fluorescence emitted from Cy5 attached on the interactive molecules was detected by the photomultiplier, which was placed in front of the sensing plate. In this experiment, we used the cut filter with a wavelength of 680 nm, which is suitable for Cy5. The light reflected from the sensing plate was recognized by a photodiode and recorded by a computer.

4.3.9. Analyses of target-binding sites on the aptamer

To analyze the binding region of the target protein on the selected aptamer, we performed mapping analyses. Mapping analyses were performed with the ethylnitrosourea (ENU) modifications on the backbone of phosphate molecules. This modification was done with ENU that was saturated with ethanol. To perform this mapping analysis, the selected aptamer was labeled with PcP (P^{32}) and purified. The labeled aptamer was reacted with ethanol saturated ENU, in the reaction buffer

containing 20 mM HEPES, pH 8.0, and 1 mM EDTA and 2.5 µg of tRNA; it was precipitated using a Dr. GenTLE precipitation carrier. From this ENU-modified aptamer, approximately 100 kcpm was kept separate for the negative reaction containing no targets. Approximately 900 kcpm of the aptamer reacted with 40 µg/mL of target (Tokio-virus or Jilin-HA) in the HEPES binding buffer, and unbound molecules were removed by membrane filtration followed by washing with 1 mL of the HEPES binding buffer. The aptamers that were bound on the membrane were treated with a mild alkali solution (100 mM Tris-HCl, pH 9.0) for 10 min at 50ºC. The ENU-modified aptamer, which was not reacted with the target, was simultaneously treated in the same manner. These mild alkali-treated products were ethanol precipitated in the presence of the Dr. GenTLE precipitation carrier and were fractionated on 12% polyacrylamide gel containing 7 M urea. To locate the position of the cleaved bases on the gel, the labeled aptamers that reacted with alkali solution and were digested with T1 were used as markers. For the alkali ladder, labeled products (approximately 20 kcpm) were treated with 50 mM sodium carbonate, pH 9.2 at 90ºC for 10 min. For the T1 enzyme (enzyme that specifically cleaves G bases) digestion, a similar amount of labeled aptamer was treated with 0.06 units of enzyme in the 16.5 mM sodium citrate, pH 5.0, 0.85 mM EDTA, 7 M urea for 10 min at room temperature.[22] To avoid over-cleavage, both reaction mixtures were also added to 0.3 µg of yeast RNA. The reactions were stopped by adding 2× urea buffer containing bromophenol blue, and the reaction mixtures were loaded on a 12% polyacrylamide gel containing 7 M urea.

4.3.10. Setup of the waveguide-mode sensor

A monolithic sensing plate designed for waveguide-mode sensor comprises a SiO_2 glass substrate, a single-crystalline Si layer, and a thermally grown SiO_2 waveguide.[23] The sensing plate, which is illuminated using the Kretschmann configuration, operates as a sensor that is capable of detecting modifications in the dielectric environment near the waveguide-mode sensor surface by measuring changes in reflectivity. A halogen lamp was used as a light source. The light from the lamp

was guided to a collimator lens, and a polarizer, and a prism was irradiated with the s-polarized collimated light; the incident angle of the light was parallel to the bottom face of the prism. Then, the sensing plate that was placed on the bottom of the prism was illuminated, and a spectrum of the reflected light was detected using a spectrophotometer (Ocean Optics, USA). The prism was made of SiO_2 glass, and its bottom angle was 38°. The optical measurements in this study were taken around 520 nm to show a dip in reflectance, which corresponds to the optical absorption of GNPs. If GNPs are attached to the waveguide-mode sensor surface, the dip will be deepened by the optical absorption of the GNPs.[24]

The surface of the sensing plate was treated similar to the surface modification carried out for the SPFS sensing plate. After immobilizing the aptamer, the free extended end of the aptamer with A_{24} was duplexed with biotin-dT_{20}. Finally, the biotin–streptavidin interactions were monitored by immobilizing SA-GNP in the presence of N6-PEG (0.5 mg/mL). The OD of the SA-GNP solution was measured, and the dilutions were prepared using the HEPES binding buffer to obtain a 1 OD SA-GNP solution from the original stock supplied. Each reaction was performed for 30 min on the sensor chip, after which the sensing surface was thoroughly washed 3 times with 300 µL of HEPES binding buffer. The interaction between Tokio-virus (from 0.8 ng/mL to 8 µg/mL) and the aptamer (100 nM) were compared with that between Tokio-virus and antibody (100 nM).

4.4. Results and Discussion

Before being test the interactions of selected molecules from the SELEX process, initially tested the non-specific attachment on the Glu-modified surface following blocking with ethanolamine and PEG-*b*-PAAc. Upon injecting a Cy5-labelled ssDNA (poly-A), the author could observed higher non-specificity on the ethanolamine-blocked surface, whereas non-specificity was completely quenched on PEG-*b*-PAAc immobilized surface (Figure 4.5). With this surface having non-fouling was used for

further analyses.

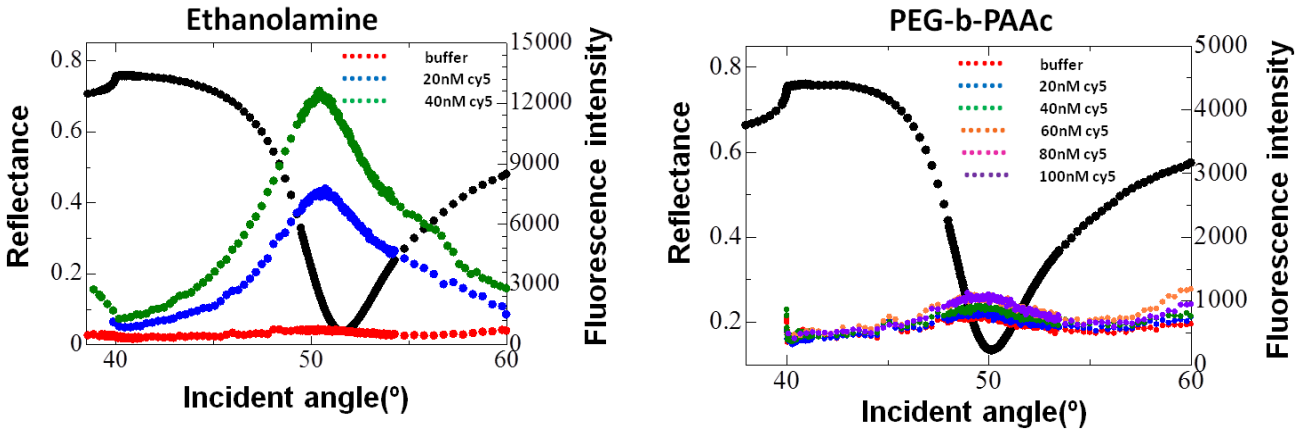

Figure 4.5. Determination of blocking efficiency. Non-specific interaction was evaluated and compared between ethanolamine and PEG-*b*-PAAc.

4.4.1. Evaluation of SELEX processes by SPFS and radioisotope-labeling

SPFS analyses showed that the binding affinity of the initial randomized library against Tokio-virus (8 μg/mL) was 1.5 times higher than the background level and that the fluorescence count (count per second) was 1400 (blue line in the Figure 4.6a), whereas the partially selected molecules from different selection cycles (4th, 7th, and 11th cycles) exhibited fluorescence counts of 3700, 27,000, and 36,000, respectively (Figure 4.6a & b). The reflectance spectra obtained during measurements are also shown (black line in the figure). The fluorescence intensity show the peaks as positions where the reflectance spectra show dips, indicating that the fluorescence is induced by the electric field enchanced by SPR. The background fluorescent count with HEPES binding buffer (red line in the figure) was approximately 1000, indicating the acceptable levels of signal to noise ratio (S/N). Similarly, we also checked the binding affinity of the initial library and the molecules from the 11th cycle with Jilin-HA. It was noticed that the fluorescence count increased from 2400 to 8100 (Figure 4.6c & d). The same molecules were also tested by filter-binding assays, aided by radioisotope-labeling with Tokio-virus concentration of 2.5 to 10 μg/mL; these assays confirmed the progress in the selection

cycles in this study with binding percentages of molecules against Tokio-virus as 0%, 3.7%, 9%, and 13.5% for the initial library, 4th, 7th, and 11th cycles, respectively. In the case of Jilin-HA (8 μg/mL), the selected molecules from the 11th cycle showed binding percentage of 13% and there was no binding with the initial library. The results obtained from both SPFS (Figure 4.6a–d) and filter-binding assays (Tables 4.1 & 4.2) clearly showed that the selected molecules include potential aptamer candidates for each target.

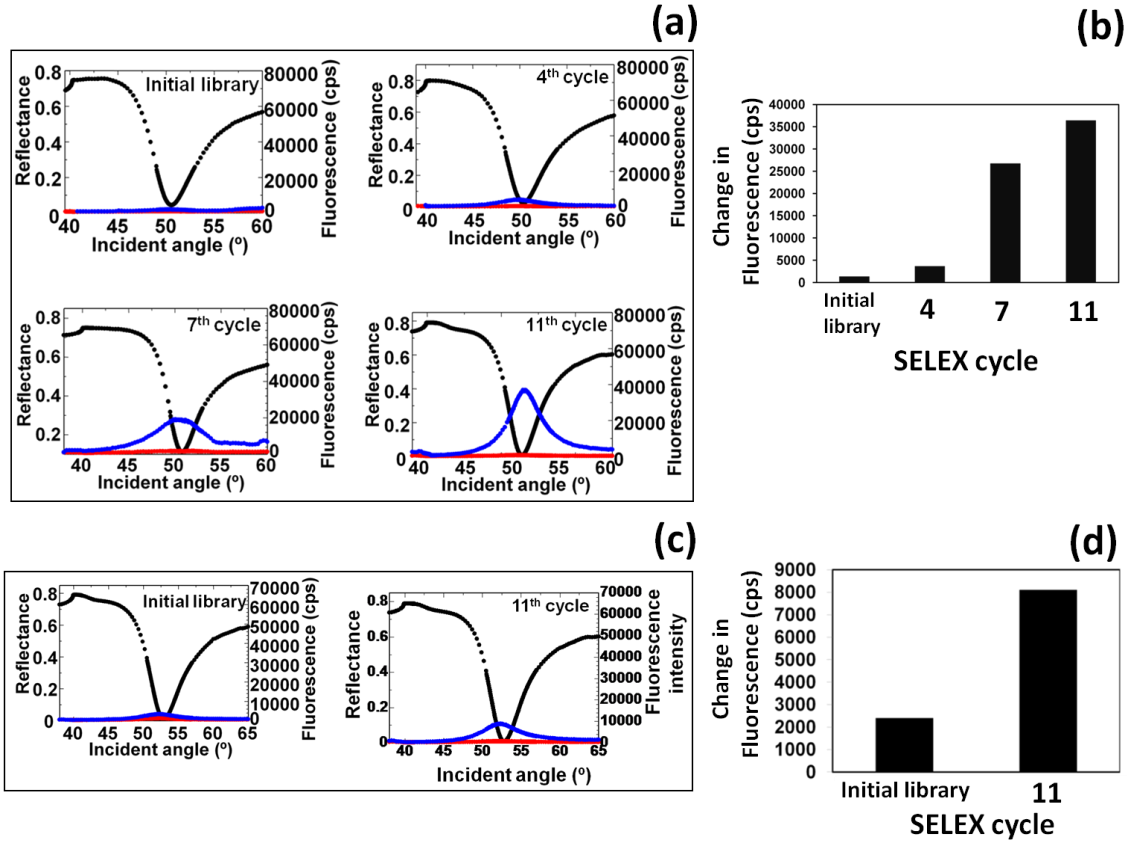

Figure 4.6. Analyses of interactions between the targets and the molecules selected from different stages of selection cycles by SPFS. (a) Spectral changes with different selection cycles against Tokio-virus. The initial, 4th, 7th, and 11th cycles are shown. The red and blue spectral lines indicate the fluorescence levels for HEPES binding buffer and aptamer-target interactions, respectively. (b) Graphical representation for the fluorescence intensities in Figure 4.6 (a). (c) Spectral changes with different selection cycles against the target Jilin-HA. The initial and 11th cycles are shown. The red and blue spectral lines indicate the fluorescence levels for HEPES binding buffer and aptamer-target interactions, respectively. Reflectance spectra (black lines) of the sensing surface covered with buffer, obtained by irradiation with laser having wavelength of 632.8 nm. (d) Graphical representation for the fluorescence intensities if Figure 4.6(c).

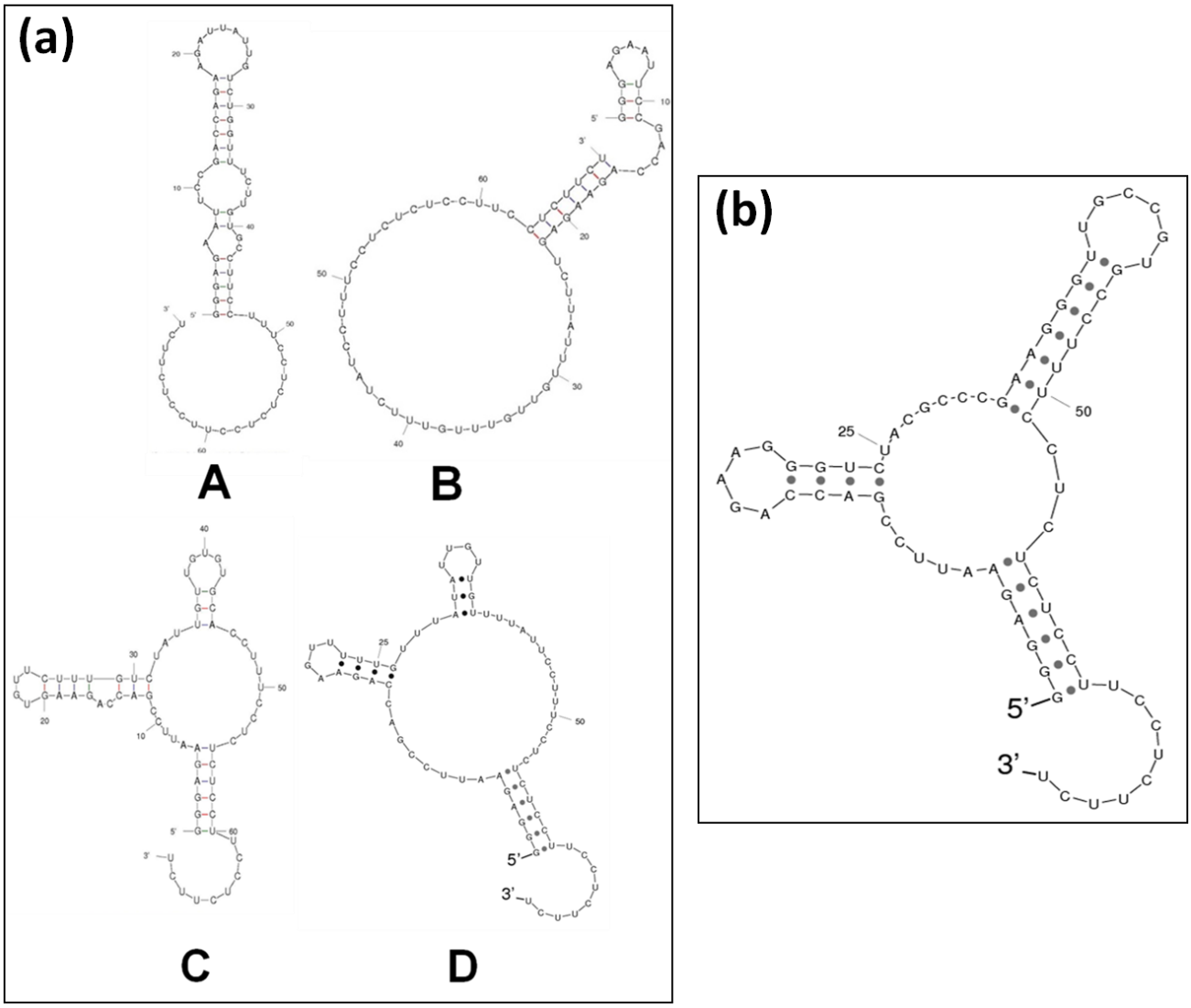

Figure 4.7. Secondary structure of the selected clones against (a) Tokio-virus (clones A,B,C and D), predicted by the Sfold software (b) Secondary structure of the selected clone against Jilin-HA, predicted by the Sfold software.

4.4.2. Aptamer binding analyses

Because the 11th-cycle molecules had a sufficient binding affinity with their targets, the molecules from the 11th cycle were cloned into a TA-vector system, and the individual clones were sequenced. Based on the sequence homologous regions, 4 dominant clones were found for Tokio-virus and single clone for Jilin-HA (Figure 4.7a & b). From all the sequenced clones, the frequency of

these 4 clones represented 16% of the total population; these molecules contained the common sequence motif “GUU”, and these motifs were positioned in the single-stranded regions of the secondary structures of the selected clones (Figure 4.8). These independent clones (A, B, C, and D) were tested by the filter-binding assay against the Tokio-virus. Among these 4 clones, clone D was chosen as the best aptamer, it showed the highest binding percentage with 16 µg/mL of Tokio-virus, that is, 20% (Figure 4.9a). On the other hand, only 1 predominant clone was found to exist for Jilin-HA (Figure 4.7b), and it represented 56% of the total isolated population and exhibited a binding percentage of 14% with 16 µg/mL of Jilin-HA (Figure 4.9b).

	Forward primer	Randomized region	Reverse primer
	GGGAGAAUUCCGACCAGAAG	AUUCAUUUCUCAACCAUCGUCUCAA	CCUUUCCUCUCUCCUUCCUCUUCU
	GGGAGAAUUCCGACCAGAAG	ACUACUUCAUCAUUAGGCCUCGUUG	CCUUUCCUCUCUCCUUCCUCUUCU
	GGGAGAAUUCCGACCAGAAG	CCAAAGUUAACCGUAAUGUCUUGUA	CCUUUCCUCUCUCCUUCCUCUUCU
	GGGAGAAUUCCGACCAGAAG	CCUUUAGUGUUGCUUGUGUCUUUA	CCUUUCCUCUCUCCUUCCUCUUCU
	GGGAGAAUUCCGACCAGAAG	ACGUACUGUCGGCGUAGUACUGGAU	CCUUUCCUCUCUCCUUCCUCUUCU
A	GGGAGAAUUCCGACCAGAAG	AUUAUUGUCUGGUUUCUUGUGCCUU	CCUUUCCUCUCUCCUUCCUCUUCU
	GGGAGAAUUCCGACCAGAAG	UGUGUUCCUGUUUCUUCNUUUGUUA	CCUUUCCUCUCUCCUUCCUCUUCU
	GGGAGAAUUCCGACCAGAAG	UAGCCUCACAUUGAACAUUUAUAU	CCUUUCCUCUCUCCUUCCUCUUCU
	GGGAGAAUUCCGACCAGAAG	UAGGUCCAGAAUCUUGUUUAACUGU	CCUUUCCUCUCUCCUUCCUCUUCU
	GGGAGAAUUCCGACCAGAAG	UUUGUGGCUCCUUUGGGCCGCCGUU	CCUUUCCUCUCUCCUUCCUCUUCU
B	GGGAGAAUUCCGACCAGAAG	AGUCUUAUUUGUUGUUUGUUUCUAU	CCUUUCCUCUCUCCUUCCUCUUCU
	GGGAGAAUUCCGACCAGAAG	UCACAUUGAUACUUAGACGGUUUAC	CCUUUCCUCUCUCCUUCCUCUUCU
	GGGAGAAUUCCGACCAGAAG	UUUAUGCUCGUGGUUUGUGCUCUGU	CCUUUCCUCUCUCCUUCCUCUUCU
C	GGGAGAAUUCCGACCAGAAG	UGUUCUUUGUCUAUUGUUGUGUGCA	CCUUUCCUCUCUCCUUCCUCUUCU
	GGGAGAAUUCCGACCAGAAG	UUUGCCUAACGACCUGUGUGGGGGU	CCUUUCCUCUCUCCUUCCUCUUCU
	GGGAGAAUUCCGACCAGAAG	CGAUUCUGCAACAAGUUCGACUCCG	CCUUUCCUCUCUCCUUCCUCUUCU
	GGGAGAAUUCCGACCAGAAG	AUAAUUUUCAUGAUCGGCCCACUGU	CCUUUCCUCUCUCCUUCCUCUUCU
D	GGGAGAAUUCCGACCAGAAG	UUUUUGUUUAUAUUGUUGUUUUAUU	CCUUUCCUCUCUCCUUCCUCUUCU
	GGGAGAAUUCCGACCAGAAG	GGCGUCGUGCGAGAAGCCAACGAG	CCUUUCCUCUCUCCUUCCUCUUCU
	GGGAGAAUUCCGACCAGAAG	UCAUGUUUUUUCGAGCGUUUUUCAU	CCUUUCCUCUCUCCUUCCUCUUCU

Figure 4.8. Sequences obtained after SELEX process against Tokio-virus. Four major clones are obtaining having a consequence region of ‘GUUU’. Other than these clones having ‘GUU’ region.

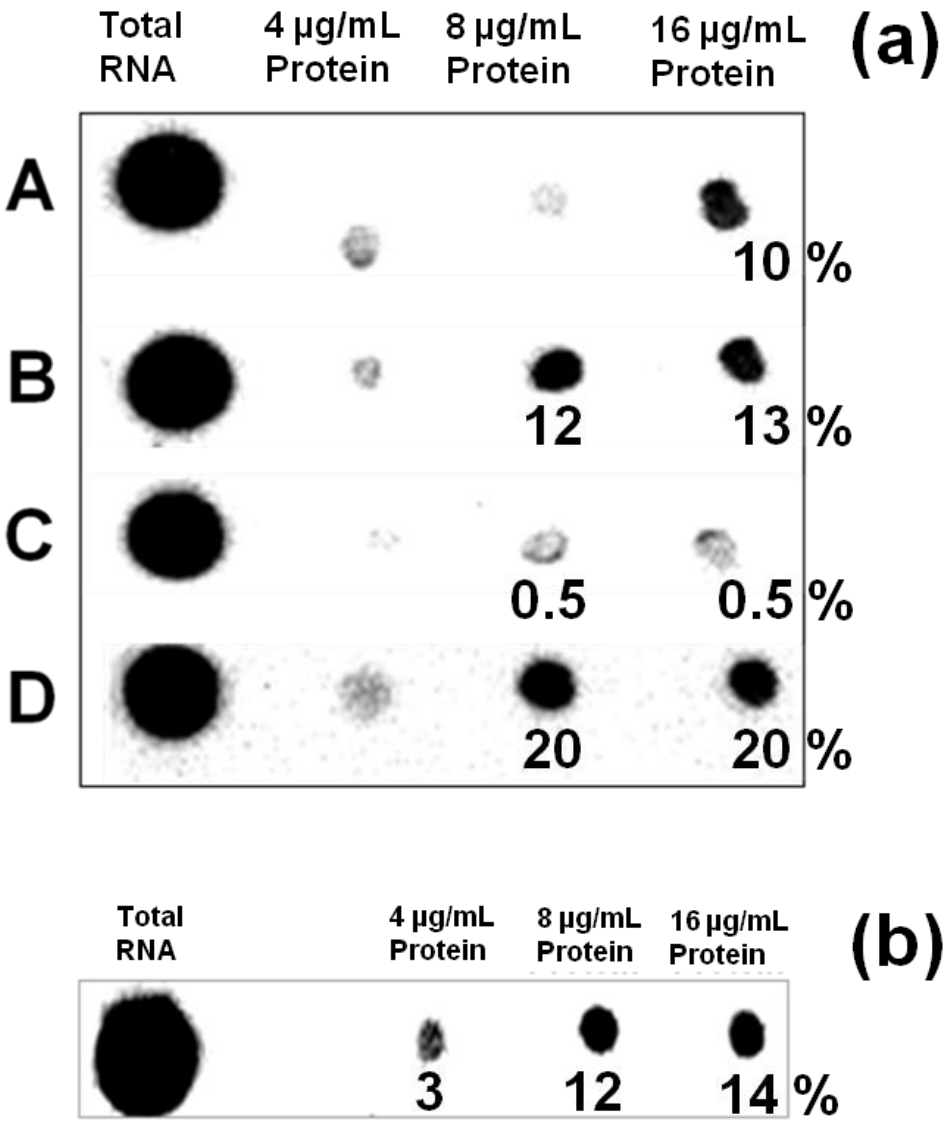

Figure 4.9. Results of the filter binding analyses. (a) Selected aptamers (clone A,B, C and D) from SELEX process vs Tokio –virus and (b) selected aptamer from SELEX process vs Jilin-HA. Aptamers were labeled by incorporating α-ATP (P^{32}) in the transcription reaction and separated on the gel. After making the labeled aptamer and target complex, it was filtered on a nitrocellulose membrane. An imaging film was exposed on the membrane and counts were measured.

4.4.3. Determination of the detection limit of the selected aptamers

To check the detection limit of the selected aptamers, we titrated the target concentration from low ng/mL levels to μg/mL levels against a constant concentration of the aptamer.

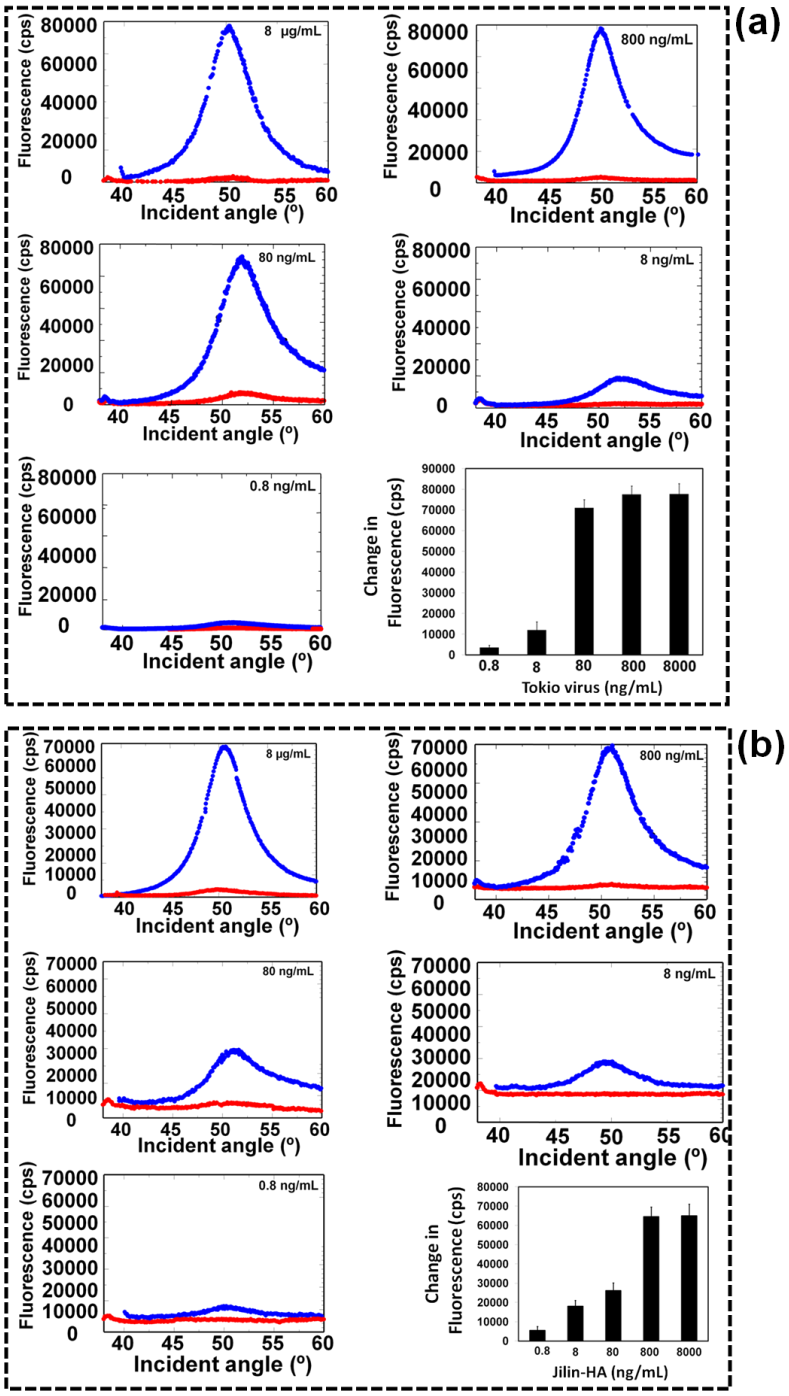

Figure 4.10. Analyses of the selected aptamer against (a) Tokio-virus. Graphical representation for the binding analysis with the selected aptamer (clone D) against 0.8 ng/mL to 8 µg/mL of Tokio-virus is shown. (b) Jilin-HA by SPFS. Interactive analyses were performed with the aptamer (100 nM) against dose dependent target (8 µg/mL to 0.8 ng/mL). Graphical representation for the binding analysis of the selected aptamer against 0.8 ng/mL to 8 µg/mL of Jilin-HA is shown. The red and blue spectral lines indicate the fluorescence levels for the HEPES binding buffer and aptamer-target interactions, respectively. The changes in the fluorescence were observed from 8 ng/mL of the targets, and clear increase was noticed in a concentration dependent manner.

The changes in the fluorescence was observed from 8 ng/mL of Tokio-virus with the selected aptamer (clone D), and clear increase was noticed in a concentration dependent manner, and the change were saturated at the concentration of 80 ng/mL (Figure 4.10a). Similarly, the binding between the Jilin-HA and aptamer for it was also tested, in this case, the sensitivity level was almost the same as in the case of Tokio-virus (about 8 ng/mL) (Figure 4.10b). Both selected aptamers showed limit of detection against the targets at low ng/mL. Detection limit is calculated with the value from 3 times higher fluorescence counting than the control experiment.

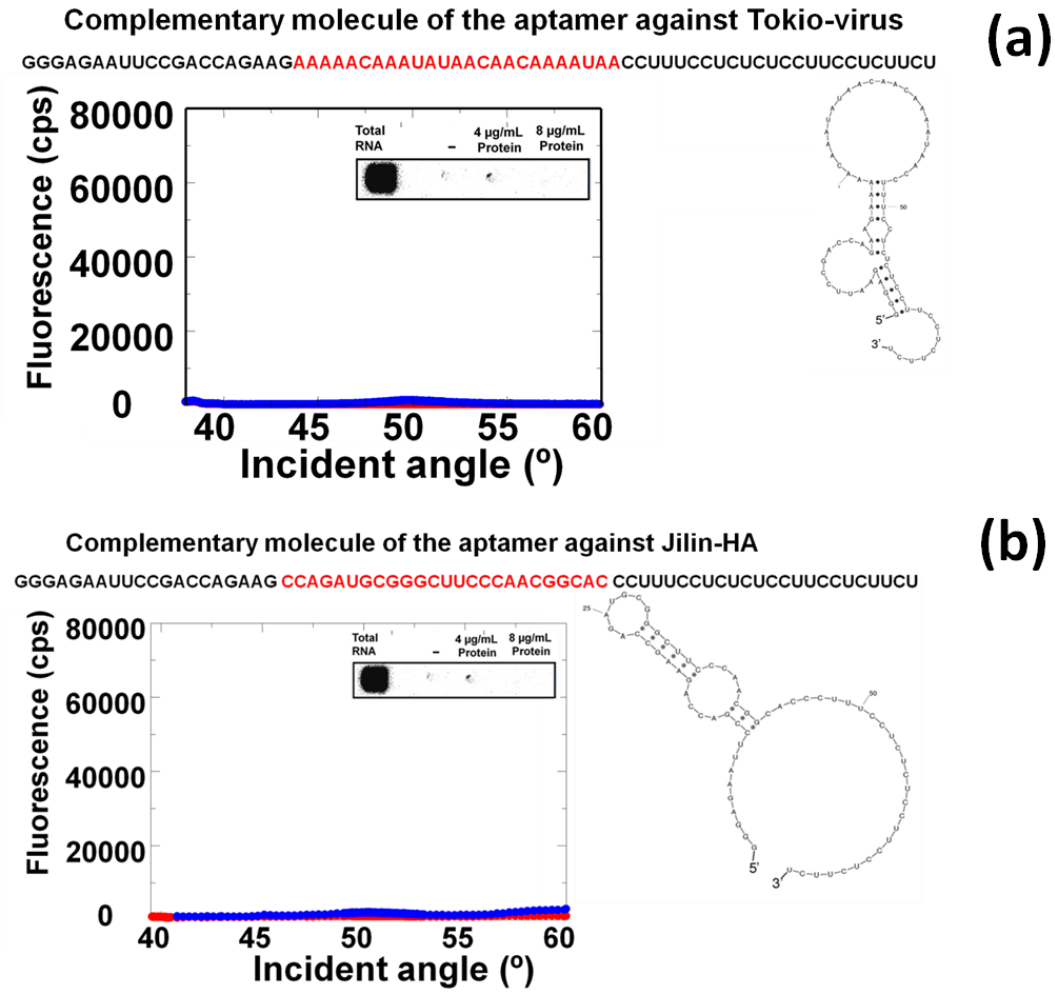

Figure 4.11. SPFS analyses of complementary sequences of the selected aptamers against Tokio-virus (a) and Jilin-HA (b). Secondary structures predicted by the Sfold software are shown. The red and blue spectral lines indicate the fluorescence levels for the HEPES binding buffer and interactions of aptamer-target, respectively. The insets are the results obtained from the filter binding assay. Complementary sequences are failed to bind with the targets in both cases.

Developing high affinity sensing systems for the detection of influenza viruses has been highly encouraged.[25,26] Previously, Lee et al.[27] proposed an analytical kit to detect influenza viruses and showed the sensitivity level of 73 ng/mL. The present analytical detection with the aptamers has one-order higher sensitivity. The aptamer generated against the Tokio-virus reached saturation at 80 ng/mL whereas the aptamer against Jilin-HA reached saturation at 800 ng/mL (Figure 4.10a & b); this difference might be attributable to the larger size of the virus compared to that of the HA protein. Quantitative work will be required in order to clarify this point. For a control experiment, the author also tested the complementary sequences against the targets, and these sequences completely lost their binding capacity against the targets (Figure 4.11a & b).

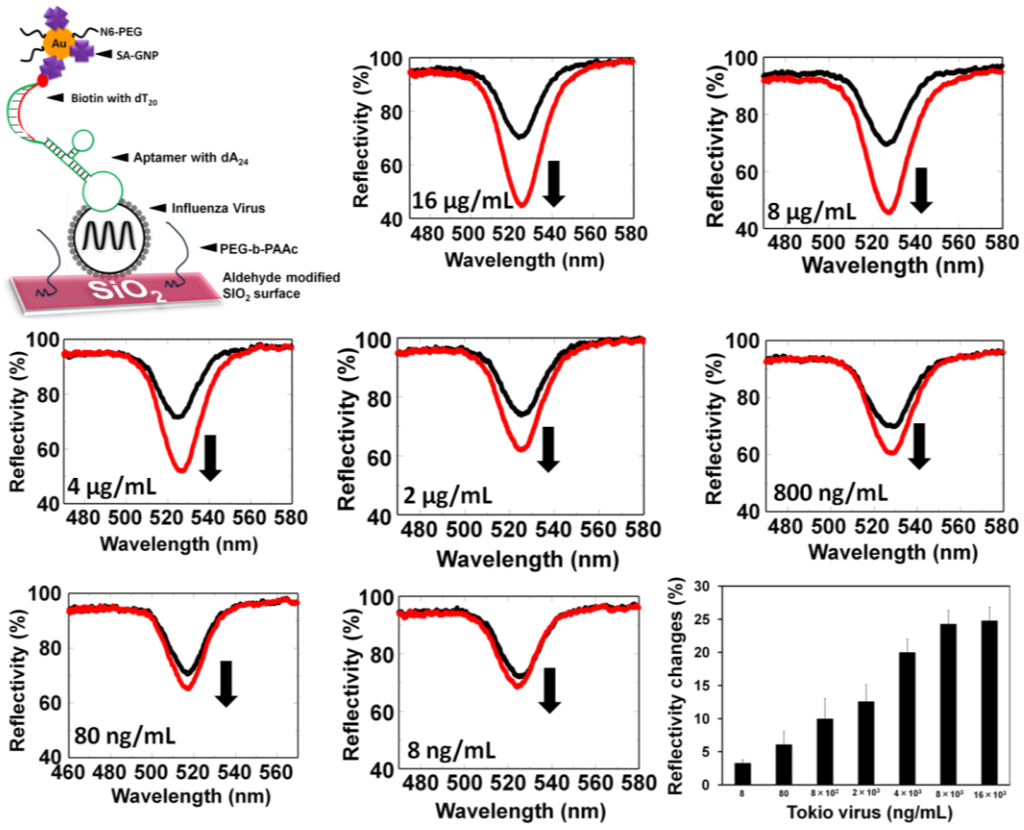

Figure 4.12. Determination of detection limit of the aptamer against Tokio-virus using the waveguide-mode sensor. Representation for the surface modification is shown. Interactive analyses were performed with the aptamer (100 nM) against dose dependent Tokio-virus. The black and red curves are the spectra before and after the attachment of SA-GNP, respectively. Arrows indicate the direction of changes in the spectra. Graphical representation of reflectivity changes of selected aptamer vs Tokio-virus is shown.

Furthermore, these detection limit levels were also confirmed by the waveguide-mode sensor by using the aptamers and targets, the measurements were carried out using SA-GNPs. This GNP hybrid sensing system was previously demonstrated to have high sensitivity for the interactions of biotin and streptavidin[24] and antibody-based detection of influenza viruses.[28] Similarly, the aptamer generated in this study was evaluated with the respective target in a dose-dependent manner.

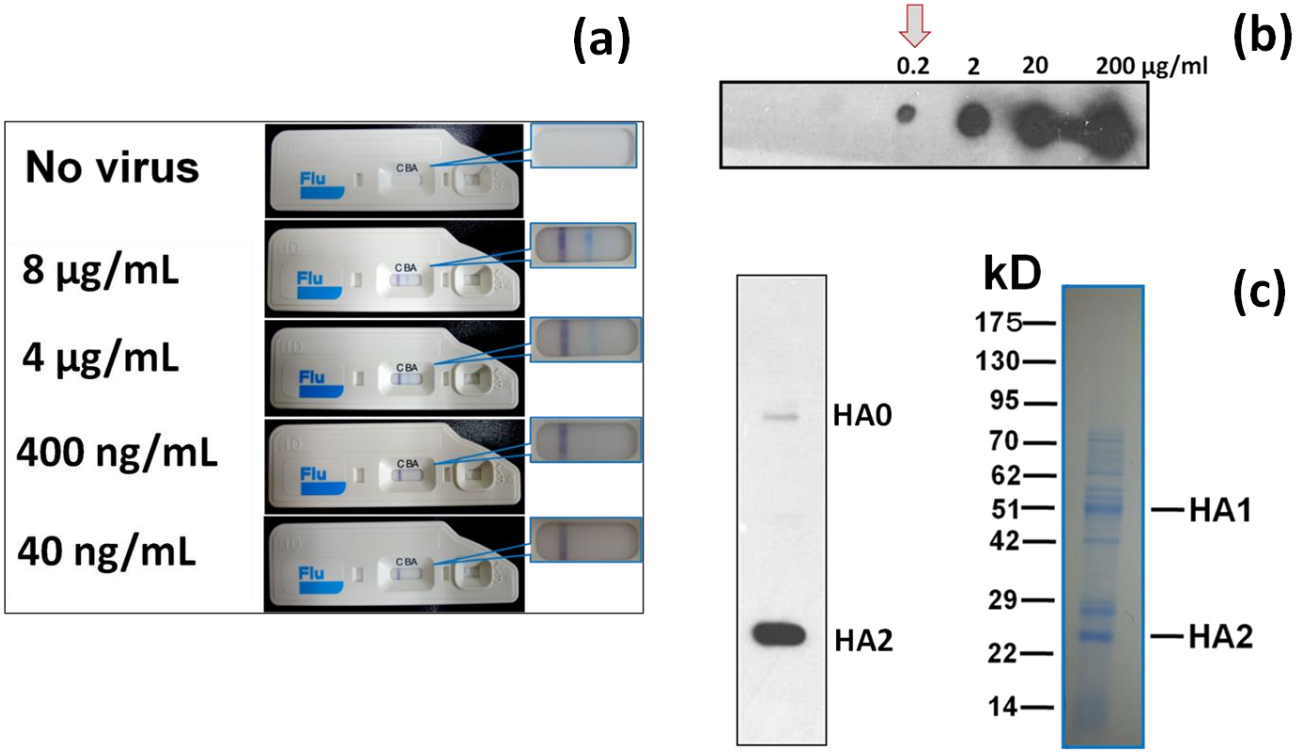

Figure 4.13. Specificity of the target molecules were determined by (a) Immunochromagraphy test. Different amounts of virus was dissolved in the supplied buffer and loaded on the windows of ICT. After 10 min of incubation the photographs were taken. Positive band appeared at the virus concentration 4 µg/mL and above. (b) Dot-blot analyses for primary antibody vs secondary antibody. Different amount of viruses (0.2 to 200 µg/mL) were spotted on the nitrocellulose membrane. After blocking, the specificity of primary antibody interactions with secondary antibody was analyzed using a 1:1000 dilution of secondary antibody, followed by ECL-plus blotting detection. (c) Western blot analyses for antibody and Tokio-virus. After transfer the protein, the membrane was blocked with 3% nonfat milk then treated with a 1:10,000 dilution of the primary antibody. After washing, the membrane was incubated with horseradish peroxidase-conjugated goat anti-mouse immunoglobulin G (secondary antibody). The immunocomplexes thus formed were visualized by staining with ECL-plus western blotting detection solution.

To check the detection limit, we titrated the Tokio-virus concentration from 8 ng/mL to 16 μg/mL against constant concentrations of aptamer, PEG-*b*-PAAc (4 mg/mL), biotin-dT_{20} (100 nM), and SA-GNP (1 OD) mixed with 0.5 mg/mL of N6-PEG. Inclusion of PEG-polymers in the reaction mix for biomolecular interactions was reported to increase specificity.[21,29] 8 ng/mL of Tokio-virus shows the reflectivity changes of 4% and the saturation level was 8 μg/mL (Figure 4.12). Immunochromatography (ICT) was carried out to compare the detection levels of the SPFS and the waveguide-mode sensor, and it was clear that both sensors showed higher sensitivity than ICT (Figure 4.13a).

4.4.4. Comparison of anti-influenza antibody and aptamer

To compare the aptamer with antibody, the specific interaction of anti-influenza B antibody and detection antibody was analyzed by dot-blot analysis, which showed that 200 ng/mL of anti-influenza antibody was the ideal dilution (Figure 4.13b).

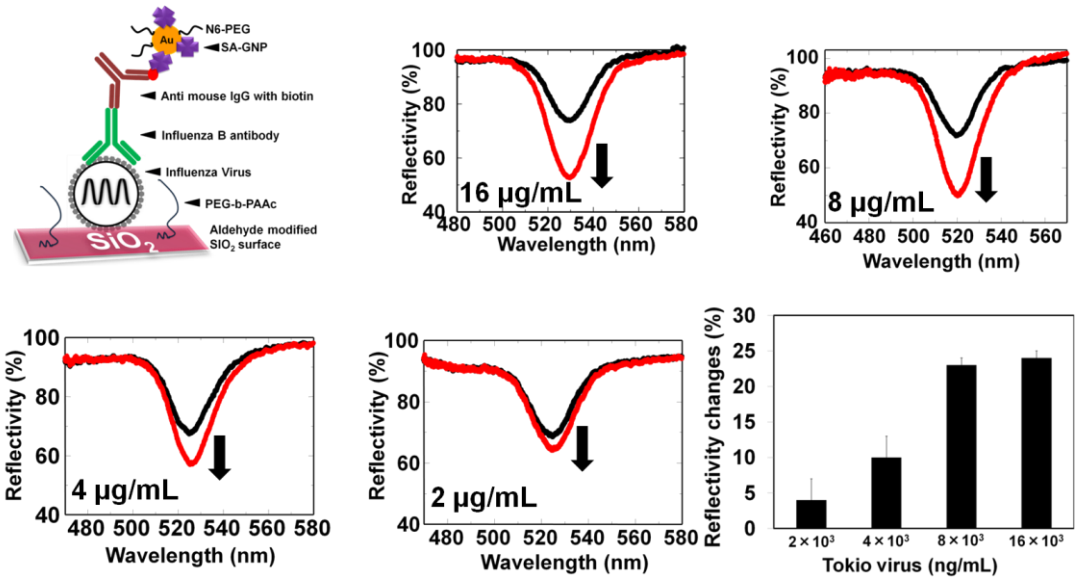

Figure 4.14. Binding analyses of antibody against Tokio-virus by waveguide-mode sensor. Representation for the surface modification is shown. Interactive analyses were performed with the antibody (100 nM) against dose dependent Tokio-virus. The black and red curves are the spectra before and after the attachment of SA-GNP, respectively. Arrows indicate the direction of changes in the spectra. Graphical representation of reflectivity changes of antibody vs Tokio-virus is shown.

The anti-influenza antibody was also evaluated against Tokio-virus by western blot analysis, the results clearly showed that the antibody predominantly interacted with HA2 (Figure 4.13c). Analyses with the waveguide-mode sensor by using the antibody against Tokio-virus clearly showed the spectral changes until 2 μg/mL of Tokio-virus. Concentrations lower than 2 μg/mL did not result in significant changes in the spectrum. The saturation point was 8 μg/mL (Figure 4.14). Similar titration was also carried out by SPFS analyses in a dose-dependent manner by using Tokio-virus against the Alexa Fluor-conjugated antibody; and the sensitivity was μg/mL level (Figure 4.15), which was similar to the result obtained in the waveguide-mode sensor.

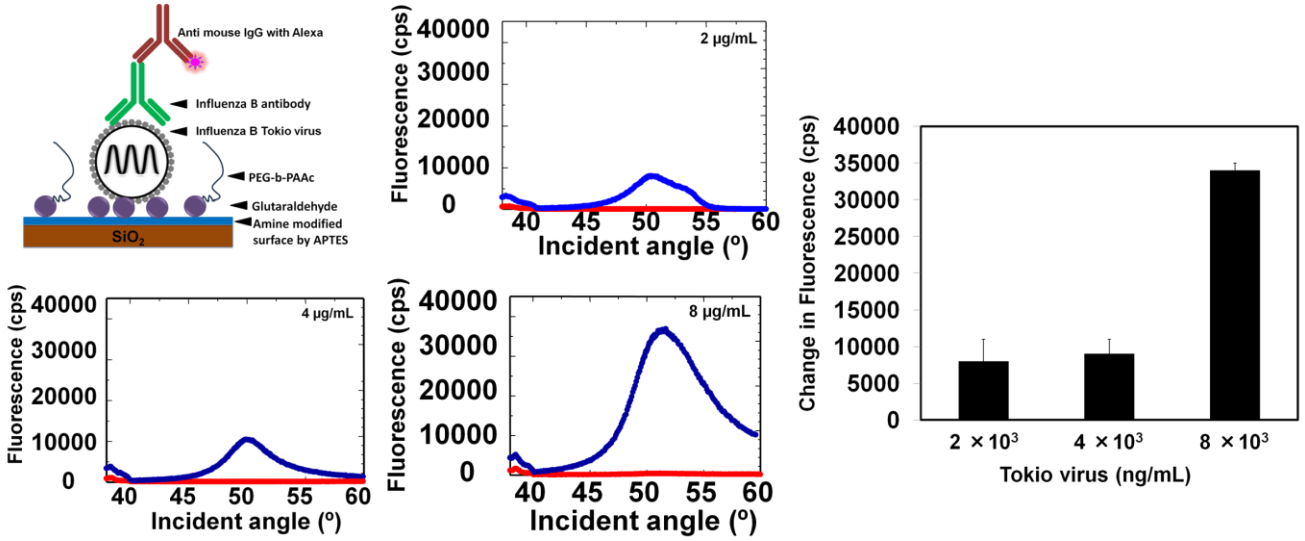

Figure 4.15. Binding analyses of antibody against Tokio-virus by SPFS. Interactive analyses were performed with the antibody (100 nM) against dose dependent Tokio-virus. Clear increment was noticed in a concentration dependent manner. The red and blue spectral lines indicate the fluorescence levels for the HEPES binding buffer and antibody-Tokio-virus interactions, respectively. Graphical representations for the binding analysis of the antibody vs Tokio-virus is shown.

Based on these results with both aptamer and antibody, it was clear that the sensitivity (8 ng/mL) of the aptamer is approximately 250-fold higher than that (2 μg/mL) of the tested antibody. The K_d values of the abovementioned generated aptamers were evaluated by the filter-binding assay by using the targets against the PcP (P^{32}) 3′ end-labeled aptamers. Different concentrations of the targets ranging

from 0 to 51.2 μg/mL were used against a constant aptamer concentration. Based on the statistical calculation, the K_d values were determined to be 0.7 ± 0.2 μg/mL and 1.2 ± 0.2 μg/mL, respectively (Figure 4.16a & b), for Tokio-virus and for Jilin-HA.

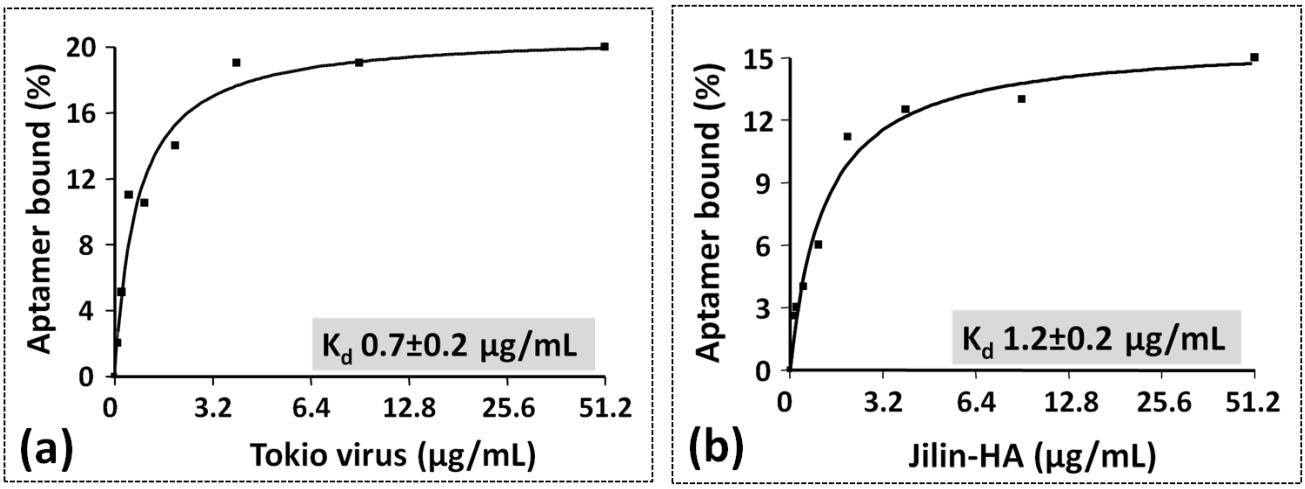

Figure 4.16. Determination of the dissociation constants (K_d) for the selected aptamers. Targets were used in concentrations from 0 to 51.2 μg/mL of target (a) K_d of the selected aptamer against Tokio-virus. (b) K_d of the selected aptamer against Jilin-HA.

4.4.5. Potential binding regions of the aptamers

Using the aptamers generated in this study, we attempted to identify the target-binding regions of the aptamer by mapping analyses. To map the binding region, we performed phosphate interference analysis. Initially, phosphates in the backbone of the aptamers were modified by ethanol-saturated ENU at 90ºC with 20 mM HEPES, pH 8.0, and 1 mM EDTA. With this reaction, phosphates are modified to a phosphotriester, which would create an ideal situation for mild alkaline cleavage. It is expected to be the modification or incorporation of the ENU in each phosphate moiety. The modified aptamers reacted with their target separated from the unbound molecules by membrane filter. Images obtained from the fractionation of these samples by 12% polyacrylamide gel containing 7 M urea showed clear profiles and indicated the binding regions for the aptamers by comparing the uncleaved

regions in the absence of the target in the gel pattern. The position of the interferences was predicted with alkali- and T1 enzyme-digested aptamer bases. In the case of the Tokio-virus aptamer, 2 major domains were involved in the binding regions. One was in the region from 4 to 26 bases and the other was between bases 34 and 38 (Figure 4.17a).

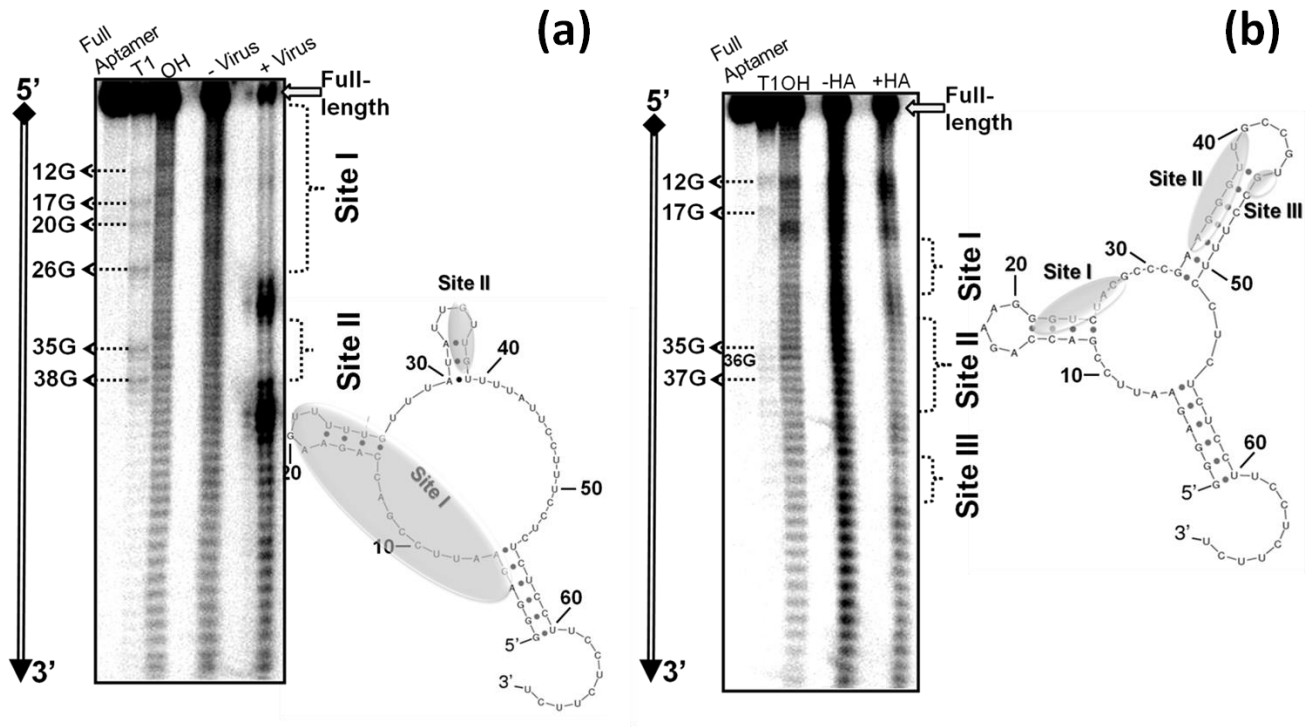

Figure 4.17. Ethylnitrosourea mapping of interfering phosphates of the selected aptamer against (a) Tokio-virus and (b) Jilin-HA. Binding regions are displayed on the secondary structures.

Similarly, in the case of Jilin-HA, the binding regions were found in the following phosphate regions: bases 21–27, 33–39, and 44-45 (Figure 4.17b). In both cases, the region of phosphate inferences was on the single-strand loop regions of the secondary structures that were predicted by the Sfold online software (http://sfold.wadsworth.org/cgi-bin/index.pl).

4.4.6. Discrimination of influenza viruses

With the purpose of discriminating the influenza viruses with the selected aptamer in this study,

we performed filter-binding analyses with different proteins obtained from different subtypes of the influenza viruses belonging to either the A or B type. Based on the results obtained, the selected aptamers against the targets failed to interact with HA of other influenza strains A/California/07/2009 (H1N1), A/India/NIV33487/2006 (H5N1), and A/Japan/305/1957 (H2N2), or intact virus of A/Panama/2007/1999 (H3N2) (Figure 4.18 & Table 4.3).

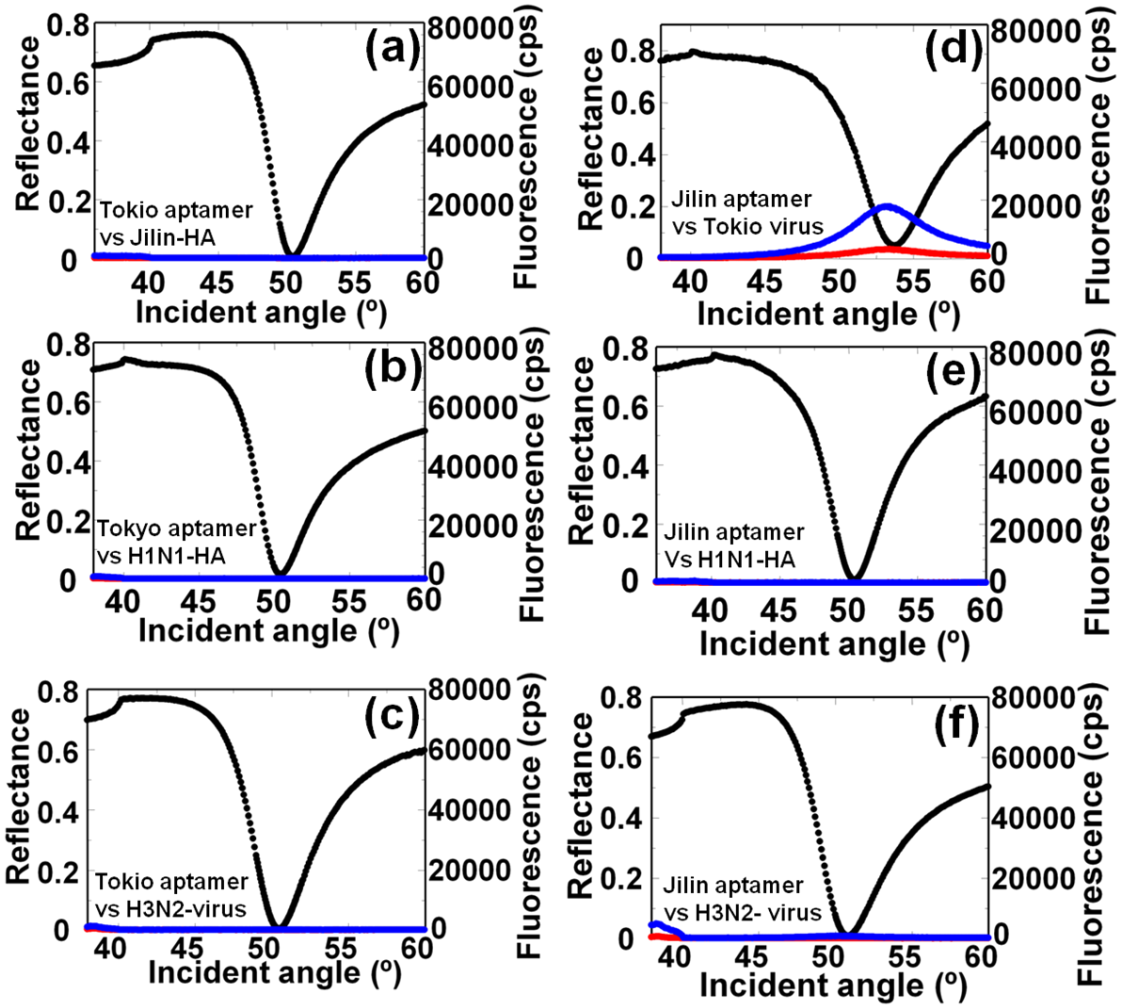

Figure 4.18. Analyses of the selected aptamer against different viruses or HA by SPFS. Spectral changes with the anti-Tokio-virus aptamer against, (a) HA from Jilin-HA, (b) HA of A/California/07/2009 (H1N1), (c) virus A/Pananma/2007/1999 (H3N2). Spectral changes with the anti- Jilin-HA aptamer against, (d) Tokio-virus, (e) HA of A/California/07/2009, and (f) virus A/Pananma/2007/1999. The concentration of the virus and HA was 8 μg/mL. The red and blue spectral lines indicate the fluorescence levels for the HEPES binding buffer and aptamer interactions, respectively. Reflectance spectra (black lines) of the sensing surface covered with buffer, obtained by irradiation with laser having wavelength of 632.8 nm.

These results imply that the selected aptamers are not able to bind with influenza A types. We also investigated the cross-reactivity between the aptamers against Tokio-virus and Jilin-HA. Similarly, discrimination studies were also carried out by SPFS and similar results were obtained (Figure 4.19a–f). Based on both studies, aptamer generated against Tokio-virus has predominant binding with whole Tokio-virus and there is a possibility that this aptamer may bind to one of the major surface proteins [Hemagglutinin (HA) or Neuraminidase (NA)] of Tokio-virus. More possibility with HA, because it is the major protein among all proteins resides in influenza virus. This aptamer lost its binding with Jilin-HA, so that the selected aptamer may discriminate Tokio-virus from Jilin-virus. On the other hand, aptamer generated against Jilin-HA has a little affinity to Tokio-virus, but it can recognize the Jilin-HA efficiently. Taken together, the sensing system shown here, based on fluorescent labeling (SPFS) and GNP-conjugates (waveguide-mode sensor), will pave the way to develop higher sensititve detection of influenza viruses in clinical relevant samples using the generated aptamers.

Type	Subtype/ Lineage	Strain	Binding
B	Victoria	B/Tokio/53/1999	positive
A	H1N1	California/07/2009	Negative
A	H5N1	A/Chicken/India/ NIV33487/2006	Negative
A	H2N2	Japan/305/1957	Negative
A	H3N2	Panama/2007/1999	Negative
B	Yamagata	B/Jilin/20/2003	Negative

Type	Subtype Lineage	Strain	Binding
B	Yamagata	B/Jilin/20/2003	positive
A	H1N1	California/07/2009	Negative
A	H5N1	A/Chicken/India/ NIV33487/2006	Negative
A	H2N2	Japan/305/1957	Negative
A	H3N2	Panama/2007/1999	Negative
B	Victoria	B/Tokio/53/1999	Positive

Table 4.3. Results of discrimination analyses using the selected aptamer against (a) Tokio-virus and (b) Jilin-HA obtained by the filter binding assays.

4.5. Conclusions

Two aptamers were generated with random regions of 25 nucleotides against the Tokio-virus (Victoria) and Jilin-HA (Yamagata). The progression in the selection processes was evaluated by the SPFS and conventional radioisotope labeling strategies. Both aptamers have K_d around 1 µg/mL

against their targets. With the SPFS system and the waveguide-mode sensor, the detection limits were determined to be low ng/mL. Furthermore, the selected aptamers could discriminate HA proteins of different influenza viruses. Sensing system with the generated aptamers shown here can be an alternate approach to distinguish the strains belonging to the same type, which would be useful to speed up the surveillance of emerging influenza strains.

4.6. References

1. Ellington, A.D., Szostak, J.W., *Nature* **1990**, 346, 818–822.
2. Tuerk, C., Gold, L., *Science* **1990**, 249, 505–510.
3. Robertson, D.L., Joyce, G.F., *Nature* **1990**, 344, 467–468.
4. Gopinath, S.C.B., Misono, T., Mizuno, T., Kawasaki, K., Kumar, P.K.R., *J. Gen. Virol*. **2006**, 87, 479-487.
5. Gopinath, S.C.B., Hayashi, K., Kumar, P.K.R., *J. Virol.* **2012**, 86, 6732–6744.
6. Ardjomandi, N., Niederlaender, J., Aicher, W.K., Reinert, S., Schweizer, E., Wendel, H.P., Alexander, D. *Nucleic Acid Ther.* **2013**, 23, 44-61.
7. Ninomiya, K., Kaneda, K.; Kawashima, S., Miyachi, Y., Ogino, C., Shimizu, N., *Bioorg. Med. Chem. Lett.* **2013**, 23, 1797-1802.
8. Jayasena, S.D., *Clin. Chem.* 1999, 45, 1628-1650.
9. Gopinath, S.C.B., In.: Encyclopedia of Analytical Chemistry, eds R.A. Meyers, John Wiley: Chichester. Published on 15th March 2011, pp 1–27.
10. Scholtissek, C., Burger, H., Kistner, O., Shortridge, K.F., *Virology* **1985**, 147, 287-294.
11. Webster, R.G., Bean, W.J., Gorman, O.T., Chambers, T.M., Kawaoka, Y., *Microbiol. Rev.* **1992**, 56, 152-179.
12. Biere, B., Bauer, B., Schweiger, B., *J. Clin. Microbiol.* **2010**, 48, 1425–1427.
13. Wongphatcharachai, M., Wang, P., Enomoto, S., Webby R.J., Gramer, M.R., Amonsin, A., Sreevatasan, S., *Clin. Microbiol.* **2013**, 51, 46–54.
14. Jeon, S.H., Kayhan, B.,Ben-Yedidia, T., Arnon, R., *J. Biol. Chem.* **2004**, 279, 48410-48419.
15. Ishida, A., Sakata, Y., Majima, T., *Chem. Commum.* 1998, 1, 57-58.
16. Liebermann, T., Knoll, W., *Colloids Surf. A* **2000**, 171, 115-130.
17. Fukuda, N., Mitsuishi, M., Aoki, A., Miyashita, T., *J. Phys. Chem. B* **2002**, 106, 7048–7052.

18. Neumann, T., Johansson, M., Kambhampati, D., Knoll, W., *Adv. Func. Mater.* **2002**, 12, 575–586.
19. Yamamoto-Fujita, R., Kumar, P.K.R., Anal. Chem., **2005**, 77, 5460–5466.
20. Gopinath, S.C.B., Awazu, K., Fujimaki, M., Shimizu, K., Mizutani, W., Tsukagoshi, K., *Analyst* **2012**,137, 3520-3527.
21. Lakshmipriya, T., Fujimaki, M., Gopinath, S.C.B., Awazu, K., Horiguchi, Y., Nagasaki, Y., *Analyst* **2013**, 138, 2863-2870.
22. Urvil, P.T., Kakiuchi, N., Zhou, D., Shimotohno, K., Kumar, P.K.R., *Eur. J. Biochem.* **1997**, 248, 130–138.
23. Fujimaki, M., Rockstuhl, C., Wang, X., Awazu, K., Tominaga, J., Koganezawa, Y., Ohki, Y., Komatsubara, T., *Opt. Exp.* **2008**, 16, 6408–6416.
24. Fujimaki, M., Nomura, K., Sato, K., Kato, T., Gopinath, S.C.B., Wang, X., Awazu, K., Komatsubara, T., Ohki, Y., *Opt. Exp*. **2010**, 18, 15732–15740.
25. Suenaga, E., Mizuno, H., Kumar, P. K. R., *Biosens. Bioelectron.* **2012**, 32, 195–201.
26. Wang, R., Li, Y., *Biosens. Bioelectron.* **2013**, 42, 148–155.
27. Lee, G., Jeon, E., Kim, W., Le, D.T., Yoo, J., Chong, C., *Virology J.* **2010**, 7, 244–248
28. Gopinath, S.C.B., Awazu, K., Fujimaki, M., Shimizu, K., Shima, T., *Plos One* **2013**, 8, e69121.
29. Nagasaki, Y., *Polymer J.* **2011**, 43, 949–958.

Chapter 5

Summary

Developing high-performance nano-biosensors is highly relying on sensitivity and specificity to recognize the analyte in the mixture of sample. To fulfill these criteria, the construction of sensing surface with high non-fouling and the choice of probe are mandatory. The sensing surface construction with synthetic polymers is reported to have higher non-fouling, whereas the natural polymers are giving non-specificity in most of the cases. Regarding the specific probe, antibody and aptamer are commonly considered in sensors developments. However, aptamers are found to have several advantageous over antibodies and the consistent developments in the aptamer-based sensors (aptasensors) are widely reported. In the present investigation, using the common sensing substrates (Au and SiO_2) the high-performance aptasensors are demonstrated with the assistance of Poly(ethylene glycol)-(PEG) block polymers (PEG-*b*-polymers); {PEG-*b*-poly(acrylic acid) (PEG-*b*-PAAc), pentaethylenehexamine-terminated PEG (N6-PEG) and PEG-*b*-poly[2-(N,N-dimethylamino)ethyl methacrylate] (PEG-*b*-PAMA)} using the clinically relevant analytes, human blood clotting protein (FIX) and influenza B viruses.

The results obtained are gleaned into 3 chapters (chapters 2, 3 & 4) as summarized below.

Chapter 2: *Evanescent-field-coupled Waveguide-mode sensor (PEG-b-PAAc and N6-PEG hybridized SiO_2 surface)*

(i) PEG-*b*-PAAc blocking treatment completely prevents non-specific binding on the SiO_2 sensor surface and reached the sensitivity to 100 pM for FIX-aptamer interaction.

(ii) Coating of SA-GNPs by N6-PEG increases the sensitivity by 1000 times (to 100 fM).

(iii) Higher sensitivity arises from the crowding effect of N6-PEG on the SA-GNPs, which occupy the active binding sites on the streptavidin, determined by competition assay and SEM.

(iv) FIX detection limit of 100 fM was attained even in the presence of other coagulation factors or a realistic albumin concentration.

Chapter 3: *Surface Plasmon Resonance (PEG-b-PAMA and N6-PEG hybridized Au surface)*

(i) PEG-b-PAMA treated Au surface promoted the proper orientation of thiolated DNA oligos.

(ii) Co-immobilization of PEG-b-PAMA and N6-PEG completely abolished the bio-fouling, whereas BSA has shown higher non-specificity.

(iii) The dissociation constant of FIX and aptamer was found as 37 pM in the presence of *PEG-b*-PAMA and N6-PEG.

(iv) With dual polymer construction the sensitivity was attained to 800 fM with aptamer-FIX-antibody sandwich and detected by GNP-conjugated anti-mouse IgG.

(v) Selective FIX detection was shown with albumin, glubulin containing samples and in human blood serum.

Chapter 4: *Surface Plasmon Fluorescence Spectroscopy (PEG-b-PAAc hybridized SiO_2 surface)*

(i) Two aptamers were generated against influenza viruses (Tokio-virus and Jilin-HA).

(ii) Both aptamers have the values of K_d in the range of 0.7 to 1.2 µg/mL against their targets.

(iii) PEG-*b*-PAAc completely suppresses the non-specific binding of Cy5-conjugated ssDNA on the sensing surface.

(iv) With the SPFS system in the presence of PEG-*b*-PAAc, the detection limits were determined to be low ng/mL, ~ 250-fold higher sensitivity than that of the commercial antibody.

(iv) Target-binding sites on the aptamer were predicted by mapping analyses.

(vi) Selected aptamers could discriminate other influenza viruses.

Through this work, it can be concluded that PEG-b-polymer constructed sensing surface is the potential way to develop high-performance faithful sensing systems and herein it is clearly demonstrated with different aptasensors. Further, preference of dual polymers on a given sensing system is shown to be with higher sensitive non-biofouling detections. This work will pave way to generate various sensing systems with the assistance of PEG-b-polymers for a wide range of ligand and analyte in clinical diagnosis.

List of Publications

1. **Lakshmipriya, T**., Fujimaki, M., Gopinath, S.C.B., Awazu, K., Horiguchi, Y., Nagasaki, Y., High-performance waveguide-mode biosensor for detection of FIX uses PEG-based blocking agents to suppress non-specific binding and improve sensitivity. *Analyst* **2013**, 138: 2863-2870.
2. **Lakshmipriya, T**., Fujimaki, M., Gopinath, S.C.B., Awazu, K., Generation of anti-influenza aptamers using systematic evolution of ligands by exponential enrichment for sensing applications. *Langmuir* **2013,** 29(48), 15107-15115.
3. **Lakshmipriya, T**., Horiguchi, Y., Nagasaki, Y., Co-immobilized poly(ethylene glycol)-b-poly[2-(N,N-dimethylamino)ethyl methacrylate] and pentaethylenehexamine-terminated poly(ethylene glycol) promotes sensitivity and restrict bio-fouling on gold sensor surface for detecting Factor IX in human plasma. **2013** (Submitted to Analyst).

List of Presentations

International conference: Oral Presentation

Lakshmipriya, T., Horiguchi, Y., Nagasaki, Y., Aptamer/PEG hybridized sensing surface for sensitive detection of human Factor IX by Surface Plasmon Resonance. Second International conference on Advanced Materials, Energy and Environments (ICMEE`13), Yokohama, Japan, 8-9 August, **2013**.

International conferences: Poster Presentation

1. **Lakshmipriya, T**., Horiguchi, Y., Nagasaki, Y., Poly(ethylene glycol)-block-polymers mediated anti-fouling for aptamer-factor IX interaction. MANA International symposium, 2014, Epochal Tsukuba, Japan. 5-7 March, **2014**.
2. **Lakshmipriya, T**., Horiguchi, Y., Nagasaki, Y., PEG-oriented aptamer immobilization on sensing surface for highly sensitive detection of human blood clotting Factor IX. Tsukuba International Conference on Materials Science (TICMS), University of Tsukuba, Japan, August 29-30, **2013**.
3. **Lakshmipriya, T**., Fujimaki, M., Gopinath, S.C.B., Awazu, T., Horiguchi, Y., Nagasaki, Y., Detection of FIX by Waveguide mode sensor-High performance by RNA-aptamer/gold nanaoparticle-PEG hybridized sensing. 2nd International conference on Biomaterials science in Tsukuba (ICBS 2013), Epochal Tsukuba, Japan. 19-22 March, **2013**.
4. **Lakshmipriya, T**., Fujimaki, M., Gopinath, S.C.B., Awazu, T., Horiguchi, Y., Nagasaki, Y., Detection of influenza viruses by Fluorescence based SPR - High performance sensing by RNA-aptamers/PEG hybridized sensor. MANA International Symposium 2013, Jointly with ICYS, Epochal Tsukuba, Japan. February 27- 1 March, **2013**.
5. **Lakshmipriya, T.,** Fujimaki, M., Gopinath, S.C.B., Koichi Awazu., Horiguchi, Y. and Nagasaki, Y., Protein sensing on aptamer/PEG hybrid surface by monolithic waveguide sensing plate. International

Worhskp on Soft Interface Sciences for Young Scientists 2012 (SISYS 2012), Tsukuba, Japan. November 21-22, **2012**.

6. **Lakshmipriya, T.,** Fujimaki, M., Gopinath, S.C.B., Horiguchi, Y., Nagasaki, Y., Detection of influenza viruses by SPFS-High performance sensing by RNA-aptamers/PEG hybridized sensor. International Union of Materials research societies-International conference on Electronic Materials 2012 (IUMRS-ICEM 2012), Yokohama, Japan. September 23-28, **2012**.
7. **Lakshmipriya, T.,** Fujimaki, M., Gopinath, S.C.B., Horiguchi, Y., Nagasaki, Y., Evaluation of anti-influenza aptamer generation by surface Plasmon Fluorescence Spectroscopy. Softinterface International Minisymposium on Biointerface-interface between Bio and Materials (SIMS2012) March 17–19, **2012**.
8. **Lakshmipriya, T.,** Fujimaki, M., Gopinath, S.C.B., Horiguchi, Y., Nagasaki, Y.,. Poly(ethylene glycol)-b-Poly(acrylicacid) (PEG-b-PAAc) mediated signal enhancement for aptamer-protein interactions by Surface Plasmon Fluorescence Spectroscopy. MANA International Symposium 2012 Jointly with ICYS. Tsukuba, Japan. February 29-March 2, **2012.**
9. **Lakshmipriya, T.,** Fujimaki, M., Gopinath, S.C.B., Horiguchi, Y., Nagasaki, Y., Optimization of fluorescence labeling and label free aptasensors for the detection of influenza virus. The 21st MRS-Japan Academic Symposium, Yokahama, Japan, December 19-21, **2011**.

First and foremost, I would like to express my heartiest and the grateful gratitude to Professor Yukio Nagasaki for providing me the opportunity to pursue Ph.D. degree and his instructive guidance with encouragement and beneficial comments throughout the duration of the present study.

I am also grateful to Professor Hiroaki Suzuki, Professor Osamu Niwa and Professor Seiya Tsujimura for their constructive comments to improve my thesis.

I wish express my gratitude to Dr. Makoto Fujimaki for his constant guidance, hearty encouragements and beneficial comments throughout the duration of the present study.

The author is deeply grateful to Dr. Yukuchi Horiguchi, for his encouragements and helpful discussions to improve this work.

I am deeply grateful to Dr. Yutaka Ikeda, Dr. Toru Yoshitomi and Dr. Chonpathompikunlert Pennapa for their hearty encouragements.

The author would like to thank from the bottom of the heart to all members of Nagasaki Laboratory for their warm assistance and making friendly environment.

The present thesis is a compilation of the studies performed at the University of Tsukuba and National Institute of Advanced Industrial Science and Technology (AIST) during 2011-2014.

My sincere gramercy to everyone involved directly or indirectly with this work.

Finally, I sincerely express my appreciation to my family members for their assistance and encouragements during my study.

Thangavel Lakshmipriya

NAGASAKI LABORATORY

筑波大学
University of Tsukuba

Appendices

List of Abbreviations and Symbols

A	Adenine
Ag	Silver
AMA	2-(*N*,*N*-dimethylamino)ethyl methacrylate
APS	Ammonium persulfate
APTES	3-aminopropyltriethoxysilane
ATP	Adenosine 5'-triphosphate
Au	Gold
Bis	N, N'-methylene bisacrylamide
bp	Base pair(s)
BSA	Bovine serum albumin
C	Cytosine
°C	Degrees Celsius
$CaCl_2.6H_2O$	Calcium chloride hexahydrate
CM5	Carboxymethyl-dextran
Cr	Chromium
Cy5	Cyanine 5
dATP	Deoxyadenosine triphosphate
dCTP	Deoxycytidine triphosphate
ddH_2O	Double-distilled water
dGTP	Deoxyguanosine triphosphate
DNA	Deoxyribonucleic acid
DNase	Deoxyribonuclease
dNTP	Deoxyribonucleotide triphosphate
dsDNA	Double-stranded DNA
DTT	Dithiothreitol
dTTP	Deoxythymidine triphosphate
ECL	Enhanced chemiluminescence
EDC	*N*-ethtyl-*N'*-(3-dimethylaminopropyl)carbodiimde hydrochloride
E. coli	*Escherichia coli*
EDTA	Ethylenediaminetetraacetic Acid
EFC-WM	Evanescent-field-coupled waveguide-mode
ENU	Ethylnitrosourea
ELISA	Enzyme-Linked Immunosorbent Assay
et al.	and others
EtBr	3, 8-diamino-5-Ethyl-6-phenyl phenanthridinium Bromide
fM	Femtomolar
FIX	Factor IX
g	Gravitational acceleration
g	Gram
G	Guanine
$Gd_2O_3:Er^{3+},Yb^{3+}$	gadolinium oxide
Glu	Glutaraldehyde
GNP	Gold nanoparticle
GTP	Guanosine 5'-triphosphate
h	Hour(s)
HA	Hemagglutinin
HCG	Human Chorionic gonadotrophin
HCl	Hydrochloric acid
HEPES	4-(2-hydroxyethyl)-1-piperazineethanesulfonic acid

He-Ne	Helium-Neon
HIV-1	Human immunodeficiency virus-1
HRP	Horseradish peroxidise
ICT	Immunochromatography test
IEF	Isoelectric focusing
Ig	Immunoglobulin
IgE	Immunoglobulin E
IgG	Immunoglobulin G
IgG-GNP	Immunoglobulin G conjugated gold nanoparticle
IPTG	Isopropyl-β-D-thiogalactopyranoside
Jilin-HA	Influenza B/Jilin/20/2003
KCl	Potassium chloride
kcpm	Kilo counts per Minute
K_d	Dissociation constant
kDa	Kilodalton
Kg	Kilogram
KOH	Potassium hydroxide
KH_2PO_4	Monopotassium phosphate
K_2HPO_4	Dipotassium phosphate
LB	Luria Bertani medium
M	Mol/Liter, molar
MeO-PEG-OH	Hydroxyl-terminated poly(ethylene glycol)
mg	Milligram
$MgCl_2.6H_2O$	Magnesium Chloride hexahydrate
Min	Minute(s)
mL	Milliliter
mM	Millimolar
N6-PEG	pentaethylenehexamine-terminated poly(ethylene glycol)
NA	Neuraminidase
Na^+	Sodium ion
NaCl	Sodium chloride
ND	Not determined
NaOAc. $3H_2O$	Sodium acetate trihydrate
NaOH	Sodium hydroxide
ng	Nanogram
NHS	N-Hydroxysuccinimide
nM	Nanomolar
nt	Nucleotide(s)
OD	Optical density
OH	Hydroxyl
PAGE	Polyacrylamide gel electrophoresis
PBS	Phosphate buffered saline
PCR	Polymerase chain reaction
PAAc	poly(acrylic acid)
PEG	Poly(ethylene glycol)
PEG-*b*-PAAc	Poly(ethylene glycol)-*b*-poly(acrylic acid)
PEG-*b*-PAMA	Poly(ethylene glycol)-*b*-poly[2-(N,N-dimethylamino)ethyl methacrylate]
pg	Picogram
pH	Potential hydrogen
pM	Picomolar
pI	Isoelectric point
poly A_{24}	24-mer of poly adenosine
poly dA	poly deoxyadenosine

ppm	Parts per million
PVDF	Polyvinylidene difluoride
rf	Radio Frequency
RNA	Ribonucleic acid
RNase	Ribonuclease
rpm	Rotations per minute
RT	Room temperature
RT-PCR	Reverse transcription-PCR
RU	Response Unit
s	Second(s)
SA-GNP	Streptavidin-conjugated gold nanoparticle
SDS	Sodium dodecyl sulfate
SELEX	Systematic Evolution of Ligands by Exponential Enrichment
SEM	Scanning Electron Microscope
SH-dT	Thiolated Deoxythymidine
Si	Silicon
SiRNA	Small interfering Ribonucleic acid
SiO_2	Silicon dioxide
S/N	Signal-to-noise
SPR	Surface Plasmon Resonance
SPFS	Surface Plasmon Fluorescence Spectroscopy
ssDNA	Single-stranded DNA
T	Thymine
TBE	Tris-Boric Acid-EDTA
TBS-T	Tris Buffered Saline with Tween 20
TEMED	N,N,N',N'-Tetramethylethylenediamine
THF	tetrahydrofuran
Tokio-virus	Influenza B/Tokio/53/99
Tris	Tris-(Hydroxymethyl)-Aminomethane
tRNA	Transfer RNA
U	Units of enzymatic activity
UTP	Uridine 5'-triphosphate
UV	Ultraviolet
Y_2O_3	Yttrium oxide
V	Volt (s)
VEGF	Vesicular Endothelial Growth Factor
v/v	Volume per volume
w/v	Weight per volume
X–gal	5'-Bromo-4'-Chloro-3'-Indolyl-β-D-galactoside
µA	Microampere
µg	Microgram
µL	Micro liter
µM	Micro molar
2'-F	2'-fluoro
2'-NH_2	2'-amino
^{32}P	Phosphorus-32
$\gamma^{32}P$	Gamma-phosphate

Preparation of Buffers & Reagents

Ammonium Persulphate, APS (10%)

1 g of APS powder was dissolved in 10 mL of ddH_2O, aliquoted in several tubes and stored at -20°C.

Ampicilin (100 mg/mL)

0.5 g of ampicilin was dissolved in ddH_2O that amounts up to a final volume of 5 mL. Following filter sterilization, the solution was stored in aliquots at -20°C.

Calcium Chloride (1M)

21.91 g of Calcium chloride hexahydrate ($CaCl_2.6H_2O$) powder was dissolved to a final volume of 100 mL of ddH_2O. The solution was autoclaved at 121°C for 20 min and stored at RT.

Coomassie Briliant blue R250 (0.5%)

5 g of Coomassie Briliant blue R250, 300 mL of methanol and 100 mL of glacial acetic acid were mixed together and made up to a final volume of 1 L with ddH_2O. The solution was kept at RT.

Denaturing-urea Polyacrylamide Gel (12%, 7 M)

420 g of urea, 100 mL of 10X TBE and 400 mL of Acrylamide/Bis–acrylamide (30%) were dissolved in ddH_2O to a final volume of 1 L. The solution was stored at 4°C. The bottle containing the solution was wrapped up with aluminium foil for protection from light. For polymerization, each 10 mL of the solution was mixed with 100 µL of 10% APS and 10 µL of TEMED.

Destaining Solution

300 mL of methanol and 100 mL of glacial acetic acid were mixed together and made up to a final volume of 1 L with ddH_2O. The solution was kept at RT.

EDTA (Ethylenediaminetetraacetic) (0.5 M, pH 8.0)

93.06 g of EDTA, Disodium Salt (Dihydrate) was dissolved in 450 mL of ddH_2O. The solution was stirred while the addition of 10 N NaOH was taking place till the pH of 8.0. Next, the solution was topped up to a final volume of 500 mL, autoclaved at 121°C for 20 min and stored at RT.

HEPES-KOH (10X SELEX Binding Buffer) (100 mM HEPES-KOH [pH 7.4], 1500 mM NaCl)

23.83 g of HEPES and 87.66 g of NaCl were dissolved in 800 mL of ddH_2O. The pH was adjusted to 7.4 with 10 N of KOH. After adjusting the volume to 1 L, the solution was filter-sterilized. The working solution, which is 1X, was prepared by mixing 100 mL of the stock solution with 900 mL of autoclaved ddH_2O.

Isopropyl-β-D-thiogalactopyranoside (IPTG) (100 mM)

0.238 g of IPTG was dissolved in ddH_2O to a total volume of 10 mL, filter-sterilized, aliqouted and stored at -20°C. Tubes were covered with aluminium foil for protection from light.

LB Agar containing 100 µg/mL Ampicilin

10.5 g of LB agar powder was dissolved in ddH_2O to a final volume of 300 mL and autoclaved at 121°C for 20 min. After cooling to about 50°C, 300 µL of 100 mg/mL of ampicilin was added into the solution and approximately 20 mL of the solution was poured into each petri plate. After solidification, the petri plates were stored at 4°C. For blue-white selection, 50 µL of 40 mg/mL X-Gal and 50 µL of 100 mM IPTG were spread on top of the agar and incubated at 37°C for 20 min before used for transformation.

LB Broth/ LB Broth containing 100 µg/mL Ampicilin

6 g of LB broth powder was dissolved in ddH_2O to a final volume of 300 mL and autoclaved at 121°C for 20 min. The solution was stored at RT. To prepare overnight-grown culture of bacteria, 5 µL of 100 mg/mL of ampicilin was added into 5 mL of the LB broth before incubation at 37°C with shaking at 200 rpm for 16 hrs.

Magnesium Chloride ($MgCl_2$) (1 M)

20.33 g of Magnesium Chloride Hexahydrate ($MgCl_2.6H_2O$) powder was dissolved in ddH_2O to a final volume of 100 mL and autoclaved at 121°C for 20 min. The solution was stored at RT.

Native PAGE (10%)

50 mL of 10X TBE and 175 mL of Acrylamide/Bis–acrylamide (30%) were dissolved in ddH_2O to a final volume of 500 mL. The solution was stored at 4°C. For polymerization, each 10 mL of the solution was mixed with 100 µL of 10% APS and 10 µL of TEMED.

Phosphate Buffered Saline (PBS) (0.01 M)

5 PBS tablets were dissolved in ddH_2O to a final volume of 1 L and autoclaved at 121°C for 20 min. The solution was stored at RT.

PBS containing 3% BSA

3 g of BSA was added to a final volume of 100 mL of PBS buffer and stored at 4°C.

PBS containing 0.05% Tween-20

500 µL of Tween-20 was added into 1 L of PBS buffer and stored at RT.

RNA loading dye (2X)

4.8 g of urea and 0.5 mL of 1% bromophenol blue were dissolved in 1X TBE to a final volume of 10 mL.

The solution was filter-sterilized and stored at RT.

SDS-PAGE Resolving Gel

2.5 mL of 1.5 M Tris-HCl (pH 8.8), 100 µL of 10% SDS, 4.0 mL Acrylamide/Bis-acrylamide (30%) and 3.3 mL ddH_2O were mixed together. Following this, 100 µL of 10% (w/v) APS and 10 µL of TEMED were added for polymerization and poured into the gel casting system. The mixture was overlayed with water.

SDS-PAGE Sample Buffer (5X)

2 mL of Tris-HCl (0.5 M pH 6.8), 5 mL of 100% glycerol, 1 g of SDS and 0.5 mL of 1% bromophenol blue were dissolved in ddH_2O to a volume of 10 mL. The mixture was aliquoted 1 mL into each microcentrifuge tube and stored at RT. Prior to use, 50 µL of Beta-mercaptoethanol was added into each aliquot.

SDS-PAGE Stacking Gel

2.0 mL of 0.5 M Tris-HCl (pH 6.8), 80 µL of 10% SDS, 1.3 mL of Acrylamide/Bis-acrylamide (30%), 5.14 mL of ddH_2O were mixed together. Following this, 80 µL of 10% (w/v) APS and 8 µL of TEMED were added for polymerization. The mixture was poured on top of the solidified resolving gel and comb was inserted.

SDS Running Buffer (10X)

30.2 g of Tris Base, 144 g of glycine and 10 g of SDS were added into ddH_2O, which was adjusted to a final volume of 1 L. The solution was stored at RT and was diluted to a working concentration of 1X by mixing 100 mL of the stock solution with 900 mL of ddH_2O.

Sodium Acetate (NaOAc) (3 M, pH 5.2)

40.8 of Sodium Acetate Trihydrate (NaOAc. $3H_2O$) was dissolved in 80 mL of ddH_2O. After adjusting the pH to 5.2 with glacial acetic acid, the solution was topped up to a final volume of 100 mL. The solution was autoclaved at 121°C for 20 min and stored at RT.

Sodium Phosphate (50 mM, pH 7.6)

0.11 g of Monosodium Phosphate, Monohydrate and 1.13 g of Disodium Phosphate, Heptahydrate were added to a final volume of 1 L of ddH_2O. The solution was autoclaved at 121°C for 20 min and stored at RT.

Tris-Borate-EDTA (TBE) (10X)

108 g of Tris Base, 55 g of Boric acid and 40 mL of 0.5 M EDTA (pH 8.0) were added to a final volume of 1 L of ddH_2O. Autoclaving of this stock solution was made at 121°C for 20 min. Working solution (1X) was prepared by diluting 100 mL of the stock solution with 900 mL of ddH_2O.

Tris Buffered Saline with Tween 20 (TBS-T) (10X)

24.23 g of Tris Base, 87.66 of NaCl and 5 mL of Tween-20 were added in ddH_2O to a volume of 800 mL. After adjusting the pH to 7.5 using 10 N HCl, the solution was topped up to a final volume of 1 L. The solution was stored at RT and diluted to a working concentration of 1X by mixing 100 mL of the stock solution with 900 mL of ddH_2O. The working solution was used as the washing buffer for Western Blot analysis. For blocking and antibody preparation, the stock solution was diluted to 1X containing 5 % skimmed milk and stored at 4°C.

Tris-HCl (0.5 M, pH 6.8)

6.1 g of Tris Base powder was dissolved to a final volume of 80 mL of ddH_2O and the pH was adjusted to 6.8 with 10 N of HCl. The volume was brought up to 100 mL. This solution was then autoclaved at 121°C for 20 min and stored at RT.

Tris-HCl (1 M, pH 8.3)

12.2 g of Tris Base powder was dissolved to a final volume of 80 mL of ddH_2O and the pH was adjusted to 8.3 with 10 N of HCl. The volume was added up to 100 mL. This solution was then autoclaved at 121°C for 20 min and stored at RT.

Tris-HCl (1.5 M, pH 8.8)

18.3 g of Tris Base powder was dissolved to a final volume of 80 mL of ddH_2O and the pH was adjusted to 8.8 with 10 N of HCl. The volume was added up to 100 mL. This solution was then autoclaved at 121°C for 20 min and stored at RT.

Tris-HCl (1 M, pH 9.0)

12.2 g of Tris Base powder was dissolved to a final volume of 80 mL of ddH_2O and the pH was adjusted to 9.0 with 10 N of HCl. The volume was added up to 100 mL of ddH_2O. This solution was then autoclaved at 121°C for 20 min and stored at RT. For mild alkaline hydrolysis in ENU mapping analysis, working concentration of 1X was prepared by mixing 100 mL of the stock solution with 900 mL of autoclaved ddH_2O.

X-Gal (5-bromo-4-chloro-3-indolyl-β-D- galactopyranoside) (20 mg/mL)

100 mg of X-Gal powder was dissolved to a final volume of 5 mL of Dimethyl Sulfoxide. After filter-sterilization, the solution was aliquoted and stored at -20°C. Tubes were wrapped up with aluminium foil for protection from light.